STUDY THE EFFECT OF DENSITY DEPENDENCE OF SYMMETRY ENERGY ON FRAGMENTATION IN HEAVY-ION COLLISIONS AT INTERMEDIATE ENERGIES

A THESIS

submitted to the

THAPAR UNIVERSITY, PATIALA

for the degree of

DOCTOR OF PHILOSOPHY

IN THE FACULTY OF SCIENCE

By

Karan Singh Vinayak

Regn. No. 900912024

SCHOOL OF PHYSICS AND MATERIALS SCIENCE

THAPAR UNIVERSITY

PATIALA-147004, PUNJAB, (INDIA)

THAPAR UNIVERSITY, PATIALA

CANDIDATE'S DECLARATION

I hereby certify that the work which is being presented in this thesis entitled "**STUDY THE EFFECT OF DENSITY DEPENDENCE OF SYMMETRY ENERGY ON FRAGMENTATION IN HEAVY-ION COLLISIONS AT INTERMEDIATE ENERGIES**" is partial fulfillment of the requirements for the award of Degree of Doctor of Philosophy and submitted in the School of Physics and Materials Science, Thapar University, Patiala, is an authentic record of the my own work carried out during a period from May 2010 to May 2013 under the supervision of **Dr. Suneel Kumar**, Associate Professor, Thapar University Patiala.

The matter presented in this thesis has not been submitted by me for the award of any other degree of this or any other university/institute.

Karan S. Vinayak

(Karan Singh Vinayak)

This is to certify that the above statement made by the candidate is correct to the best of our knowledge.

S Kumar

Dr. Suneel Kumar

(Supervisor)

Signature of HOD

Signature Dean R & SP

Signature of External Examiner

Date: 24/09/13

Acknowledgments

First and foremost, I would like to express my most sincere gratitude to my thesis supervisor **Dr. Suneel Kumar** *Associate Professor, Thapar University, Patiala.* His intuition and persistency are the key reasons that I could successfully finish each of the research topics. He is a unique combination of great intellects and genuine caring for those persons for whom he has some responsibility. I was very fortunate to be one of these people. To me, he is not only a world class advisor, but also an influential mentor. He is the source of endless inspiration even during the most stressful times. His guidance, support, and vision will be a long-lasting influence in my professional and personal life.

Special thanks go to **Dr. Rajeev K. Puri** *Professor, Panjab University, Chandigarh* for his support during my whole research work. He has especially contributed a lot to this thesis. He is an inexhaustible source of intellectual and creative energy. His good sense in finding general physics laws to explain complicated theoretical data was an excellent lesson to me. I am extremely impressed by his ability to get an intuitive feel of the most difficult ideas. It is a fortunate for me being associated with him in research field.

I offers special thanks to **Dr. Kulvir Singh**, *Associate Professor and Head, School of Physics and Materials Science, Thapar University, Patiala*, for providing all the necessary facilities in the department and teaching assistantship during the time when I need it a lot. Also, I wishes to express thankfulness to all the faculty and staff of the School for their kind support. I am thankful to **Prof. K. K. Raina**, *Deputy Director,* for their encouragement and constant moral support to accomplish this task. I acknowledges the useful suggestions of the members of my doctoral committee **Dr. A. K. Lal** and **Dr. Manoj Kumar Sharma**. Thanks to **Dr. P. K. Bajpai,** *Dean, research and sponsored projects* for providing the possible research facilities here at Thapar University campus. Many thanks are due to head of computer science department, Thapar University, Patiala for providing me the supercomputing facility. Special thanks to **Dr. O. P. Pandey** for providing me useful and valuable tips regarding research.

Here, I will not forgot to thank **Dr. Rohit Dhir** (now doing Post Doctorate at Yonsei University, South Korea) for useful suggestions, moral support and joyous company. It was only he, who supported me during the tough phases and provided me a vision to solve the problems in life.

I am fortunate enough to have worked with my lab mates Dr. Sanjeev Kumar, Anupriya Jain and Rubina Bansal at Thapar University, Patiala. I am thankful to them for their sincere help and cooperation. I acknowledges with thanks the co-operation and encouragement extended by colleagues in the Heavy Ion Reactions Theory group at Chandigarh, particularly, Dr. Sakshi, Dr. Supriya, Rajni and Sukhjit Kaur for their fruitful discussions and novel views.

A special word of thanks to my senior **Dr. Akshay Kumar** (now Assistant Professor at S.G.G.S.W. University), for his help and encouragement.

Of course, none of this could have happened without the support of my parents, **Mr. Anoop Vinayak and Mrs. Swaran Lata**, my brother, **Shakti Singh Vinayak**, my cousin **Puneet Bhandari**, who always stand by me and boost my confidence to achieve my goals in life. Also, I would love to mention my close and ever cheerful friends Sumit Nagpal, Dheeraj Sharma and Neeraj Saini for moral support and all fantastic moments we spent together.

And above all, I would like to thank God who has given me this life and provided me an opportunity to work in this esteem institution and complete my task successfully.

Karan S. Vinayak

Date : 24/09/13

Patiala

(Karan Singh Vinayak)

List of Publications :

A. International Journals :

1. Multifragmentation around the transition energy in intermediate-energy heavy-ion collisions.
   Karan Singh Vinayak and Suneel Kumar,
   Physical Review C 83, 034614 (2011) [5 pages].

2. Influence of density dependent symmetry energy on elliptical flow.
   Karan Singh Vinayak and Suneel Kumar,
   European Physical Journal A 47, 144 (2011) [6 pages].

3. Thermalization and temperature reached in heavy-ion collision using the isospin-dependent quantum molecular dynamics model.
   Karan Singh Vinayak and Suneel Kumar,
   European Physical Journal A 48, 96 (2012) [7 pages].

4. Effect of density-dependent symmetry energy on nuclear stopping.
   Karan Singh Vinayak and Suneel Kumar,
   Journal of Physics G: Nuclear Particle Physics 39, 095105 (2012) [9 pages].

5. Effect of density dependent symmetry energy on fragmentation.
   Karan Singh Vinayak and Suneel Kumar,
   Journal of Physics Conference Series 381, 012032 (2012) [5 pages].

6. On the role of density-dependent symmetry energy and momentum dependent interactions in multifragmentation.
   Karan Singh Vinayak and Suneel Kumar,

Physics of Particle and Nuclei Letters 9(8), 583 (2012) [6 pages].

7. Optimizing the rapidity limit for nuclear stopping in intermediate energy heavy-ion collisions.
   Karan Singh Vinayak and Suneel Kumar,
   Physics of Atomic Nuclei 76, 286 (2013) [8 pages].

8. Impact of momentum dependent equation of state and isospin-dependent cross section on the elliptical flow.
   Karan Singh Vinayak and Suneel Kumar,
   American Institute of Physics, Proceedings 1524, 228 (2013) [4 pages].

9. Effect of nucleonic cross section and momentum dependent interactions on directed flow v_1.
   Anupriya Jain, Karan Singh Vinayak and Suneel Kumar,
   Annals of Physics 334, 334 (2013) [7 pages].

10. On the role of isospin momentum dependent interactions in multifragmentation.
    Navjot Kaur Virk, Karan Singh Vinayak and Suneel Kumar,
    Physical Review C (Submitted).

B. National Journals :

11. Effect of density dependent symmetry energy and Coulomb interactions on the evolution of intermediate mass fragments.
    Karan Singh Vinayak and Suneel Kumar,
    Pramana Journal of Physics (Accepted).

B. Symposia/Workshops/Conferences:

12. Reduced NN cross section and fragment production.
    Karan Singh Vinayak and Suneel Kumar,
    DAE Symposium for Nuclear Physics, December 19-24, BITS, PILANI, **Vol. 55**, 496 (2010).

13. Influence of density dependent symmetry energy on fragmentation.
    Karan Singh Vinayak, Mohinder Singh and Suneel Kumar
    5^{th} Chandigarh Science Congress, Feb 26-28, Panjab University, Chandigarh **PS-16**, Page-56 (2011).

14. Role of density dependent symmetry energy in nuclear stopping.
    Karan Singh Vinayak and Suneel Kumar,
    DAE symposium for Nuclear Physics, December 26-30, Andhra University, Vishakhapatnam **Vol. 56**, 770 (2010).

15. Effect of density dependent symmetry energy on Elliptical flow.
    Suneel Kumar and Karan Singh Vinayak,
    DAE symposium on Nuclear Physics, December 26-30, Andhra University, Visakhapatnam, **Vol. 56**, 814 (2011).

16. Neutron-proton P_t-differential sideward flow as a probe for symmetry energy.
    Suneel Kumar and Karan Singh Vinayak,
    DAE symposium on Nuclear Physics, December 3-7, University of Delhi, New Delhi, **Vol. 57**, 704 (2012).

17. On the directed transverse flow and the relation between symmetric and asymmetric

collisions.

Karan Singh Vinayak, Rubina Bansal and Suneel Kumar,

DAE symposium on Nuclear Physics, December 3-7, University of Delhi, New Delhi, **Vol. 57**, 698 (2012).

18. Role of isospin momentum dependent interactions in multifragmentation.

    Karan Singh Vinayak, Navjot Kaur Virk and Suneel Kumar,

    DAE symposium on Nuclear Physics, December 3-7, Bhabha Atomic Research Center (BARC), Mumbai, 2013.

19. Effect of isospin momentum dependent interactions on elliptical flow.

    Navjot Kaur Virk, Karan Singh Vinayak and Suneel Kumar,

    DAE symposium on Nuclear Physics, December 3-7, Bhabha Atomic Research Center (BARC), Mumbai, 2013.

20. Effect of density dependent symmetry energy on intermediate energy heavy-ion collisions.

    Karan Singh Vinayak,

    DAE symposium on Nuclear Physics, December 3-7, Bhabha Atomic Research Center (BARC), Mumbai, 2013.

Abbreviations	
EOS	equation of state
QGP	quark gluon plasma
RQMD	relativistic quantum molecular dynamics
UrQMD	ultra-relativistic quantum molecular dynamics
CMD	classical molecular dynamics
IQMD	isospin dependent quantum quantum molecular dynamics model
IBUU	isospin dependent boltzmann uehling uhlenbeck model
FN	free nucleons
LCP	light charged particles
MMF	medium mass fragments
IMF	intermediate mass fragments
HMF	heavy mass fragments
MST	minimum spanning tree
MSTM	minimum spanning tree (with momentum cut)
MDI	momentum dependent interactions

Contents

ABSTRACT

In the present study, we aim to investigate the effect of density dependence of symmetry energy on multifragmentation, fragment's flow (i.e. elliptical flow) as well as on nuclear stopping. The present work is performed within the framework of microscopic dynamical isospin-dependent quantum molecular dynamics *(IQMD)* model. We shall here attempt a descriptive analysis of the fragment production, elliptical flow associated with nucleons and fragments, nuclear dynamics (density & temperature) and nuclear stopping (or thermalization) reached in heavy-ion collisions subjected to different forms of density dependence of symmetry energy. Present study includes a detailed discussion of the consequences of different forms of symmetry energy in heavy-ion collisions at intermediate energies (i.e. between 10 MeV/nucleon and 1 GeV/nucleon).

The present thesis is divided into seven chapters.

Chapter 1 includes the general introduction regarding the isospin-dependence of the nuclear equation of state. The behavior of symmetry energy and its variation with the density is explained. The role of density dependent symmetry energy in heavy-ion reactions as well as theoretical and experimental work done in this domain is discussed. Also a brief outline of the various observables such as multi-fragmentation, collective flow and nuclear stopping is reported. We shall review the status of the work done regarding the density dependence of the symmetry energy by different collaborations at *MSU (USA), RIKEN (JAPAN), and GSI (Germany), INFN (Italy), University of Liverpool (UK), University of Arizona (USA), Texas (USA).* The attempts made by different theoretical groups are also discussed.

Chapter 2 gives the details of various theoretical models used in the literature and clusterization algorithms which clusterize the phase space of nucleons. This chapter is divided mainly into three parts. In the first part, different theoretical models used to study heavy-ion collisions without isospin effects, shall be discussed. On the other hand, second part consists of different theoretical models which are capable of exploring the heavy-ion

collisions with isospin effects. These models are the primary models used to follow the reaction from the start where one has two well separated nuclei to the end where matter is fragmented and cold. The third part presents different secondary algorithms used to analyze the phase space of nucleons generated by the primary models. We shall discuss the *QMD, IQMD* models in detail, while, MST and MSTM methods are also presented.

In **Chapter 3** we shall carry out the investigation for the fragmentation of light charged particles at their respective transition energies to see that whether any particular structure exits at these incident energies (energy at which elliptical flow vanishes in the mid-rapidity region) or not.

Chapter 4 sheds light on the consequences of various forms of density dependent symmetry energy on the multifragmentation. This work highlights the variation in the fragment production with the inclusion of density dependent symmetry energy and momentum dependent interactions (MDI). We shall present the percentage variation in the production of free nucleons and light charged particles over the whole colliding geometry subjected to the different forms of density dependent symmetry energy (with and without MDI). Also a comparison of the theoretical predictions with the experimental data of *ALADIN* Collaboration has been made to study the collective effect of density dependent symmetry energy and MDI on the fragment production. We shall discuss the role of Coulomb interactions in the formation of heavier fragments. The charge distribution of nuclear matter is studied and the results are compared with experimental findings.

Chapter 5 shows the effect of density dependent symmetry energy on the transverse momentum and excitation energy dependence of the elliptical flow. The elliptic flow (or squeeze-out flow) is highly sensitive towards the different forms of the density dependent symmetry energy in the mid-rapidity region (participant zone) from where the squeeze-out is actually generated. The elliptical flow vanishes at a particular incident energy where the shadowing of the spectator matter is counter balanced by the expansion of the compressed and heated participant matter. The transition energy (energy at which the elliptic flow vanishes) is found to vary drastically with respect to the different forms of the

density dependent symmetry energy. The theoretical results are in good agreement with the experimental findings, where the inclusion of the density dependence of symmetry energy tends to give the larger squeeze-out for the Z $\leq$ 2 particles and protons. Also, we shall discuss the impact of momentum dependent equation of state and different forms of cross sections (isospin-dependent and independent) on the elliptical flow. The momentum dependent interactions and isospin dependent cross section are found to affect the elliptic flow of both protons and neutrons considerably.

In Chapter 6, we discussed the role of density dependence of symmetry energy in nuclear stopping. The global nuclear stopping is mildly affected by the density dependence of the symmetry energy for the isospin asymmetric systems at peripheral collisions. System mass dependence and excitation energy dependence of anisotropy ratio (global nuclear stopping) shows no sensitivity towards the various forms of the density dependent symmetry energy. The dN/dY as a function of reduced rapidity $Y_{red.}$ shows a considerable effect of symmetry energy for peripheral collisions when subjected to different forms of symmetry energy. Overall, the nuclear stopping decreases with an increase in the stiffness of the symmetry energy. Also, nuclear stopping which is generated from the participant zone is severely affected by the size and type of the rapidity bin. The global stopping of protons increases, while of the neutrons decreases with an increase in N/Z of the system.

The knowledge about the temperature and density reached in heavy-ion collisions is of great importance to understand the properties of compressed and thermalized nuclear matter. We shall show that the temperature and density tends to increase with the stiffness of the symmetry energy. Our findings concludes that the nuclear stopping can act as a good probe for the temperature reached in heavy-ion collisions. The statistical correlation of global nuclear stopping with the temperature is also potentially justified as the stopping of target with projectile indicates the thermalization reached in the heavy-ion collisions. The theoretical findings are compared with the data of *INDRA* and *ALADIN* Collaboration.

In **Chapter 7** we summarize our results, that follows with an outlook.

Chapter 1

Introduction

" Take up one idea. Make that one idea your life - think of it, dream of it, live on that idea. Let the brain, muscles, nerves, every part of your body, be full of that idea, and just leave every other idea alone. This is the way to success.".....*Swami Vivekananda* (1863-1902).

1.1 Introduction

The intermediate energy heavy-ion collisions (HIC's) are signified as an excellent tool to unfold the complex nuclear interactions inside the extremely dense and heated nuclear matter having density 3 - 4 times the normal nuclear matter density (0.15 - 0.17 fm^{-3}). The intermediate energy range (10 MeV/nucleon to 1 GeV/nucleon), provides an opportunity to extract the properties of nuclear matter away from the saturation density. The quest for the nuclear equation of state (equation that describes the relation between pressure, temperature, energy and density of the heated nuclear matter) is the major motivation for the study of HIC's from low to relativistic energies. At low incident energies, the phenomena of fusion, fission and dynamical cluster decay dominate the physics. For low energy reactions, Malik *et al.* [1] had proposed a model for the mechanism of cluster formation and then penetration of the confining nuclear interaction barrier in radio-active nuclei. Investigations performed by Rath *et al.* [2] near the barrier energies reported the suppression of the complete fusion for a particular system. Trautmann *et al.* [3] studied the thermal and chemical freeze-out in spectator fragmentation. Recently, Rafi *et al.* [4] described the equation of state and nucleon optical potential with three body forces. On

the other hand, the high energy reactions corresponds to the formation of quark-gluon plasma (QGP) and the break-up of nucleons into smaller constituents (quarks and gluons). Though, protons and neutrons are the basic building blocks of the nature, yet they are not the fundamental particles, as they are composed of quark-gluon matter. A clear understanding of the behavior of protons and neutrons is essential to unfold the various mysteries of nuclear as well as astro-physics. More in-depth probes reported that the quarks are even more dense and hard. During the collision phase, the density becomes few times of the normal matter density and the conditions created are similar to those which prevailed during the creation of the universe. In the overlapping stage, the temperature of the nuclear matter is even larger than that of the surface of the sun. Therefore, the HIC's can act as a tool to understand the behavior of highly compressed nuclear matter under the extreme conditions.

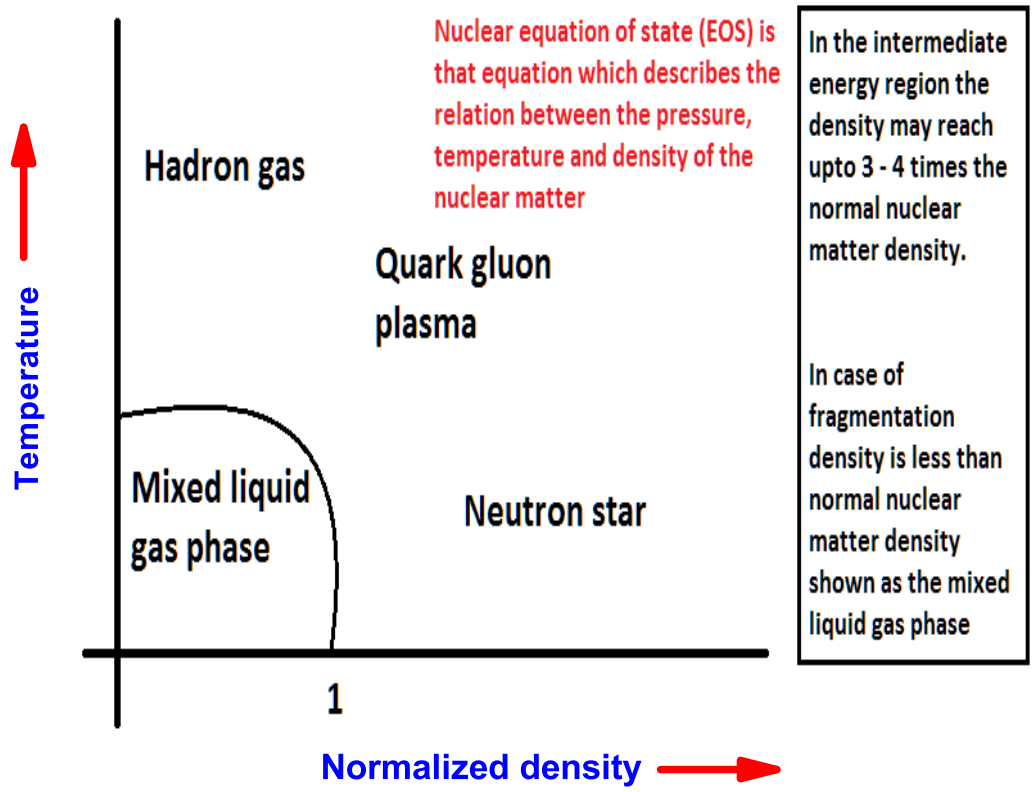

Figure 1.1: Phase diagram of nuclear matter.

The enormous developments made by the HIC's in this field, in the present and last few decades has gone through great developments, where the questions regarding

the nuclear equation of state (EOS), transport coefficients, momentum dependence of the nucleon-nucleon (NN) interactions, in-medium cross sections and their isospin dependence are well studied. Further the collective flows (directed, elliptical and higher order anisotropic flow) have revolutionized the study of the EOS and its isospin dependence. The multifragmentation and nuclear stopping are well suited to study the nuclear matter interactions at low densities.

The reactions at relativistic energies are more pronounced in the exploration of quark gluon plasma. While the low energy reactions shed light on the structure of the nuclei, the intermediate energy range is best suited to analyze the relation between the density and pressure, the so-called nuclear equation of state and the interactions among the protons and neutrons inside an excited nucleus (composed of target and projectile). HIC's can provide an access to the various rare phenomenon related to the astrophysics. Though, astrophysical phenomenon can provide only an indirect information regarding the neutron stars and supernova explosions [5, 6]. The nuclear equation of state plays a crucial role in the structure, composition and evolution of neutron stars and can shed light on the conditions which existed just after the formation of the universe [6, 7]. The intermediate energy reactions provide us an opportunity to understand the conditions which prevailed during the formation of the universe. It gives a brilliant access to the conditions when the QGP and Hadron gas (HG) existed just after the big-bang. This is due to the fact that dramatic changes takes place when the nuclear matter is subjected to the conditions of very high temperatures and densities. Interestingly, at intermediate energies, the density drops below normal nuclear matter density at the later stages of the reaction. This state is basically mixed liquid-gas phase at low density nuclear matter shown in Fig. 1.1. Overall, the compressed nuclear matter generated in heavy-ion collisions gives us a stance of the super nuclear equation of state and can provide an excellent exposure to the environments which are remote in space and cannot be accessed due to the limitations of huge time span.

1.2 Asymmetric nuclear matter

One should keep in the mind that the neutron to proton (N/Z) ratio of the systems has a significant impact on the reaction outcome in the intermediate energy heavy-ion collisions.

The neutron (proton) content of the whole system justify the strength and interplay of symmetry energy in HIC's. Larger proton content increases the Coulomb repulsion as well. That is why, the Coulomb effect tends to increase with proton number of a nucleus. Therefore, larger number of neutrons are needed to compensate the additional Coulomb effect. However, the larger neutron content tends to increase the role of symmetry energy. M*ü*ller and Serot have shown that the asymmetric EOS has quite distinct new features compared to the symmetric one [8]. In isospin-asymmetric nuclear matter, it has been concluded that the evolution of symmetry energy is due to the variation in the freeze-out density rather than the temperature [9]. Particularly, the density and compressibility at saturation are predicted to decrease as the nuclear matter becomes more neutron-rich [10]. The effect of temperature and density dependence of the asymmetric nuclear matter properties within the extended relativistic mean field (ERMF) model [5, 11] was studied, which includes the contribution from the self and mixed interaction terms by using different parameterizations [12]. It was observed that the symmetry energy, its slope and incompressibility coefficients decrease with increasing temperatures up to saturation densities [12]. Also, the information about the density dependent Skyrme effective interactions for normal and isospin rich nuclei can be extended to the neutron skin thickness and isoscalar giant monopole, dipole and quadrupole resonances [13]. Therefore the role of symmetry energy becomes more prominent in case of neutron rich isospin-asymmetric nuclear matter. One is interested to understand the role of symmetry energy at densities away from the normal nuclear matter density. The equation of state of isospin asymmetric nuclear matter is a longstanding problem in both, the nuclear physics and the astro-physics. With the development of radioactive beam facilities around the world during the last few decades, it has become possible experimentally to study the properties of nuclear matter or nuclei under the extreme conditions of large isospin asymmetry in terrestrial laboratories, and also there has been a surge of research activities in this direction. In general, the parameter nuclear symmetry energy $E_{sym}(\rho)$ is the energy related to the neutron-proton asymmetry in the EOS of isospin-asymmetric nuclear matter. The details regarding the symmetry energy are discussed in the next section.

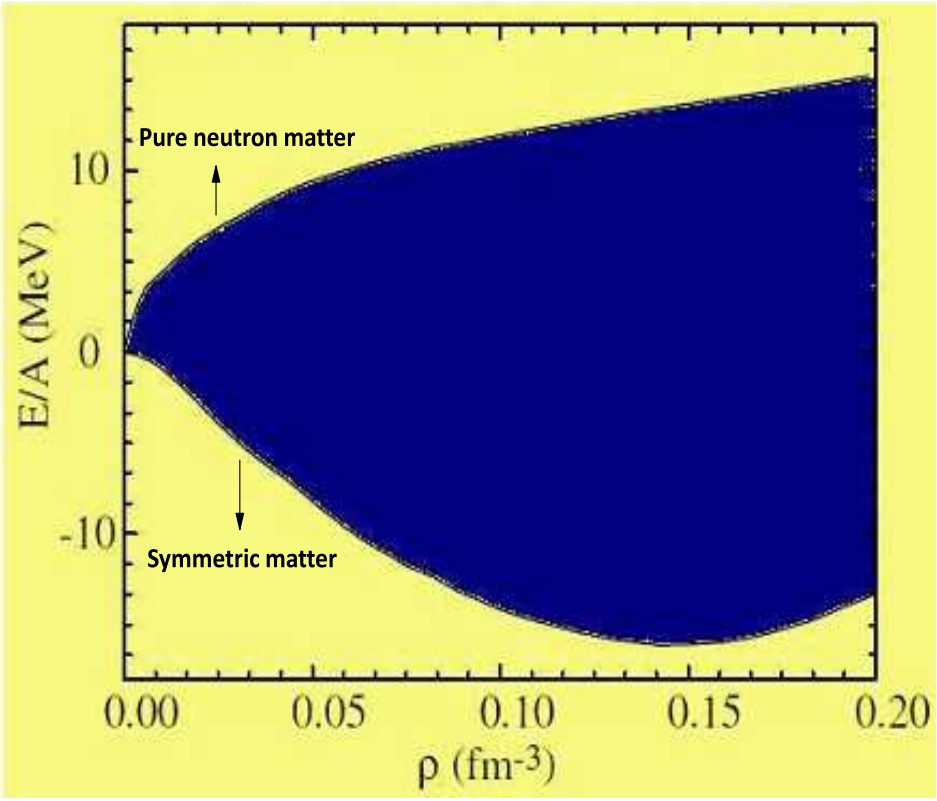

Figure 1.2: The representation for the symmetry energy. The top line is the energy density for pure neutron matter and lower line is that for symmetric nuclear matter. The difference between the two lines signifies the symmetry energy (Figure taken from Ref. [14] Copyright @ 1998 World Scientific).

1.3 Symmetry energy

The equation of state is a fundamental property of nuclear matter, that can be further divided into the charge symmetric nuclear matter (i.e. independent of the isospin asymmetry) and an isospin term (known as the symmetry energy) [15-17]. Many approaches involving different physical approximations and numerical techniques are available which are equipped to deal with the many-body problem of the isospin-asymmetric nuclear matter. The equation of state of nuclear matter refers to the complete understanding of the thermodynamical properties of the nuclear matter which depends strongly on the density, temperature and the neutron-proton asymmetry (i.e., isospin content). It also includes the in-medium properties of the nuclear matter such as Pauli blocking and in medium

nucleon-nucleon (NN) cross section as well as its isospin dependence. An elementary illustration of the symmetry energy strength with density is shown in Fig. 1.2. The difference between the two lines express the effect of symmetry energy in the nuclear matter. The lower line represents the symmetric matter and upper line represents the pure neutron matter.

The term isospin refers to the pair of similar particles (i.e., protons and neutrons), which are almost identical in nuclear matter but have different charge states. The interactions among the proton-proton, neutron-neutron, and neutron-proton are entirely different. The symmetry energy basically accounts for the larger neutron content in the isospin asymmetric systems. The term symmetry energy can be defined as the difference of the energy per nucleon between pure neutron matter and symmetric nuclear matter [18]. The extraction of the exact form and strength of the symmetry energy is a challenging task for the nuclear physics community in the present decade.

As we know, the average binding energy per nucleon is the 8.5 MeV. The binding energy formula E_{bind} = E(A,Z) can be expressed in terms of charge Z and mass A. The Bethe-Weizsäcker (BW) mass formula [19, 20] can be defined as the sum of following five terms:

$$E_{bind} \;=\; a_V A \;+\; a_S A^{2/3} \;+\; \frac{a_C Z(Z-1)}{A^{1/3}} \;+\; \frac{a_A (N-Z)^2}{A} \;+\; \delta_p \tag{1.1}$$

The details of these terms are available in [20]. The fourth term $\frac{a_A(N-Z)^2}{A}$, signifies the symmetry energy. From Refs. [21, 22] symmetry potential can be stated as:

$$V^{sym} = t\frac{1}{\varrho_0} T_3^i T_3^j \delta(\vec{r_i}' - \vec{r_j}) \tag{1.2}$$

The symmetry energy as a function of density can be parameterized in different forms [23, 24] which are described below:

$$V_{sym}^1 = cF_1(u)\delta_a\tau_z, \tag{1.3}$$

$$V_{sym}^2 = cF_2(u)\delta_a\tau_z \;+\; \frac{1}{2}cF_2(u)\delta_a^2, \tag{1.4}$$

$$V^3_{sym} \;=\; cF_3(u)\left[\delta_a\tau_z \;-\; \frac{1}{4}\delta_a^2\right], \tag{1.5}$$

where $\tau_z = 1$ for neutrons and -1 for protons. Here, $F_1(u) = \mathrm{u}$, $F_2(u) = u^2$, $F_3(u) = u^{1/2}$ and $u = \frac{\rho}{\rho_0}$; δ_a is the relative neutron excess $\delta_a = \frac{\rho_n - \rho_p}{\rho_n + \rho_p}$; $\rho,\ \rho_o,\ \rho_n$ *and* ρ_p are the total, normal, neutron and proton densities respectively. The strength c is of the order of 32 MeV to reproduce the fourth term of the Bethe Weizsacker mass formula.

The details regarding the density dependence of symmetry energy are discussed in next section.

1.4 The density dependence of the symmetry energy

The energy per particle of an asymmetric nuclear matter with density ρ and an isospin asymmetry $\delta_A = (\rho_n - \rho_p)$, can be determined by a parabolic law [18], i.e.,

$$E_{sym}(\rho, \delta_A) = E_{sym}(\rho, 0) + E_{sym}(\rho)\delta_A^2, \tag{1.6}$$

where $E_{sym}(\rho,0)$ is the energy per particle of symmetric nuclear matter and E_{sym} represents the nuclear symmetry energy. This understanding does not remain valid as one goes away from the normal nuclear matter density and $\beta-$ stability line [18]. The equation given below provides us the parametrization for the density dependence of symmetry energy [25-37]:

$$E_{sym}(\rho) = E_{sym}(\rho_0)\left(\frac{\rho}{\rho_0}\right)^{\gamma} \tag{1.7}$$

The value of γ determines the stiffness (or strength) of the symmetry energy at densities above and below the saturation density. Constraining the above said equation for the different values of gamma, and its effects on various observables such as multifragmentation, collective flow and nuclear stopping which define the nuclear matter EOS is a much talked about thing in the present nuclear physics research.

The strength of the symmetry energy is different for different values of γ at the densities above and below saturation density. Generally, two different forms of density dependence of symmetry energy have been observed.

1. Soft density dependence: Here the symmetry energy increases upto normal nuclear matter density and decreases afterwards at high densities.

2. Stiff density dependence: Here the symmetry energy tends to increase monotonically with the density.

The stiff symmetry energy will result in a large neutron skin thickness and can lead to larger neutron star radii and rapid cooling of a neutron star [38-40]. There are various studies available in the literature which suggest different forms of the symmetry energy. The predictions made by *ab* initio microscopic calculations prescribed different forms of the nuclear EOS at sub-supra saturation densities [41-44]. Many studies predicted the symmetry energy to increase continously at all densities [34, 45]. However, some studies [46] advocated that the symmetry energy first increases to a certain value and then decreases at supra-saturation densities.

During the past two decades, a lot of work has been done to extract the strength of the symmetry energy as well as its density dependence. The recent developments through nucleon-nucleon collisions give some estimation about the density dependence of the symmetry energy in the sub-saturation region. However, the situation becomes more complex at supra-saturation densities, and still needs more investigation to be done.

1.5 Symmetry energy and nucleon-nucleon collisions

In HIC's, there is an abrupt variation in the density along the whole time span of the reaction. The density of the system becomes 3 - 4 times the normal nuclear matter density around 10 - 15 fm/c, which further depends upon the incident energy and impact parameter of the reaction. Also, the density becomes less than the saturation density during the expansion stage (freeze-out stage). The symmetry energy tends to play a significant role during the overlapping stage and the dissociation stage. The density dependence of the symmetry energy affect the nuclear dynamics at the time when system density is above and below the normal nuclear matter density. The large variation of density during the reaction leads to a significant variation in the symmetry energy strength. Therefore, the accurate form of density dependent symmetry energy can give a more realistic picture of the reaction dynamics. This density dependence of the symmetry energy has a considerable impact on the various observables which can reveal the facts of HIC's.

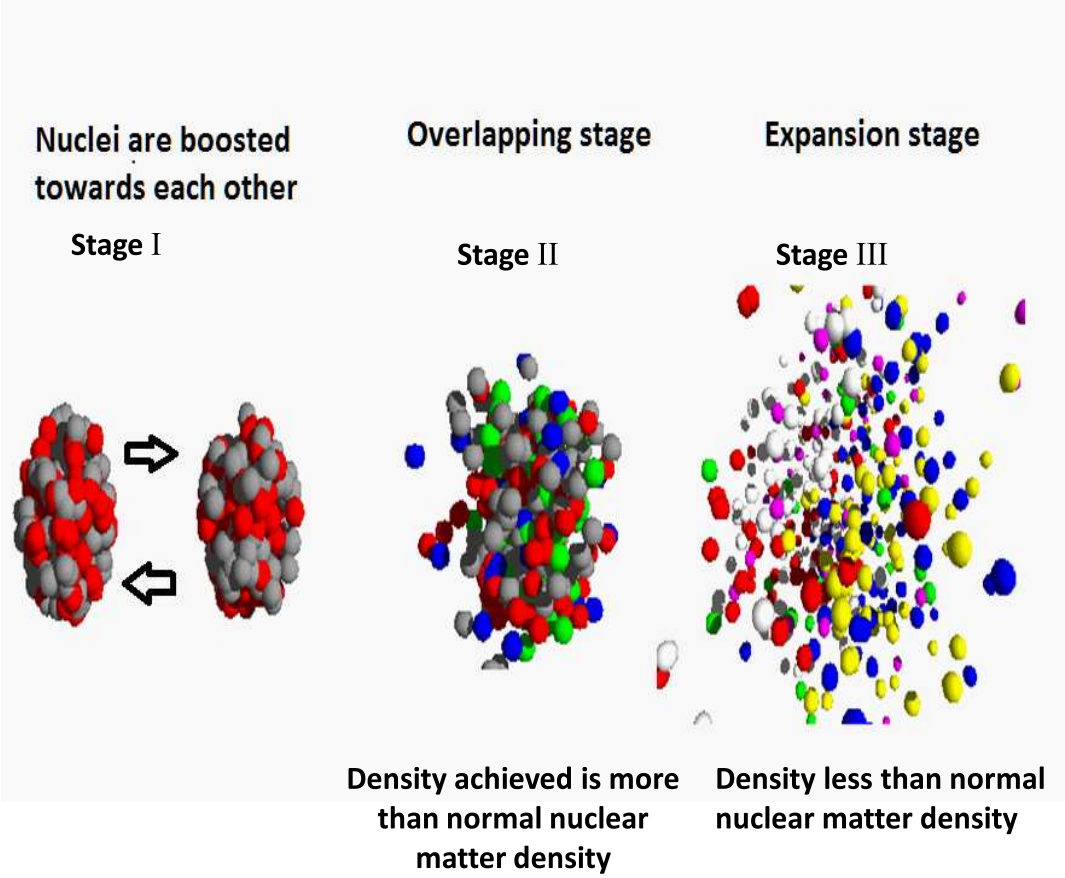

Figure 1.3: Different stages of nuclear collisions, resulting in density and phase changes of nuclear matter.

To have a more precise view of the role of symmetry energy, we display the overlapping and the dissociation stage during the nucleon-nucleon collisions in Fig. 1.3. The overlapping stage is best suited to understand the nuclear EOS where the density becomes few times the normal nuclear matter density. At the next stage, the density of the system decreases, and the phenomenon of fragmentation takes place. During the NN collisions, the strength of symmetry energy changes drastically at stage II and stage III, as shown in Fig. 1.3. Therefore the question arises about the exact parametrization of the density dependence of symmetry energy. The radii, moments of inertia, and the relative binding energies of neutron stars is highly sensitive to the behavior of the nuclear symmetry energy [6].

The stiff density dependence of symmetry energy causes the early emission of nucleons from the reaction zone. In case of the soft density dependence of symmetry energy,

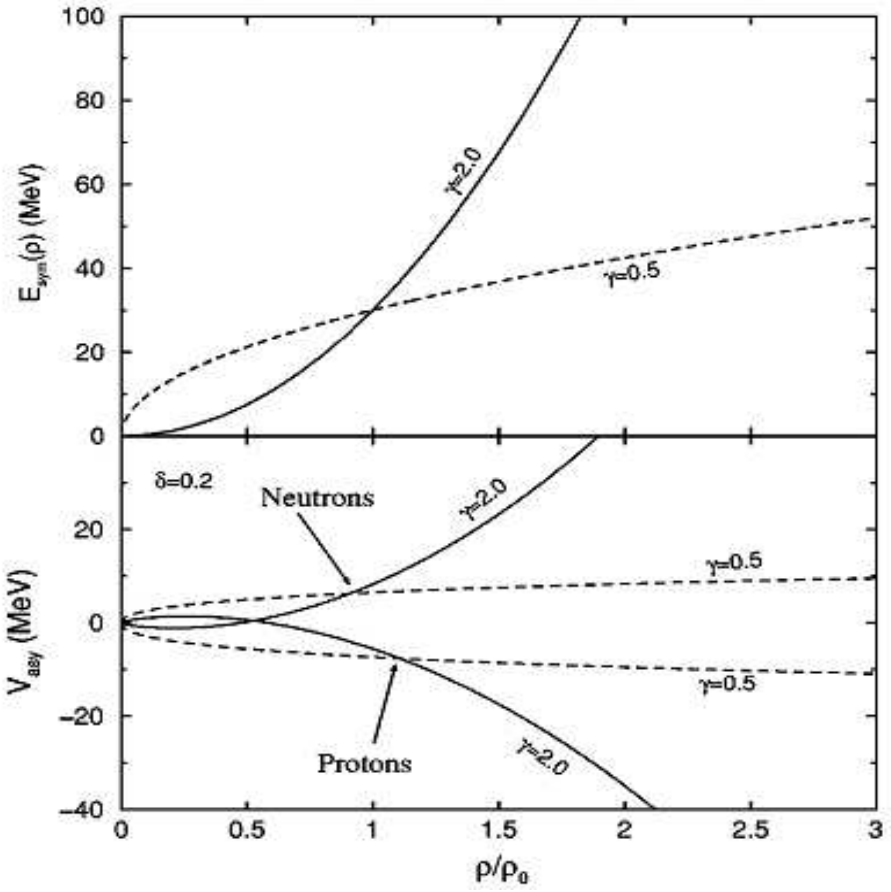

Figure 1.4: The symmetry energy (upper window) and symmetry potential (lower window) variation with the density of the system for an isospin asymmetry of $\delta = 0.2$ and the $\gamma = 0.5$ and 2, respectively. The Figure has been taken from [36].

the symmetry potential is highly repulsive (attractive) for neutrons (protons) in the low density region compared to the stiff dependence as shown in Fig. 1.4. This interesting observation has given new method to probe the symmetry energy strength via. light cluster production in HIC's [35, 36].

From Fig. 1.4, it is clear that the role of symmetry energy varies for the protons and neutrons for the different values of γ. The comparative study of ${}^{100}_{50}Sn + {}^{124}_{50}Sn$ and ${}^{100}_{30}Zn + {}^{124}_{50}Sn$ reactions at the incident energy of 30 MeV/nucleon and 40 MeV/nucleon proved that the neutron/proton ratio at mid rapidity is highly sensitive towards the symmetry energy at densities away from nuclear matter density [36]. At supra normal densities, the π^-/π^+ ratio is most sensitive to the density dependence of the symmetry energy at the incident energy of 400 MeV/nucleon [36]. However, exact form and strength

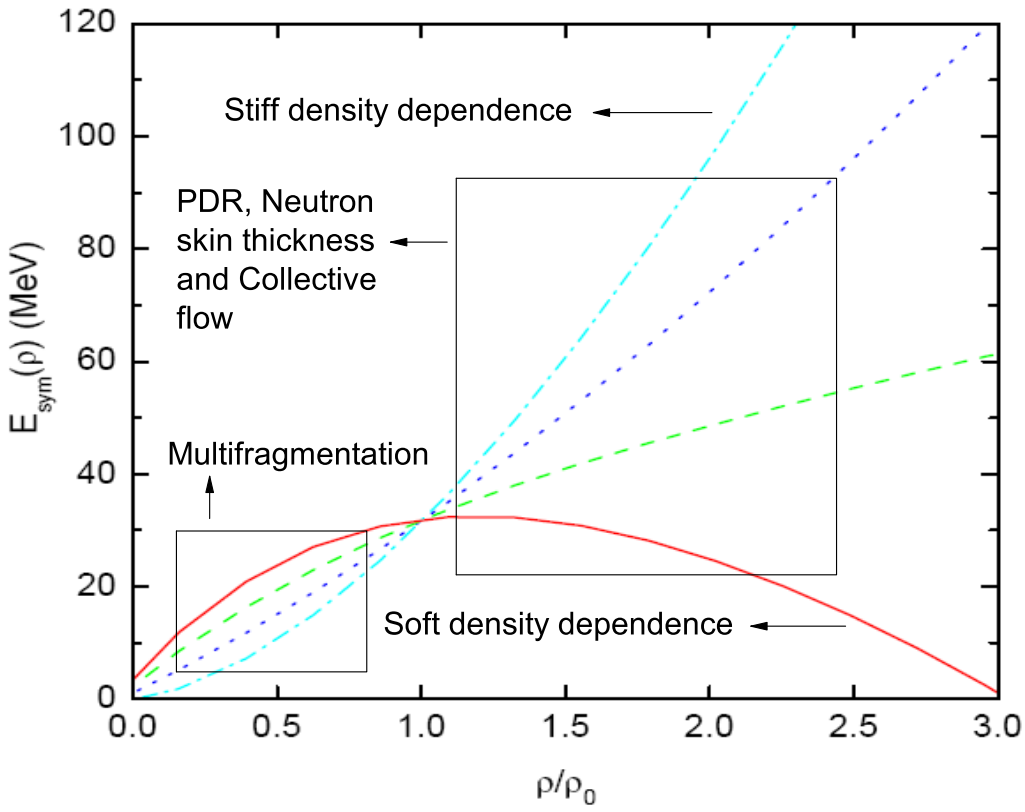

Figure 1.5: The stiff and soft density dependences of symmetry energy. The study of multi-fragmentation is much more suited to extract the behavior of symmetry energy at low densities. While symmetry energy behavior at supra-densities can be traced from the analysis of pygmy dipole resonance, neutron skin thickness and collective flow.

of the symmetry energy at sub-supra saturation densities is still an open question for the nuclear physics community. Fig. 1.5, shows that for soft density dependence, the strength of symmetry energy decreases above the normal nuclear matter density. However, in case of stiff density dependence, the symmetry energy tends to increase at supra-saturation densities.

The multifragmentation can yield an estimation for the strength of symmetry energy at sub-saturation densities as the fragment formation takes place when the highly excited and compressed nuclei tends to expand and the density becomes less than the normal nuclear matter density [26, 47], which is shown in Figure 1.5. A soft behavior of symmetry energy is predicted in the low density region. Indeed, the collective flow, pygmy dipole resonance (PDR) and neutron skin thickness are more suited to track the symmetry energy

behavior at high densities [6, 48, 49].

1.6 Attempts to understand the symmetry energy

From the last two decades, the density dependence of the symmetry energy is a topic of wide interest for the nuclear physics community. A large amount of work has been done on the density dependence of the symmetry energy. Though, the exact parametrization for the density dependence of the symmetry energy is still not available in the literature. Some fairly consistent constraints are available in the sub-saturation region.

Russotto *et al.* [49] studied the elliptical flow ratio of neutrons with respect to protons in reactions of neutron rich systems at relativistic energies. The results obtained from the *FOPI* Land data [50] for $^{197}_{79}Au + ^{197}_{79}Au$ collisions at 400 MeV/nucleon in comparison with the *UrQMD* model [51, 52] favor a moderately soft symmetry energy term with a density dependence of the potential term proportional to $(\rho/\rho_o)^\gamma$ with $\gamma = 0.9 \pm 0.4$ [49]. Chen *et al.* [53] determined the stiffness of nuclear symmetry energy from the degree of isospin diffusion in HIC's with the isospin-dependent Boltzmann-Uehling-Uhlenbeck *(IBUU04)* Transport model [30, 54]. At sub-normal densities, nuclear symmetry energy was found to be $E_{sym}(\rho) = 31.6\left(\frac{\rho}{\rho_0}\right)^{1.05}$, which was consistent with the *NSCL-MSU* data [32]. Shetty *et al.* [26] concluded that the $\gamma = 0.69$ (with $E_{sym} = 31.6\ MeV$) is among the best candidates to study the density dependent symmetry energy for theoretical calculations. This fact can be justified from the Fig. 1.6. This form of the density dependence of symmetry energy is also adopted by Heiselberg and Hjorth-Jensen in their study on neutron stars [37].

Li *et al.* [31] concluded that using the in-medium nucleon-nucleon cross sections, a symmetry energy of the form $E_{sym}(\rho) \approx 31.6\left(\frac{\rho}{\rho_0}\right)^{0.69}$ was found most acceptable when compared with the *MSU* isospin diffusion data [32]. Also, the soft behavior of symmetry energy is recommended at supra densities [33]. Li *et al.* [9] showed that the experimentally observed decrease of nuclear symmetry energy with increasing centrality or excitation energy in isotopic scaling analysis of heavy-ion reactions can be well understood analytically within a degenerate Fermi gas model. It was found that the density dependence of the nuclear symmetry energy affects significantly the nucleon emission time in these collisions, leading to larger values of two-nucleon correlation functions for a symmetry energy that

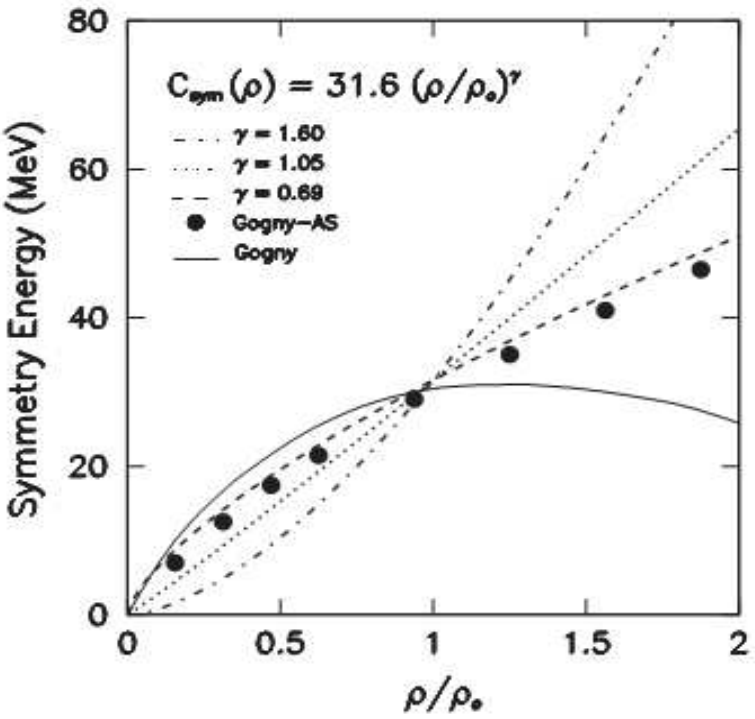

Figure 1.6: Various parameterizations of the density dependent symmetry energy used in the dynamical analysis measurements on iso-scaling data and the isospin diffusion measurements of *NSCL-MSU* [53]. The Figure has been taken from Ref. [26].

has a stronger density dependence. Two-nucleon correlation functions are signified as useful tools for extracting information about the nuclear symmetry energy from HIC's [55]. Yong *et al.* [56] studied the double neutron-proton differential transverse flow and termed it as a good probe for the high density behavior of nuclear symmetry energy.

Some studies predicted the symmetry energy to increase continously at all densities [45]. However, others [46] predicted that symmetry energy first increases to a certain value and then decreases at supra-saturation densities. The present situation clearly shows that the theoretical predictions on the symmetry energy at supra-saturation densities show extremely diverse results. To overcome this, one needs to have a qualitative observable which can help to understand whether the symmetry energy at high densities is soft or stiff. This has been done originally by comparing the n/p ratio of light and heavy, early

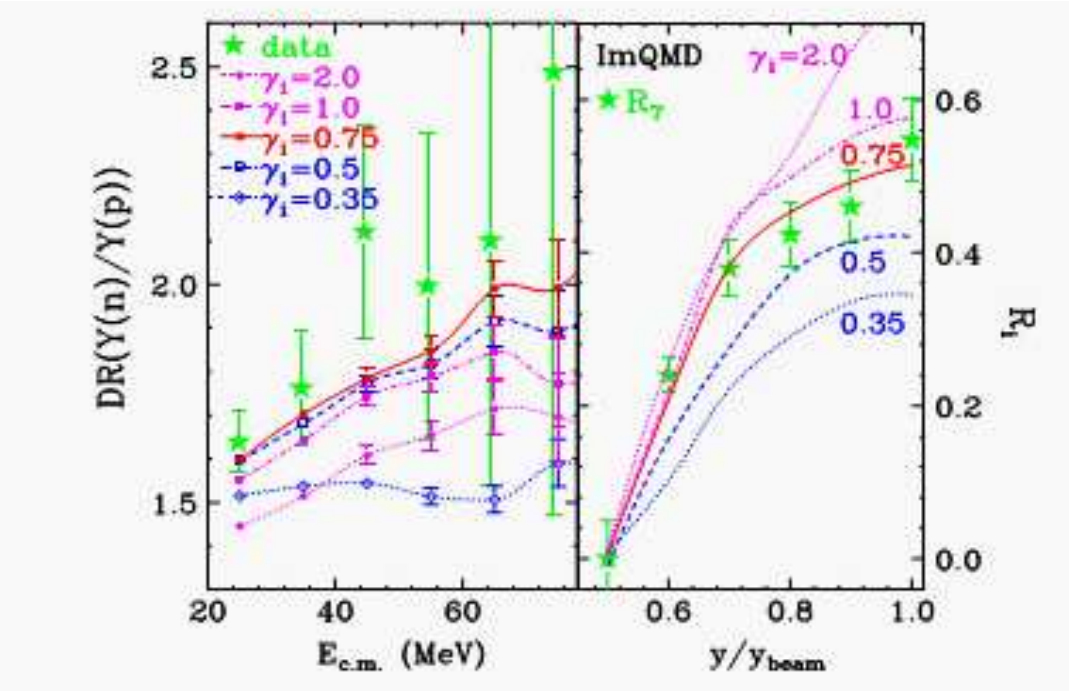

Figure 1.7: Left panel: comparison of experimental double neutron-proton ratios (star symbols), as a function of nucleon center of mass energy, to ImQMD calculations (lines) with different density dependences of the symmetry energy parameterized in terms of γ. Right panel: comparison of experimental isospin transport ratios obtained from the yield of A = 7 isotopes (star symbols), as a function of the beam rapidity, to the ratios from ImQMD calculations (lines) for b = 6 fm. The Figure is taken from [34].

emitted clusters from the reaction zone [57].

Lynch *et al.* [58] reported that the neutron rich and neutron deficient HIC's can provide constraints on the EOS of neutron rich nuclear matter at sub-saturation densities. Tsang *et al.* [34] made an attempt by applying the experimental constraints on the density dependence of symmetry energy at subsaturation density. Fig. 1.7, shows that $\gamma = 0.7$ is more compatible with the data as compared to other forms [34]. Various studies regarding the form of symmetry energy are described in Table 1.1.

The theoretical studies can provide an estimation for the behavior of symmetry energy at sub-supra saturation densities [18, 26, 37, 59]. The experimental results can provide an indirect information about the symmetry energy, through the observables related to the symmetry energy [27-30, 60]. To extract an exact form of the density dependence

Heiselberg *et al.* [37]	$32.0(\rho/\rho_0)^{0.60}$	Variational Calculation
Danielewicz *et al.* [15]	$31(33)(\rho/\rho_0)^{0.55(0.79)}$	BE, skin, isospin analog states
Tsang *et al.* [32]	$31(33)(\rho/\rho_0)^{2}$	Isospin diffusion
Chen *et al.* [53]	$31.6(\rho/\rho_0)^{1.05}$	Isospin diffusion
Li *et al.* [31]	$31.6(\rho/\rho_0)^{0.69}$	Isospin diffusion
Piekarewicz *et al.* [85]	$32.7(\rho/\rho_0)^{0.64}$	Giant resonances
Shetty *et al.* [26]	$31.6(\rho/\rho_0)^{0.69}$	Isotopic distribution
Famiano *et al.* [28]	$32.0(\rho/\rho_0)^{0.55}$	neutron-proton emission ratio
Tsang *et al.* [86]	$23.4(\rho/\rho_0)^{0.60}$	Isotopic distribution

Table 1.1: The various parameterized forms of the density dependence of the symmetry energy obtained from various independent studies. This table is taken from Ref. [26].

of symmetry energy, an international collaboration, consisting of an interdisciplinary, experimental and theoretical team of scientists, has been formed [61] to conduct a series of experiments at unique facilities based in the United States (the National Superconducting Cyclotron Laboratory *NSCL*) at Michigan State University, Japan (the Radioactive Ion Beam Factory at *RIKEN*) and *GSI*, Germany. As stated above, the situation at supra-saturation densities become much more complex. At *GSI*, experiments are being performed to explore the constraints on the symmetry energy especially at supra densities [25].

Tsang *et al.* [25] concluded that within the framework of quantum molecular dynamics *(QMD)* model it is possible to reproduce both isospin diffusion data and double ratio of neutron proton spectra data, which can be an important step to obtain the information about the symmetry energy in heavy-ion collisions. At the supra-saturation densities, the strength of symmetry energy can be estimated with the single and double ratios of neutrons to protons [30, 36, 62-67]. The single and double ratios of π^-/π^+, Σ^-/Σ^+, and K^-/K^+ are also useful probes for the density dependence of the symmetry energy [33, 68-72]. Overall, π^-/π^+ ratio [73] is considered as a powerful tool to extract the behavior of symmetry energy at higher densities.

Ma *et al.* [74] recently made an attempt to extract the symmetry energy from fragments in relativistic energy HIC's induced by ${}^{124,136}_{54}Xe$. Recently, S. Kumar *et al.* [47] showed that the results from isospin dependent quantum molecular dynamical *(IQMD)* model [22] for the dependence of the sum of the charge number for fragments with Z $\geq$ 2 (Z_{bound}) on the multiplicity of neutrons (M_n) from the projectile spectator fragmentation of ${}^{124}_{50}Sn$ and ${}^{124}_{54}La$ at 600 MeV/nucleon and their comparison with the data of

ALADIN-2000 Collaboration [75] suggested the soft symmetry energy. It was concluded that the Z_{bound} dependence of R(n/p) is most sensitive observable toward the symmetry energy [47]. Recently, the systematic study [76] within the framework of statistical multi-fragmentation [77, 78] model has been performed on the effect of secondary decay on the symmetry energy coefficient extracted by iso-scaling and the recently proposed isobaric yield ratio methods. The analysis includes the correlation between the input symmetry energy coefficients and the calculated ones from both primary and secondary fragment yields [76].

In present analysis, we explore the role of symmetry energy via. multifragmentation, nuclear stopping, and elliptical flow. These crucial observables are discussed in next sections.

1.7 Observables to study heavy-ion collisions

There are number of observables which can be used to pin down the dynamics of reactions at intermediate energies e.g., multifragmentation, fragment flow, stopping and sub-threshold particle production etc.. We shall brief them one by one.

1.7.1 Multifragmentation

The multifragmentation is an interesting process where one is interested to know the reason of this break up that whether it is a statistical process, making micro canonical phase space model a proper tool or it is driven by the fluctuations during the reaction [79-84]. The shattering of the colliding nuclei into pieces leads to the phenomenon of multifragmentation. After the collision, the nuclear matter undergoes a phase transition. The highly thermalized and concentrated nuclear matter gets condensed by the emission of large number of fragments. The fragments are classified on the basis of their size and termed as the free nucleons (FN's) [$A_f = 1$], light charged particles (LCP's) [$2 \leq A_f \leq 4$], medium mass fragments (MMF's) [$5 \leq A_f \leq 9$] as well as intermediate mass fragments (IMF's) ($5 \leq A_f \leq (A_f)_{tot}/6$). The size and multiplicity of the fragments is highly specific to the reaction conditions (i.e., incident energy, impact parameter, size of the colliding partners and reaction cross section etc.). At central collisions, more FN's and LCP's are produced due to the violent phase of the reaction. However, peripheral collisions enhance

the production of IMF's and heavy mass fragments (HMF's) [$5 \leq A_f \leq (A_f)_{tot}/3$]. In higher incident energies, the matter is subjected to large compression and the decompression stage is followed by the emission of light fragments (FN's and LCP's). The fragments produced are signified as a probe for the nuclear EOS and can provide excellent knowledge about the various microscopic features of the nuclear matter. The fragment production in HIC's can act as a probe for the behavior of symmetry energy at the sub-saturation density ($\rho < \rho_0$) because the phenomena of multifragmentation takes place during the dissociation phase when the density is below the normal nuclear matter density. Generally, soft density dependence of symmetry energy is recommended at these densities [62].

1.7.2 Experimental attempts to study multifragmentation

In the earlier time, the cosmic rays were assumed to be naturally accelerated beams, which led to the first experiment in 1930's, using cosmic radiation as projectiles and ionization chambers and Geiger counters as detectors [87]. In 1980's Jacobsson *et al.* [88] confirmed the multiple emission of IMF's in the emulsion irradiated by the carbon beam at the incident energy of 250 MeV/nucleon. Warwick *et al.* [89] concluded the fact that the multifragmentation is a dominant reaction channel if the incident energy is more than 35 MeV/nucleon. Further, Purdue group [90], stated that the phenomenon of multifragmentation evolves the mixed liquid gas phase transition of nuclear matter. At the time of fragmentation the density becomes less than the normal nuclear matter density. Experimental facility provided the first ever evidence for the formation of compressed nuclear matter in 1984 at Berkeley lab in California. This was also the first ever milestone in the search of QGP. The first accelerator to study multifragmentation was BEVALAC accelerator at Lawrence Berkeley Laboratory in California.

EOS Collaboration at Berkeley investigated the crucial parameters like symmetry energy, volume energy, and surface energy [91]. After this attempt, the Grand Accelerateur National D'ions Lourds *(GANIL) (France)*, the Relativistic Heavy-Ion Collider *(RHIC) (USA)*, the Superconducting SuperCollider *(SSC)* at *BNL (USA)*, the *NSF-Arizon* accelerator at the university of *Arizona (USA)*, the *Vivitron* Accelerator in *Strasbourg (France)*, the Superconducting Cyclotron *(SC)* at *Texas (USA)*, the Superconduct-

ing Cyclotron *(SC)* with the *CHIMERA* detector at Laboratori Nazionali del Sud *INFN, Catania (Italy)* and the Heavy-ion Synchrotron *SIS* accelerator at *GSI (Germany)* etc. have made good progress to understand the fragmentation. In the present times, these accelerators has been upgraded to study the isospin dependent part of the nuclear EOS. The facilities at Dubna, Brookhaven, and CERN have made possible to have a beam of ultra-relativistic energies. The Emulsion experiment [88, 92] was considered as the initial attempt to have a first hand information of the multifragmentation. They provided a unique possibility to study the fusion, multi-fragmentation which includes the mixed liquid-gas phase transition as well as vaporization at intermediate energies.

The *Berkeley* group studied the asymmetric reactions for the incident energy between 50 and 110 MeV/nucleon [93-96], with an aim to investigate the role of entrance-channel mass asymmetry reaction dynamics. The emphasis was on the different parameters like excitation energy, angular distribution, cross section as well as velocity distribution. The aim of the *EOS* collaboration at *BEVALAC* was to study phase transition in nuclear matter through the process of multifragmentation. Various critical exponents like surface energy, volume energy, symmetry energy, entropy etc. [91] are extracted using asymmetric reactions. Also, similar exponents were calculated for symmetric reactions of $^{197}_{79}Au + ^{197}_{79}Au$ [97].

The main focus of the *National Superconducting Cyclotron Laboratory (NSCL)* of *Michigan State University (MSU)* has been to study the asymmetric reactions like $^{129}_{54}Xe + ^{12}_{6}C$, $^{27}_{13}Al$, $^{51}_{23}V$, $^{64}_{29}Cu$, $^{89}_{39}Y$ (50 MeV/nucleon), $^{36}_{18}Ar + ^{197}_{79}Au$, $^{129}_{54}Xe + ^{197}_{79}Au$ (50-110 MeV/nucleon), $^{40}_{18}Ar + ^{64}_{29}Cu$, $^{108}_{47}Ag$, $^{197}_{79}Au$ (at 17-115 MeV/nucleon) [98, 99, 100]. The major emphasis of the *Superconducting Cyclotron* of the Laboratori Nationali del Sud of *INFN (Italy)* is to explore the facts about symmetric reactions. The reactions of $^{93}_{41}Nb + ^{93}_{41}Nb$ (at 17, 23, 30 and 38 MeV/nucleon) and $^{116}_{50}Sn + ^{116}_{50}Sn$ (at 29.6, 38 MeV/nucleon) [101] has been studied. The study includes the multiplicity of LCP's and IMF's in peripheral and semi-peripheral collisions as a function of excitation energy of emitting source, mass of the system and beam energy [101]. Recently *Isospin collaboration* at *INFN (Italy)* studied the isospin effects for neutron-rich $^{124}_{50}Sn + ^{64}_{28}Ni$ and neutron-deficient $^{112}_{50}Sn + ^{68}_{28}Ni$ systems for non-central collisions at 35 MeV/nucleon [102].

The *FOPI* and *ALADIN* groups at GSI did perform a study on multifragmentation

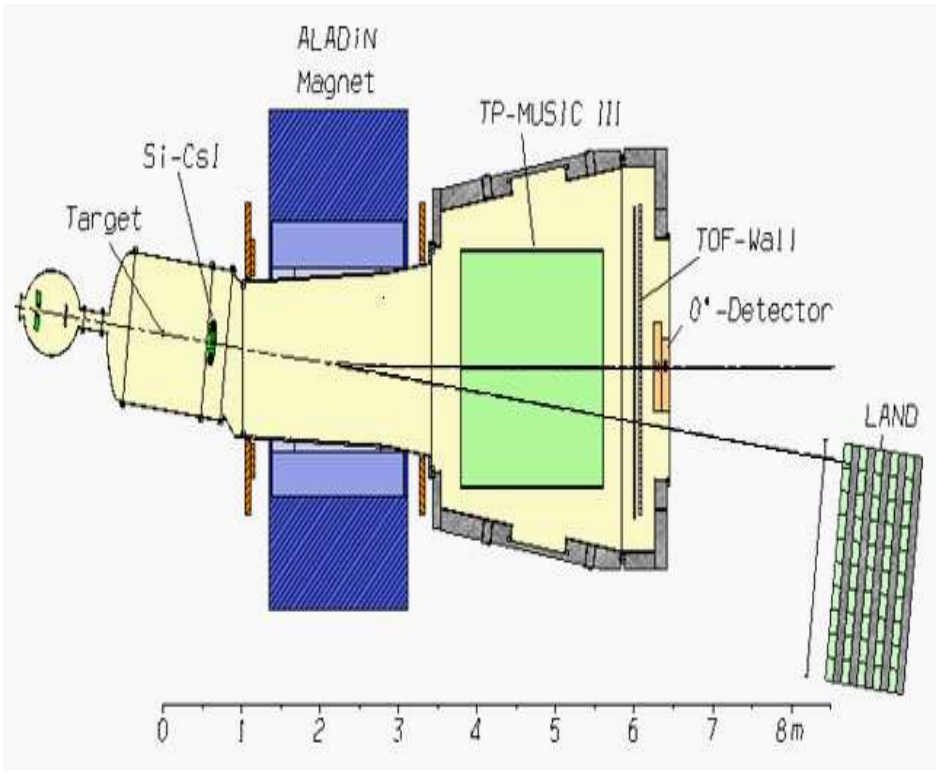

Figure 1.8: The ALADIN detector set up. The Figure has been taken from Ref. [109, 110].

over a wide range of masses with incident energies ranging from 100 to 1000 MeV/nucleon [78, 82, 103-108]. For the better understanding, the picture of *ALADIN* detector set up is shown in Fig. 1.8. Experimental observations shed light on the particle evaporation to multi fragment emission and at last total disassembly and shattering of the nuclear matter after the reaction. One of the most interesting phenomenon of rise and fall in multifragmentation is also reported by *ALADIN collaboration* for the reaction of $^{197}_{79}Au + ^{197}_{79}Au$ [78, 82, 103-106]. It was concluded that the fragment multiplicities and correlations obey the universal behavior [78, 82, 103-106]. Secondary beams has extended the domain of the study to isospin plane [111, 112].

The *NIMROD* collaboration at *TAMU* focuses on the reaction dynamics in Fermi energy domain of the HIC's [113-116]. An extensive analysis of the critical behavior in the disassembly of nuclei with $A \approx 36$ has been carried out [113]. The multiplicity and charge distribution, energy and velocity spectra has been observed for the reactions

of $^{64}_{30}Zn$ + $^{58}_{28}Ni$ (26 MeV/nucleon), $^{197}_{79}Au$ (at 47 MeV/nucleon), $^{92}_{42}Mo$ (at 35 and 47 MeV/nucleon), $^{40}_{18}Ar$ + $^{112}_{50}Sn$ (40 MeV/nucleon) and $^{27}_{13}Al$ + $^{124}_{50}Sn$ (at 55 MeV/nucleon) collisions [114]. The study of EOS for isospin asymmetric nuclear matter [117] has also been carried out by this collaboration. An extensive analysis for the observables such as symmetry energy, isotropic and isobaric yield ratio, average n/p ratio for the reactions of $^{124}_{50}Sn$ + $^{124}_{50}Sn$, $^{124}_{54}Xe$ + $^{124}_{50}Sn$, $^{112}_{50}Sn$ + $^{112}_{50}Sn$ at 28 MeV/nucleon has been performed [115, 117]. These properties are also studied by using different beams with projectiles $^{40}_{18}Ar$, $^{40}_{20}Ca$, $^{58}_{26}Fe$ and $^{58}_{28}Ni$ on $^{58}_{26}Fe$ and $^{58}_{28}Ni$ targets at 25, 30, 33, 40, 45, 47 and 53 MeV/nucleon [26, 117]. These findings showed that the isotopic distribution of the hot primary fragments are found to vary over a wide range and extend towards the neutron drip line. For the iso-scaling observables, the comparison of dynamical [118, 119] and statistical model yields [77, 78] consistent results, provided the sequential decay effect in dynamical model is small. Recently, this group has studied the mass dependence of the nuclear caloric curve [116].

The, *INDRA* group at *GANIL (France)* has also made significant advancements in the area of multifragmentation. This group mainly emphasize on the system size effects, the role of system size in entrance channel as well as Coulomb instabilities, kinetic energy spectra and fragment velocity correlation in case of nearly asymmetric reactions of $^{36}_{18}Ar + ^{58}_{28}Ni$, $^{155}_{64}Gd + ^{238}_{92}U$ and $^{129}_{54}Xe + ^{nat}Sn$ (at 30-95 MeV/nucleon), $^{58}_{28}Ni + ^{58}_{28}Ni$ (32-90 MeV/nucleon), $^{208}_{82}Pb$ + $^{197}_{79}Au$ (at 29 MeV/nucleon) and $^{36}_{18}Ar$ + KCl [83, 120, 121]. Also the entrance channel effects on the asymmetric reactions in the mass range 58 to 181 has been studied for the beam energy between 24 to 90 MeV/nucleon [122]. On the other hand, this group has also studied the symmetric reaction of $^{197}_{79}Au$ + $^{197}_{79}Au$ for the excitation energy between 40 and 150 MeV/nucleon [123]. It is concluded that the shattering of the projectile into pieces results in the formation of fragments and the phenomenon is termed as multifragmentation [124]. The collaborative work of *ALADIN-INDRA* studied the bimodal behavior of heaviest fragment distribution in the projectile fragmentation [125]. In the recent findings, it has been observed that the isospin effect has a significant role at semi-peripheral collisions for the reaction $^{58}_{28}Ni$ + $^{197}_{79}Au$ at intermediate energies [29].

1.7.3 Collective flow

The study of collective flow has contributed a lot towards the study of HIC's in the intermediate energy regime. It gives a deep insight into the thermodynamical state variables during heavy-ion collisions. Collective flow is directly related to the amount of compression generated during the overlapping of target and projectile. Information of collective flow yields essential facts about the isospin dependence of the nuclear EOS.

At earlier stages, only the matter flowing along the reaction plane in the sideward direction was observed due to pressure gradient produced in NN collisions. Later on, it was observed that the nuclear matter is squeezed out in a direction perpendicular to the reaction plane termed as elliptical flow. The study of specific processes such as collective flow provides us a clear physical knowledge of the nuclear matter which is released in decompression stage of the hot and dense highly interacting nuclear matter. The collective flow indicates the presence of strong multipole interactions between the nucleons and fragments created after the collision. The experimental analysis provided the evidence for the presence of anisotropic flow, which is the anisotropic distribution of particles in momentum space. The interactions at low incident energy leads to the negative value of directed flow. These interactions turns repulsive at higher incident energies making directed or in-plane flow positive.

After the collision phase, the nuclear matter flow is classified in terms of radial flow, directed flow and elliptical flow. The generation of radial flow is more in central collisions and is characterized by increased yields in the kinetic energy spectra of particles emitted near $\theta_{c.m.} = 90^o$ relative to the beam axis. The directed flow is highly sensitive towards the colliding geometry, and is maximum for semi-central collisions. It diminishes in case of central collisions, due to symmetry, and for very peripheral collisions due to the lack of a sizable pressure gradient [126]. The elliptical flow is basically the out-of plane or squeezed out flow of the nuclear matter. It increases with the asymmetry of the colliding nuclei which is achieved in the peripheral collisions. The ellipsoidal or almond type distribution of the nuclear matter after the collision signify the elliptical flow. The elliptical flow is generated from the participant zone, and can yield a better picture of the collective flow than the directed flow, which is the bounce-off of nuclear matter around the reaction zone and is constrained only in the reaction plane. At a particular incident energy (transition

energy), the elliptical flow vanishes in the mid-rapidity zone (or core participant region). This energy is termed as transition energy (E_{Trans}). This particular incident energy refers to the counter balancing of the shadowing of the spectator matter by the expansion of highly compressed participant matter.

While the phenomenon of multifragmentation takes place at sub-saturation densities. The collective flow reflects the intense pressure created very early in the reaction. It is considered as a good probe for the density dependence of nuclear symmetry energy at supra-densities [63, 127].

1.7.4 Experimental attempts to study collective flow

The flow generated after the collision is highly specific to the pressure gradients. That is why, the quantitative study of flow observables reveals the aspects of the nuclear EOS. The collective flow is one of the major observables which is highly sensitive to the isospin content of the system. By now, it is evident, that the collective flow, especially the elliptical one, is actually the squeezed out nuclear matter, generated from the participant zone. It can provide unique information regarding the high density behavior of the symmetry energy as compared to the directed flow, which is the bounce-off of the compressed matter in the reaction plane. The parameter elliptical flow (or out-of-plane flow) is best suited to predict the picture of the dynamics involved in the reaction.

Theoretically, the concept of elliptical flow was given by Stöcker *et al.* [128] in 1982 in terms of mid rapidity emission perpendicular to the "reaction plane". The angular distribution of protons emitted from near-central collisions in a Fluid-dynamics model led to the first ever observation for the existence of elliptical flow. They attributed that the out-of-plane emission to the fact that the compressed matter (participant matter) emitted perpendicular in the reaction plane is hindered or blocked by "spectator" matter. The out-of-plane flow (or squeeze-out flow) was first observed in 1989 at nearly the same time by two competing collaborations. The *Diogene collaboration* at the Saturne synchrotron in Saclay observed slight peaks in the azimuthal distribution of particles at mid-rapidity in 800 MeV/nucleon Ne induced reactions [129]. The *Plastic Ball group* at the Bevalac in Berkeley observed out-of-plane emission in ${}^{197}_{79}Au + {}^{197}_{79}Au$ collisions at 400 MeV/nucleon [130, 131].

The *BEVALAC* group also characterize the squeeze-out as a function of projectile energy, mass as well as the rapidity dependence by using a novel ratio of out-of-plane/in-plane emission [130, 131]. The transition from the in-plane to out-of-plane emission was first observed using the $^{64}_{30}Zn + {}^{58}_{28}Ni$ reaction at *GANIL* facility by the *NAUTILUS* collaboration in 1994 [132]. The energy of transition increases with impact parameter. Moreover, the *MINIBALL/ALADIN* collaboration observed the onset of out-of-plane emission (GSI) in $^{197}_{79}Au + {}^{197}_{79}Au$ collisions at 100 MeV/nucleon [133], where out-of-plane emission is observed for central collisions, while peripheral collisions clearly show in-plane emission.

The *NSCL* at MSU (USA) has made an in-depth analysis of the disappearance of elliptical flow for the symmetric system $^{197}_{79}Au + {}^{197}_{79}Au$ in the incident energy range from 500 MeV/nucleon to 11 GeV/nucleon [134, 135]. It was found that the elliptical flow shows a transition from negative to positive at a beam energy, E $\approx$ 4 GeV/nucleon. Later on, the investigation of the elliptical flow at $\sqrt{s_{NN}} =$ 130 & 200 GeV [136] was done by *NSCL* in collaboration with *STAR*. They show the pseudo rapidity, transverse momentum dependence and centrality dependence of the elliptical flow. In a recent study, the elliptical flow and nuclear stopping are signified as a tool to determine NN cross section in HIC's at intermediate energies [137].

Other collaborations: *FOPI, ALADIN* at *GSI*, and *INDRA* at *GANIL* performed a systematic investigation on the transition of elliptical flow and demonstrated the in-plane to out-of-plane transition of different kind of fragments in intermediate energy HIC's [50, 138-141]. Particularly, the reaction of $^{197}_{79}Au + {}^{197}_{79}Au$ is studied in the energy range of 40 to 800 MeV/nucleon, which showed that the transition of in-plane to out-of-plane is observed around 100 MeV/nucleon. The *FOPI* collaboration has successfully reported the correlation between global stopping and flow [142] as well as with the cluster formation during expansion stage [143].

For further analysis, the systems studied were: $^{40}_{20}Ca + {}^{40}_{20}Ca$ (at 0.4, 0.6, 0.8, 1.0, 1.5, 1.93 GeV/nucleon), $^{58}_{28}Ni + {}^{58}_{28}Ni$ (at 0.09, 0.15, 0.25, 0.4 GeV/nucleon), $^{96}_{44}Ru + {}^{96}_{44}Ru$ (at 0.4, 1.5 GeV/nucleon), $^{129}_{54}Xe + {}^{133}_{55}Cs$, $^{127}_{53}I$ (at 0.15, 0.25, 0.4 GeV/nucleon) and $^{197}_{79}Au + {}^{197}_{79}Au$ (at 0.09, 0.12, 0.15, 0.25, 0.4, 0.6, 0.8, 1.0, 1.2, 1.5 GeV/nucleon). The relation between stopping and flow is also presented by the *INDRA* and *ALADIN* groups

[144]. The *FOPI* collaboration reported new methodology for the analysis of anisotropic flow with various methods like the event plane reconstruction, on Lee-Jang Zeros and on multi-particle cumulants [145].

INDRA and ALADIN collaborations investigated the flow analysis for the set of reactions $^{124,129}_{54}Xe$ and $^{112,124}_{50}Sn$ (at 100 and 150 MeV/nucleon) [146]. The directed and elliptical flow as a function of centrality and transverse momentum dependence are analyzed for isotropically selected reaction products ($Z \leq 3$). Recently, J. Y. Ollitrault and co-workers [147] showed that the estimates of elliptical flow are influenced by the flow fluctuations and non-flow effects.

1.7.5 Nuclear stopping

Nuclear stopping is also one of the more pronounced phenomenon in the heavy-ion collisions. The nuclear stopping has gained a lot of interest because it provides the possibility of examining the degree of thermalization or equilibration reached in the matter. The parameter nuclear stopping is associated to the amount of energy dissipated, the amplitude of large collective motion and can shed light on the various other mechanisms [148]. The degree of stopping however, may vary drastically with incident energies, mass of colliding nuclei and colliding geometry. The central collisions result in larger stopping of the projectile by the target. Indeed, the peripheral collisions leads to lesser stopping due to smaller participant zone.

1.7.6 Experimental attempts to study nuclear stopping

The term nuclear stopping can be viewed as a measure of the degree to which the energy of the relative motion of the two colliding nuclei is transformed into other degrees of freedom [149]. Experimentally, the *FOPI* Collaboration [142] studied the nuclear stopping for the systems $^{40}_{20}Ca + ^{40}_{20}Ca$, $^{58}_{28}Ni + ^{58}_{28}Ni$, $^{96}_{44}Ru + ^{96}_{44}Ru$, $^{129}_{54}Xe + CsI$ and $^{197}_{79}Au + ^{197}_{79}Au$ at incident energies ranging from 90 MeV/nucleon - 1.93 GeV/nucleon. The latest study in the case of global nuclear stopping is performed by Lehaut *et al.* [148] in central collisions at intermediate energies by analyzing the kinematically complete events recorded with the help of 4π multi-detector *INDRA* for a large variety of symmetric and asymmetric reactions such as $^{197}_{79}Au + ^{197}_{79}Au$, $^{129}_{54}Xe + ^{118}_{50}Sn$, $^{58}_{28}Ni + ^{58}_{28}Ni$ etc. Nuclear stopping was reported to be highly sensitive towards the isospin dependence of the in-medium NN

cross section [148]. It was found that the behavior of anisotropy ratio (global stopping) shows a rapid decrease as a function of the incident energy upto 400 MeV/nucleon.

1.8 Theoretical approaches

Theoretical attempts to study the multifragmentation provide an opportunity to determine the strength of symmetry energy in the sub-saturation region ($\rho < \rho_0$). The low density region is associated to the complete dissociation and expansion of the participant and spectator matter. On the other hand, collective flow has the ability to shed light on the form and strength of the symmetry energy at supra-saturation densities ($\rho > \rho_0$), which is also discussed in sections above. It has been concluded that the ratio of neutrons to protons or charged particles in case of the neutron rich systems is highly sensitive to the form and strength of symmetry energy at supra-normal densities [49]. The best method to extract knowledge from the experimental observables is to compare them with the theoretical descriptions of HIC's utilizing different physical scenarios as input.

As far as the theoretical understanding/modelling of intermediate energy HIC's is concerned, we have to consider the complex reaction dynamics involved during the collisions. The most important point to remember is that the HIC's involves very complicated non-equilibrium physics. That is why, the numerical modeling in HIC's is not so straight forward. It is worth mentioning that the whole reaction dynamics at low incident energies is governed by the mutual two and three body interactions. At low incident energies, due to the lack of free space, 98 % of the attempted collisions are blocked. On the contrary, the availability of large phase space at relativistic energies makes the Pauli blocking very small (approximately 4 % of collisions are blocked) and hence the Cascade picture dominates the reaction dynamics. At intermediate energies, both cascade and mean field picture govern the reaction dynamics. These conditions offer the possibility to study the properties of nuclear matter in the symmetric nuclear matter and pure neutron matter.

Both nuclei which are cold before the collision, results in an abrupt rise of temperature and entropy during the collision stage. During the disassembly stage, the temperature and density fall to a value where the constituents are no longer interacting. This density is called freeze-out density. In case of microscopic models, one may follow the evolution upto asymptotic times and the concept of freeze-out density is no longer required. The

study of HIC's in the intermediate energy regime mainly involves two types of approaches (statistical and dynamical models) which are discussed below in detail.

1.8.1 Statistical models

The statistical models [77, 150] basically concentrate on the final break-up, and neglects the dynamics of the reaction. Some of the statistical models are based on the droplet description of a nucleus, while the other ones are based on the percolation theory. Statistical models include multi-particle phase space models, such as the *Statistical Multi-fragmentation Model (SMM)* [77, 150-152] and the *Berlin Multi-fragmentation Model* [153], which can incorporate specific nuclear properties directly. Accordingly, *a semi- micro canonical version of SMM* [151, 152] that incorporates detailed nuclear structure information relevant to the population and secondary decay of the excited fragments was developed [154]. Additional static models include *Percolation* [155], *Lattice Gas Approach* [156] and the *Expanding Emitting Source (EES) model* [157]. These approaches have the virtue of providing relatively simple schematic algorithms suitable for the exploration of critical phenomena in finite systems.

The utility of dynamical models is justified with the incapability of the statistical models to explore the dynamics involved in heavy-ion collisions. The major limitations of the statistical models are given below:

1. The situation at the start of reaction is based on some assumption for the degree of thermalization [151, 152].

2. Also, the statistical models give a better description only for the later/final stage of the reaction.

To study the time evolution of the reaction one needs dynamical models.

1.8.2 Dynamical models

The dynamical models, follow the reaction from two well separated nuclei to the final state where the matter is separated, fragmented and cold. The dynamical approaches such as the Time Dependent Hartree Fock *(TDHF)* [21, 158] or its semi-classical version called *Vlasov equation* (in phase space) [159-161] are suitable at low incident energies where the probability of nucleon-nucleon collisions are almost negligible. However, for a suitable and reasonable approach which can explain the physics of intermediate energy HIC's,

the nucleon-nucleon scattering and the mean field should be given an equal weightage. Some attempts were made in the literature to extend the *TDHF* theory to take care of the residual NN interactions, which are responsible for the two-body collisions. This was dubbed as *Extended Time dependent Hartree-Fock (ETDHF)* theory [162]. However, its numerical implementation prohibited its use for the large scale investigation of heavy-ion collisions.

In the first attempt, semi-classical version of *ETDHF* theory i.e. *Vlasov equation* [159, 160] was coupled with NN collisions and thus, a new realization, *named as Boltzmann -Uehling - Uhlenbeck (BUU) equation*, was developed. In *BUU*, one body distribution function is described as a collection of NA test particles, where A is the mass number and N is event number with no division of test particles. All possible collisions between the test particles are considered. Therefore, it becomes evident, that parallel runs communicate with each other. As a result, event by event correlation cannot be analyzed. However, Bonasera *et al.* [163] solved the collision integral using the concept of mean free path. Under this methodology, N parallel events are performed and the average physical values of various quantities are calculated over large number of events. In such case, N parallel runs do not communicate with each other and event by event correlations are preserved.

Keeping in mind the requirement of the intermediate energy region, one would like to have those methods where correlations and fluctuations among nucleons are preserved. The *Classical Molecular Dynamics (CMD)* [164, 165] approach (or the equation of motion), in principle, is capable of predicting the production of fragments. It also incorporates the complete classical N-body dynamics which is necessary to describe the formation of the fragments. The simple Classical Molecular Dynamics, however, needs major refinements (including quantum features). The quantum features play a very important role at low incident energies. The above approach was later extended to incorporate the quantum features by Aichelin and Stöcker [21, 166, 167]. This new approach, which explicitly incorporates the N-body correlations as well as nuclear matter equation of state and important quantum features (like the Pauli principle, Stochastic scattering and particle production), was dubbed as *Quantum Molecular Dynamics (QMD)* Model [166-175].

To extract the information about the EOS of neutron-rich matter, especially the density dependence of the nuclear symmetry energy, from heavy-ion reactions induced by

neutron rich (stable and/or radioactive) beams, one needs reliable theoretical tools. For this purpose, one must have transport models that include explicitly the isospin degree of freedom and thus the isospin-dependent physical quantities such as the iso-vector (symmetry) potential and isospin-dependent in-medium nucleon-nucleon (NN) cross sections and Pauli-blocking. As stated above, the semi-classical models include mainly the two types: the *BUU* and the *QMD* model. With the development of radioactive ion-beam physics, several rather comprehensive isospin-dependent, but mostly semi-classical transport model such as *IBUU* [23, 24], *SMF* [176] and *IQMD* [22] have been successfully developed in recent years to describe nuclear reactions induced by neutron-rich nuclei at intermediate energies.

The *isospin- dependent Boltzmann-Uehling-Uhlenbeck (IBUU)* transport model has the ability to explain several isospin dependent phenomena's successfully in HIC's at intermediate energies [23, 24]. In this model, isospin dependence was included in the dynamics by using isospin-dependent cross section and Pauli blocking factors, the symmetry potential $V^{sym}(\rho, \delta)$, and Coulomb potential. This model was used to calculate the ratio of yield of neutrons and protons in pre-equilibrium emission [63]. The *BUU* equation provides an accurate description of the time dependence of the one body distribution function. Accurate solution of the *BUU* equation average away fluctuations in the density that might lead to the formation of fragments in an individual collision. This is usually achieved by solving the *BUU* equation with a large number of test particles per nucleon N_{test}. In *BUU* equation, the density fluctuations that lead to the fragment production are suppressed, that is why, the calculation of fragment yield is not feasible via., *BUU* model. To overcome these drawbacks, alternate models such as, *Stochastic Mean Field (SMF)* model [176] and *Isospin dependent Quantum Molecular Dynamics (IQMD)* model has been developed to address the density fluctuations.

The *SMF*, like *IBUU*, has also tendency to describe the time evolution of the collision using self-consistent mean field. The application of the *SMF* model to the unstable situations relies on the knowledge of the most important unstable modes, which may be difficult to identify in case where the modes are not known a priori. The *IQMD* model [22] treats different charged states of nucleons, deltas and pions explicitly, as inherited from the *VUU* model [161]. The isospin degree of freedom enters into calculations via.

symmetry potential and cross section [161, 177-179]. This model is proven successful to study the isospin effects in HIC's at intermediate energies. The model incorporate the N-body correlations, reduces the fluctuations to minimum extent, explains the nuclear EOS and includes the many quantum features like Pauli blocking, Stochastic scattering, particle production etc..

All these dynamical models can follow the time evolution of nucleons only. These models are termed as "primary model" which generate the phase-space of nucleons. After this, the major question is how to construct a procedure to define the clusters. For this we need the algorithms which are termed as "secondary models". In a very simple picture, nucleons are connected to a cluster using space correlation method. This method identifies the two nucleons in the same fragment if their centroids are less than some distance [180-183]. This method is known as *Minimum Spanning Tree (MST)* method. Till today, it is one of the most extensively used methods. Several refinements to this method have been proposed including momentum cut and binding energy cuts [184].

As discussed in the above paragraphs, we have several theoretical models that are available to study the HIC's at intermediate energies. We shall study the phenomena of multifragmentation, elliptical flow and nuclear stopping using *IQMD* model and then analyze the output by secondary models *MST* and *MSTM* [185, 186].

The thesis is organized as follows:

In chapter 2, we will describe the methodology of various models in brief, *QMD*, and *IQMD* will be discussed in detail. Also, we shall discuss the secondary approaches (algorithms) such as *MST* and *MST(M)*, which are used to clusterize the phase space obtained from primary models.

In chapter 3, it will be shown that there is no typical structure of fragmentation at the transition energies of various fragments (energy that depends on the participant expansion and shadowing of the spectator matter) [187].

In chapter 4, we shall study the influence of density dependent symmetry energy and momentum dependent interactions (MDI) on the multifragmentation. We performed a theoretical study for the percentage change in the multiplicity of fragments i.e., free nucleons, light charged particles for the different forms of density dependence of symmetry energy. We also analyzed the collective effect of density dependent symmetry energy and momentum dependent interactions (MDI) on the intermediate mass fragment production and comparison has been made with the *ALADIN* data. We shall discuss the excitation energy and colliding geometry dependence of the mean IMF multiplicity which was more compatible with the *ALADIN* data [82, 100] with the inclusion of density dependence of symmetry energy and MDI citekaran1.

In chapter 5, we concentrate on the exploration of the various aspects of elliptical flow associated with various fragments via density dependent symmetry energy. Here, we elaborate our study with the comparative analysis of elliptical flow associated to protons and neutrons with momentum dependent EOS and isospin dependent NN cross section. The elliptical flow tends to become zero at a particular incident energy termed as the transition energy. At transition energy, the shadowing of spectator matter is balanced by the expanding and heated nuclear matter originated from the participant zone. The elliptical flow of light and heavy fragments as a function of transverse momentum and incident energy shows significant variation with the stiffness/strength of symmetry energy.

The momentum dependent equation of state and isospin dependent NN cross section have a significant impact on the elliptical flow. The comparison of theoretical results shows a good agreement with the experimental findings of *INDRA, FOPI* and *PLASTIC BALL* collaborations with density dependent symmetry energy for $\gamma = 0.66$ [189].

The nuclear stopping and temperature reached in HIC's have been studied many times in the literature. **In chapter 6**, we have described the role of density dependence of symmetry energy on nuclear stopping and reaction dynamics (density and temperature). The time evolution, system mass dependence and excitation energy dependence of nuclear stopping is studied when subjected to different forms of density dependence of symmetry energy ($\gamma = 0.66$, 1.33, 2). To have a proper understanding of nuclear stopping, we studied the nuclear stopping for neutrons and protons for various systems having different isotopic content. We shall also discuss the global nuclear stopping (anisotropy ratio) for the different rapidity zones. We shall describe the time evolution, system mass, colliding geometry and excitation energy dependence of the nuclear stopping subjected to the different types and sizes of rapidity bins. Moreover, for a better understanding of the nuclear stopping we elaborate our findings for the excitation energy dependence of global stopping for the various rapidity bins and compared the theoretical predictions with the data of *INDRA* and *ALADIN* Collaboration [190].

Also, we have tried to correlate the temperature reached during NN collisions with nuclear stopping, which is itself an indicator of the thermalization of the nuclear matter. We shall show the effect of density dependent symmetry energy on the maximum/average density and temperature reached in a reaction. Moreover, we demonstrate the system mass dependence of maximum/average density and temperature for the different forms of density dependence of symmetry energy.

Our, results are parameterized in **chapter 7**, which also contains an outlook of the work.

Chapter 2

Methodology

2.1 Introduction

In the previous chapter, we shed light on the dynamics involved in the intermediate energy HIC's. For the low energy HIC's, the conventional mean field theory [191] similar to that of Hartree-Fock and Schrödinger equation is best suited to explain the reaction mechanism. Contrary to the *TDHF* approach, the cascade model [192] is appropriate to describe the HIC's at high energies. The Cascade model approach is based on the concept of NN collisions, without considering the mean field and Pauli-blocking. However, for the theoretical interpretation of the intermediate energy heavy-ion reactions, one should take both the mean field and nucleon-nucleon collisions into account. To extract the exact reaction picture of HIC's from low to relativistic energies, it is essential to include both the mean field and NN collisions in a systematic way.

One must have an approach which can specify the exact information about the real (trajectory of nucleons) and imaginary (nucleon-nucleon collisions) parts of the potential. Furthermore, to extract information about the EOS of neutron-rich matter at intermediate energies from heavy-ion reactions induced by neutron-rich (stable and/or radioactive) beams, one must include explicitly the isospin degree of freedom. This isospin degree of freedom enter into real and imaginary part in term of iso-vector (symmetry) potential, and isospin-dependent in-medium nucleon-nucleon cross section, Pauli-blocking, respectively. Also, it is essential have the knowledge of these observables from the start (where matter is non-equilibrated) to the final state (where matter is cold and fragmented into small pieces of various sizes and velocities). The dynamical transport models dealing with intermediate energy reactions are supposed to include the essential collision physics. These dynamical

models at intermediate energies can be subdivided into two classes: (i) which follow the time evolution of that one-body phase space distribution i.e. *VUU* type, (*IBUU* approach) and (ii) others are based on N-body molecular dynamics or cascade schemes i.e *QMD* and *IQMD*. In the present chapter, we shall describe the *QMD* and *IQMD* models in detail.

Firstly, we give an overview of the models that explain the reaction mechanism without taking isospin effects into account. Later, we shall discuss the theoretical models that can explain the reaction dynamics with isospin effects. These models tend to explain the essential isospin physics which govern the complex nuclear matter interactions among the neutrons and protons (particles with different charge states interacting inside reaction zone).

2.2 Models used for the investigation of heavy-ion collisions without isospin effect

In the following, we describe in detail the *Quantum Molecular Dynamics (QMD)* model [166], which is a N-body model. We will also give an overview of other dynamical models such as *Relativistic Quantum Molecular Dynamics (RQMD)* model [171, 193, 194], and *Ultra-relativistic Quantum Molecular Dynamics (UrQMD)* model [195, 196].

2.2.1 Quantum molecular dynamics (QMD) model

After the *CMD* approach [164, 165] (the N-body theory, capable of treating both the compression and fragment formation, but on a completely classical level), Aichelin and Stocker [166, 167] designed a novel model known as Quantum Molecular Dynamics *(QMD)* model, that incorporates N-body correlations, nuclear EOS, and many important quantum features, namely, the Pauli principle, stochastic scattering as well as particle production. The *QMD* model [166] is based on the N-body theory, which simulates the intermediate energy heavy-ion reactions on an event by event basis, taking all the fluctuations and correlations into account.

The *QMD* model is considered as a simulation model which involve mainly three steps. First, one has to generate the nuclei. This procedure is termed as *initialization*. For this, some *initial checks for stability of nuclei* are carried out. After, that the nuclei is allowed to propagate under the influence of surrounding mean field. This procedure is

called *propagation*. Finally, nucleons are bound to collide if they come too close to each other. This part is dubbed as *nucleon-nucleon collisions*. At the same time, role of *Pauli blocking* is also checked. All the steps are described below in detail.

2.2.2 Initialization

It has been concluded that the time-dependent Hartree Fock *(TDHF)* [191] (Slater determinant is used for initialization) and Classical Vlasov models [197] (point-like nucleons used as initialization) yield nearly same results. This is due to the fact that different initialization methodologies do not influence the nuclear dynamics. In other words, detailed form of the wave function does not have any significant impact on the time evolution of bulk properties of the system, provided it fulfills the minimal requirements, like approximate constant density over the proper region in coordinate space. In *QMD* model, nucleons are represented by Gaussian wave packets that interact by mutual two- and three-body interactions. The model simulates the HIC's on an event by event basis and as a consequence, preserves the correlations and fluctuations.

2.2.3 Propagation

In this step, the successfully initialized nuclei are boosted towards each other with proper center of mass velocity using relativistic kinematics. The center of each distribution moves along the Coulomb trajectories. The equation of motion of many-body system is, then, calculated by means of a generalized variational principle: we start from the action

$$S = \int_{t_1}^{t_2} \mathcal{L}[\Phi, \Phi^*] d\tau, \tag{2.1}$$

with the Lagrange functional

$$\mathcal{L} = \langle \Phi | i\hbar \frac{d}{dt} - H | \Phi \rangle, \tag{2.2}$$

Where the total time derivative includes the derivation with respect to the parameters. The time evolution is obtained by the requirement that the action is stationary under the allowed variation of the wave function

$$\delta S = \delta \int_{t_1}^{t_2} \mathcal{L}[\Phi, \Phi^*] dt = 0. \tag{2.3}$$

The Hamiltonian H contains a kinetic term and mutual interactions V_{ij}, which can be interpreted as the real part of the Brückner G-matrix supplemented by the Coulomb

interactions. The time evolution of the parameters is obtained by the requirement that the action is stationary under allowed variation of the wave function. This yields an Euler-Lagrange equation for each parameter. We obtain for each parameter λ an Euler-Lagrange equation:

$$\frac{d}{dt}\frac{\partial \mathcal{L}}{\partial \dot{\lambda}} - \frac{\partial \mathcal{L}}{\partial \lambda} = 0. \tag{2.4}$$

If the true solution of the Schrödinger equation is contained in the restricted set of wave function $\psi_i(r,\ p_i(t),\ r_i(t))$, this variation of the action gives the exact solution of the Schrödinger equation. If the parameter space is too restricted, we obtain that wave function in the restricted parameter space which comes closest to the solution of the Schrödinger equation.

For the coherent states and a Hamiltonian of the form $H = \sum_i T_i + \frac{1}{2}\sum_{ij,i\neq j} V_{ij}$ ($T_i =$ kinetic energy, $V_{ij} =$ potential energy), the Lagrangian and the variation can easily be calculated and we obtain:

$$\mathcal{L} = \sum_i \dot{r}_i p_i - \sum_{j\neq i} < V_{ij} > - \frac{3}{2Lm}, \tag{2.5}$$

$$\dot{r}_i = \frac{p_i}{m} + \nabla_{p_i} \sum_j < V_{ij} > \ = \ \nabla_{p_i} < H >, \tag{2.6}$$

$$\dot{p}_i = -\nabla_{r_i} \sum_{j\neq i} < V_{ij} > = -\nabla_{r_i} < H >, \tag{2.7}$$

with $r_i = r_i + \frac{p_i}{m}t$ and $\langle V_{ij}\rangle = \int d^3r_1 d^3p_2 \langle \psi_i^* \psi_j^* | V(r_1, r_2) | \psi_i \psi_j \rangle$.

These equations represent the time evolution and can be solved numerically. The equations of motion now show a similar structure like classical Hamiltonian equations.

$$\dot{p}_i = -\frac{\partial \langle H \rangle}{\partial r_i} \ ; \ \dot{r}_i = \frac{\partial \langle H \rangle}{\partial p_i}. \tag{2.8}$$

The numerical solution can be achieved in the spirit of the classical molecular dynamics [198]. The expectation value of total Hamiltonian reads as:

$$\begin{aligned} \langle H \rangle &= \langle T \rangle + \langle V \rangle \\ &= \sum_i \frac{p_i^2}{2m_i} + V^{Skyrme} + V^{Yuk} + V^{Coul} + V^{mdi}. \end{aligned} \tag{2.9}$$

where V^{Skyrme}, V^{Yuk}, V^{Coul} and V^{mdi} are, respectively, the local (two and three body) Skyrme, Yukawa, Coulomb and momentum dependent potentials. The local Skyrme

interaction is written as:

$$V^{Skyrme} = \frac{1}{2!}\sum_{j;i\neq j} V_{ij}^{(2)} + \frac{1}{3!}\sum_{j,k;i\neq j\neq k} V_{ijk}^{(3)}, \tag{2.10}$$

Here, $V_{ij}^{(2)}$ and $V_{ijk}^{(3)}$ are the two and three-body interactions. The two-body interactions $V_{ij}^{(2)}$ is obtained by folding the two-body interactions with the densities of both particles.

$$\begin{aligned}
\sum_{j;i\neq j} V_{ij}^{(2)} &= \sum_{j;i\neq j}\int f_i(r_i,p_i,t)\ f_j(r_j,p_j,t)\ V(r_i,r_j) \\
&\quad \times d^3r_i\ d^3r_j\ d^3p_i\ d^3p_j, \\
&= \sum_{j;i\neq j}\int f_i(r_i,p_i,t)\ f_j(r_j,p_j,t)\ t_1 \\
&\quad \times\delta(r_i-r_j) d^3r_i\ d^3r_j\ d^3p_i\ d^3p_j, \\
&= \sum_{j;i\neq j} t_1\int f_i(r_i,p_i,t)\ f_j(r_j,p_j,t) \\
&\quad \times d^3r_i\ d^3p_i\ d^3p_j, \\
&= \sum_{j;i\neq j} t_1\int \frac{1}{(\pi\hbar)^3} e^{-(r-r_i(t))^2/2L} e^{-(p-p_i(t))^2 2L/\hbar^2} \\
&\quad \times\frac{1}{(\pi\hbar)^3} e^{-(r-r_j(t))^2/2L}\ e^{-(p-p_j(t))^2 2L/\hbar^2}\ d^3r_i\ d^3p_i\ d^3p_j, \\
&= \sum_j\ t_1\frac{1}{(4\pi L)^{3/2}} e^{-(r_i-r_j)^2/4L}, \\
&= t_1\sum_{j;i\neq j}\rho_{ij}.
\end{aligned} \tag{2.11, 2.12}$$

where

$$\rho_{ij} = \int d^3r\ \rho_i(r)\ \rho_j(r) = \frac{1}{(4\pi L)^{3/4}} e^{-(r_i-r_j)^2/4L}. \tag{2.13}$$

The three-body interactions can be calculated as follows:

$$\begin{aligned}
\sum_{j,k;i\neq j\neq k} V_{ijk}^{(3)} &= \sum_{j,k;i\neq j\neq k}\int f_i(r_i,p_i,t)\ f_j(r_j,p_j,t)\ f_k(r_k,p_k,t)\ V(r_i,r_j,r_k) \\
&\quad \times d^3r_i\ d^3r_j\ d^3r_k\ d^3p_i\ d^3p_j\ d^3p_k, \\
&= \sum_{j,k;i\neq j\neq k}\int f_i(r_i,p_i,t)\ f_j(r_j,p_j,t)\ f_k(r_k,p_k,t)\ t_2 \\
&\quad \times\delta(r_i-r_j)\ \delta(r_i-r_k) d^3r_i\ d^3r_j\ d^3r_k\ d^3p_i\ d^3p_j\ d^3p_k, \\
&= \frac{t_2}{(2\pi L)^3\cdot 3^{3/2}}\sum_{j,k;i\neq j\neq k} e^{-\left[(r_i-r_j)^2+(r_i-r_k)^2+(r_k-r_j)^2\right]/6L}, \\
&= \frac{t_2}{(2\pi L)^3 3^{3/2}}\sum_{j,k;i\neq j\neq k} e^{-\left[(r_i-r_j)^2+(r_i-r_k)^2\right]/6L\times\frac{3}{2}},
\end{aligned}$$

K(MeV)	A (MeV)	B (MeV)	C	EOS
200	-356	303	1.17	Soft(S)
380	-124	70.5	2	Hard(H)
200	-390	320	1.14	SMD
380	-130	59	2.09	HMD

Table 2.1: The parameter sets of potentials for the soft (S), hard (H), soft momentum dependent (SMD) and hard momentum dependent (HMD) nuclear EOS [84, 166, 169].

$$= \frac{t_2\ (4\pi L)^{3/2\times 2}}{(2\pi L)^3\cdot 3^{3/2}}\left[\sum_{j\neq i}\frac{1}{(4\pi L)^{3/2}}e^{-(r_i-r_j)^2/4L}\right]^2,$$
$$= \frac{t_2\ 2^3}{3^{3/2}}\left[\sum_{j\neq i}\rho_{ij}\right]^2. \tag{2.14}$$

From above derivation, one can observe that the three-body term reduces to two body term. The finite range Yukawa term V^{Yuk} and an effective Coulomb interaction V^{Coul} are also included to account for various effects, can be, read as:

$$V^{Yuk} = t_3\frac{exp\{-|r_i-r_j|\}/\mu}{|r_i-r_j|/\mu}. \tag{2.15}$$

$$V^{Coul} = \frac{Z_{eff}^2\ e^2}{|r_i-r_j|}. \tag{2.16}$$

The inclusion of Yukawa term (with t_3= -6.66 MeV and μ=1.5 fm) improve the surface properties of the nuclei which are very important for multifragmentation. In nuclear matter, the local potential energy constitutes two free (A and B) parameters, which can be fixed by the requirement that at normal nuclear matter density the average binding energy should be -16 MeV and total energy should have a minima at ρ_0. The values of A, B and C for soft and hard equations of state are mentioned in Table 2.1. The parametrized form of V^{loc} is shown in chapter 4.

In the study of HIC's, one usually takes the so-called the Skyrme parametrization of nuclear EOS, which contains two sets of parameters giving the same correct binding energy and saturation density, but, two different incompressibility K (one corresponds to soft EOS with K = 200 MeV (at smaller value of C), another corresponds to hard EOS with K = 380 MeV (at larger value of C). Fig. 2.1 shows the density dependence of the compressional energy per nucleon for the soft and hard interactions. When the momentum dependence of interactions is introduced, the parameters of Skyrme interactions needs to

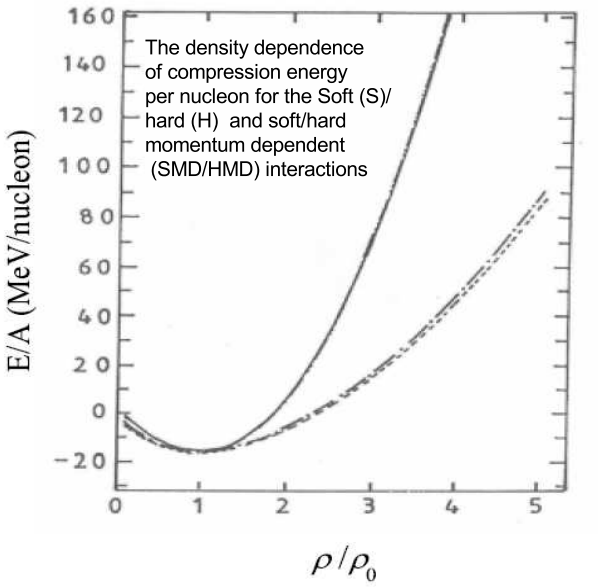

Figure 2.1: The density dependence of compression energy per nucleon. The Soft (S) and Hard (H) interactions are shown by dash-dot-dash and solid lines, respectively. The other two lines dashed/dashed double-dotted represent the soft momentum dependent (SMD)/ hard momentum dependent (HMD) interactions, and will be discussed in detail in chapter 3. The figure is taken from Ref. [84, 166, 169].

be readjusted to have correct saturation properties for normal nuclear matter and the same incompressibilities as those of the soft and hard EOS. The new parameter sets with the momentum dependence are called SMD and HMD, respectively.

2.2.4 The nucleon-nucleon binary collisions

During the propagation, two nucleons can collide if they come close to each other. The effect of N -body collisions is found to be rather small, therefore, we neglect the N - body collisions [199]. The binary collisions in *QMD* model are treated in the same way as in *BUU* model. Two particles undergo scattering if they are closer than a distance $\sqrt{\frac{\sigma^{tot}(\sqrt{s})}{\pi}}$.

This scattering is further subjected to the fulfilment of Pauli principle. If final state of scattered nucleons violates the Pauli principle, the collision is said to be blocked. Here $\sigma^{tot}(\sqrt{s})$ represents the total nucleon-nucleon cross section and $\sqrt{s}$ is the center-of-mass energy and is defined below. The employed cross sections in *QMD* model have been parametrized by Cugnon [200] on experimental data. All nucleons interact with same cross section without distinction of isospin. The total cross section ($\sigma^{tot}(\sqrt{s})$) is the sum

of cross sections for elastic and inelastic channels.

$$\sigma_{tot} \;=\; \sigma_{el} \;+\; \sigma_{inel} \;=\; \sigma_{el} \;+\; \Sigma_{channels}\sigma_i \tag{2.17}$$

For elastic channels, the total and differential cross section (labeled as σ^{el}) is:

$$\sigma_{nn}^{(el)}(\sqrt{s}) = \begin{cases} 55(mb) & \text{if}\sqrt{s} < 1.8993 \\ \frac{35}{1+100(\sqrt{s}-1.8993)} + 20 & \text{if}\sqrt{s} \geq 1.8993, \end{cases} \tag{2.18}$$

with $\sqrt{s}$, the nucleon-nucleon center of mass energy given by:

$$\sqrt{s} = \sqrt{(E_1 + E_2)^2 - (P_1 + P_2)^2}. \tag{2.19}$$

Here E_i and P_i ($i,\ j = 1, 2$) are, respectively, the energy and momentum of a nucleon. The angular distribution for these channels is given by [200]:

$$\frac{d\sigma}{dt} = ae^{bt}\ ; \qquad t = -2p^2(1 - cos\theta). \tag{2.20}$$

On the other hand, for inelastic channels, NN $\rightarrow$ N Δ the total cross section labeled as σ^{in} is parameterized as

$$\sigma_{nn\rightarrow n\Delta}^{(in)}(\sqrt{s}) = \begin{cases} 0 & \text{if}\sqrt{s} < 2.015 \\ \frac{20(\sqrt{s}-2.015)^2}{0.015+(\sqrt{s}-2.015)^2} & \text{if}\sqrt{s} \geq 2.015. \end{cases} \tag{2.21}$$

The angular distribution for in-elastic channels is assumed to be isotropic. The limit of $\sqrt{s}$=1.8993 GeV (in Eqn. 2.18) is based on the fact that the mass of two nucleons is roughly equal to 1.876 GeV. Therefore, for two colliding nucleons with very small velocity, a constant cross section (= 55 mb) is used. The mass limit of the inelastic channel (i.e. Δ formation in Eqn. 2.21) is based on the fact that mass of $\Delta(= N + \pi)$, is 1.076 GeV. Therefore, for $NN \rightarrow N\Delta$ channel, the outgoing mass should be at least 1.076 + 0.938 GeV.

The graphical representation of the elastic and in-elastic parts of the cross section is displayed in Fig. 2.2. The energy dependence of the NN cross section shows that the elastic cross section falls sharply and saturates around 20 mb. On the other hand, the inelastic cross section increases linearly with bombarding energies. At very high energies, the nucleon-nucleon cross section is fully dominated by the inelastic channels.

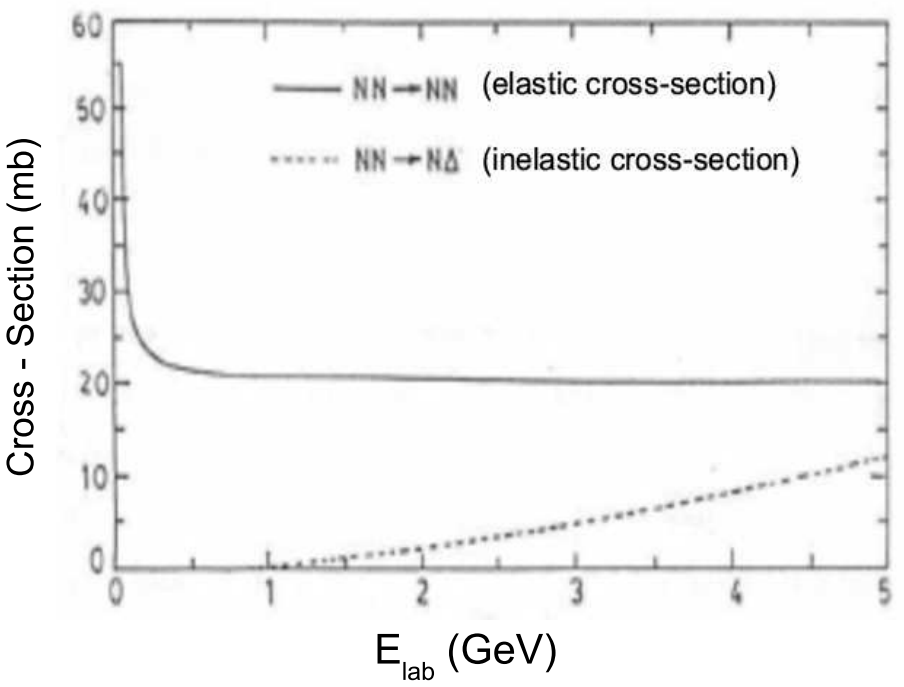

Figure 2.2: The Cugnon parametrization for the elastic (solid line) and inelastic (dashed line) cross sections of nucleon-nucleon scattering as a function of the incident energy E_{lab}. Figure is taken from Ref.[202].

2.2.5 Pauli blocking

The nucleons are Fermions, that is why, the Pauli principle (a quantum feature) is an important ingredient in the reaction dynamics. It is difficult to include the Pauli blocking properly in classical approaches because it has no classical equivalence. To overcome this, only average phenomenological treatments are usually attempted [170, 172, 174, 201]. In such a case, the basic idea is to prevent nucleons from being in overpopulated regions of phase space. With the inclusion of this methodology, whenever a binary collisions occurs, the phase space around the scattering partners is checked. For simplicity, each nucleon is assumed to occupy a sphere in the coordinate and momentum space. The results of the Pauli blocking ratio are exactly similar to those of calculated by the overlap of the Gaussians, but is much less time consuming. The fractions P_1 and P_2 of the final phase spaces are calculated for each of the two scattering partners which is already occupied by other nucleons. A binary collision is blocked with a probability:

$$P_{block} \;=\; 1 - [1 - min(P_1, 1)][1 - min(P_2, 1)], \tag{2.22}$$

and, correspondingly, allowed with a probability $(1 - P_{block})$. For a nucleus in its ground state, where all collisions should be blocked ideally, the averaged blocking probability $< P_{block} >$ is about 0.96. In the case of complete blocking, this factor should be equal to one.

2.3 Other Versions

To understand the various other aspects of HIC's at a wide range of densities, several modifications have been made in the *QMD* approach, with the principal structure being common for all. The major difference, however, lies in the details and initialization of the projectile and target. Bohnet *et al.,* [172] made several changes in the structure of original *QMD* to make it suitable for low energy fragmentation data [173]. In order to explain the mechanism of fragmentation, it was designed for describing the proper binding of a nucleus and was dubbed as *BQMD* [22] model. One of the form of *QMD* model is also termed as *HQMD* [22] model, which combines certain optional features of *BQMD* model.

Peilert *et al.* [203] developed the *PQMD* model, which includes an additional implementation of the so-called Pauli potential. The Pauli potential can be defined as a strong repulsive potential which is very effective in preventing two identical particles coming too close in phase-space. In fact, the Pauli potential, has a strong momentum-dependent nature, and also a different physical input compared to other discussed flavors. This model has also been applied for analysis of the *FOPI-data* at lower energies [204]. Another modification of the *QMD* has been done by Jaenicke *et al.* [175], in which the potentials and cross sections are replaced by those calculated from G-matrix and labeled as *G-matrix QMD* [205]. The *FOPI* collaboration has compared the data with this model also [206]. Faessler and co-workers [207] provided an another version of the Quantum Molecular dynamics model by incorporating temperature-dependent mean field potentials, dubbed as *Temperature-dependent Quantum Molecular Dynamics (TQMD)* model [207]. These temperature-dependent potentials prescribed by the model are obtained from Bethe-Goldstone equation for a realistic force in nuclear matter at finite temperature. The consequences of these temperature-dependent potentials are found to be more

in heavier nuclei [207]. At high bombarding energies, relativistic effects become very important, when velocity of particles become comparable to the velocity of light. The relativistic version of *QMD*, namely the *Relativistic Quantum Molecular Dynamics (RQMD)* [171, 193, 194] can be utilized up to relativistic energies (AGS and CERN/SPS) by including a relativistic covariant propagation scheme, similar to that proposed by Sorge [193]. This was first attempt which has shown that *RQMD* model calculations yields results similar to those of *QMD* calculations in non-relativistic limits, even for highly sensitive observables like directed transverse in-plane flow. We provide an overview of the *RQMD* model below in detail.

2.3.1 Relativistic quantum molecular dynamics (RQMD) model

The Relativistic Quantum Molecular Dynamics *(RQMD)* [171, 193, 194] model describes the propagation of all kinds of baryons and mesons in a Lorentz-invariant fashion. The Hamiltonian corresponding to N-particle system is expressed in terms of 8N variables (4N position coordinates $q_{i\mu}$ and 4N momentum coordinates $p_{i\mu}$). Since the physical events are described as world lines in a 6N dimensional phase-space, extra (2N-1) degrees of freedom have to be eliminated and a global evolution parameter τ has to be defined. This can be achieved with the help of 2N constraints. The first N constraints are chosen as Poincaré invariant mass-on shell constraints [171, 194].

$$\xi_i = p_i^\mu p_{i\mu} - m_i^2 - \tilde{V}_i = 0 \qquad ; \qquad i = 1, ..., N. \tag{2.23}$$

This choice of Poincaré invariant constraints requires that the potential part $\tilde{V}_i$ should be a Lorentz scalar and therefore, function of the Lorentz scalars only. Since in *RQMD*, a system with mutual two- and three-body interactions (like in *QMD*) has to be defined, $\tilde{V}_i$ should be given by the sum of these two-body interactions. The non relativistic Skyrme force is generalized in such a way that the force remains covariant and also reduces to the usual Skyrme in non-relativistic limit for the inclusion of relativistic effects in the dynamics. This can be done as [171, 194]:

$$\tilde{V}_i = \sum_{j \neq i}^{N} \tilde{V}_{ij}(q_{Tij}^2). \tag{2.24}$$

This shows that the two-body interactions depend only on the Lorentz invariant squared transverse distance

$$q_{Tij}^2 = q_{ij}^2 - \frac{(q_{ij}^\mu p_{ij\mu})^2}{p_{ij}^2}, \tag{2.25}$$

with $q_{ij}^\mu = q_i^\mu - q_j^\mu$ being the simple four dimensional distance and $p_{ij}^\mu = p_i^\mu + p_j^\mu$ the sum of the momenta of the two interacting particles i and j. The next set of the constraints (which fix the relative times of all particles) should be chosen in such a way that these constraints must respect the principle of casuality and (N-1) of these constraints should be Poincaré invariant so that the world line invariance can also be fulfilled. Another feature which these constraints has to fulfill is the cluster separability. This means that the system can be divided into single particles or clusters as soon as their Minkowski distances are space-like. Furthermore, a global evolution parameter should also be defined. These features can be fulfilled by choosing the following set of time constraints:

$$\chi_i = \sum_{j(\neq i)} \frac{1}{q_{ij}^2/L_C} \exp(q_{ij}^2/L_C) \;\; p_{ij}^\mu q_{ij\mu} = 0 \qquad ; \qquad i = 1, ..., N-1, \tag{2.26}$$

$$\chi_{2N} = \hat{P}^\mu Q_\mu - \tau = 0. \tag{2.27}$$

with $\hat{P}^\mu = P^\mu/\sqrt{P^2}$, $P^\mu = \sum_i p_i^\mu$, $Q^\mu = \frac{1}{N}\sum_i q_i^\mu$.

These time fixations take care that the time coordinates of the interacting particles should not be much dispersed in the center-of-mass system of two particles. The Hamiltonian is a linear combination of the Poincaré invariant constraints:

$$H = \sum_{i=1}^{2N-1} \lambda_i \Psi_i, \tag{2.28}$$

with

$$\Psi_i = \begin{cases} \xi_i & ; \;\; i \leq N \\ \chi_{i-N} & ; \;\; N < i \leq 2N-1. \end{cases} \tag{2.29}$$

This Hamiltonian then generates the equations of motion:

$$\frac{dq_i^\mu}{d\tau} = [H, q_i^\mu], \tag{2.30}$$

$$\frac{dp_i^\mu}{d\tau} = [H, p_i^\mu]. \tag{2.31}$$

Here, square brackets represent the Poisson brackets. The unknown Lagrange multipliers λ_i in Eqn. 2.28 are determined by the condition that all constraints must be fulfilled

for all times during the simulations. These equations of motion are used to propagate the baryon during the reaction.

The propagation and the "soft interaction" between baryons is combined with the quantum effects like stochastic scattering and the Pauli-blocking etc.. In *RQMD*, the collision part is treated in a covariant fashion. In *RQMD*, two baryons are allowed to collide if their distance $\sqrt{-q_{Tij}^2} \leq \sqrt{\sigma(\sqrt{s})/\pi}$ where q_{Tij}^2 is the Lorentz-invariant squared transversal distance (Eqn. 2.25) and $\sigma(\sqrt{s})$ is the cross section depending on the available invariant mass $\sqrt{s}$.

The Frankfurt group reported a new version, named Ultra-relativistic Quantum molecular dynamics *(UrQMD)* model [195], which is designed specifically for ultra-relativistic collisions and is further improved [196] by incorporating momentum-dependent Pauli potential, in-medium $NN \rightarrow N\triangle$ angular distribution and clusterization procedure. It has the ability to explain the reaction mechanism at wide incident energy range from SIS ($\approx$ 1GeV/nucleon) up to SPS ($\approx$ 200 GeV/nucleon) or even higher energies in colliders like Relativistic Heavy-Ion Collider *(RHIC)* ($\sqrt{s}$ = 20 GeV) or Large Hadron Collider *(LHC)* ($\sqrt{s}$ > 1000 GeV). This model can also be used to predict the behavior of symmetry energy as well as its density dependence at densities very much above the normal nuclear matter density [51, 208]. Here we are interested in the various phenomena linked to intermediate energies, where relativistic effects do not play any role [209].

Feldmeier introduced Fermionic Molecular Dynamics *(FMD)* [210] approach by adding an additional feature of anti-symmetrization to the *QMD* model. In *FMD* approach, a true quantum treatment is said to represent the many body state as an anti-symmetrized Slater determinant built from single particle wave packets of Gaussian form. The isospin degree of freedom has also been included, where nucleons are assumed to move in a mean-field. *FMD* utilizes quantum wave functions, provided dynamics is fully deterministic and the system remains a single determinant at all times. Another modification of the *FMD* is termed as *AMD* [211] in which stochastic terms are added so that many configurations can appear through reaction dynamics.

The *AMD* [211] and *FMD* [210] approaches can handle only lighter systems, due to the serious numerical problems. Recently improved version of *AMD* was used to show the cluster-shell competition of these nuclei [212]. To examine the Fermionic nature of N-body

system, new microscopic approach, termed as constrained molecular dynamics *(CoMD)*, was also proposed in Ref.[213]. Hoffmann *et al.* [214] put forward a new approach, dubbed as *quark molecular dynamics (qMD)*, which is capable of studying the hadrons and quarks.

Between the two above approaches namely, the statistical and dynamical, there is also possibility for statistical-dynamical phenomenology, known as *"Hybrid Models"*. In these models, the internal dynamics is described by dynamical models and the later stage by a statistical model. The heavy-ion phase space exploration *(HIPSE)* account for hybrid models [215].

No doubt, for a proper understanding of nuclear reactions at intermediate energy range, one should also take the isospin degree of freedom into account. The isospin dependence of the equation of state (symmetry energy and its density dependence) is one of the interesting topics for the nuclear physics community from the last two decades. The study of isospin-asymmetric nuclear matter has got great impetus with the recent experimental advancements made by radioactive ion beams facilities. It has further motivated the researches to include the isospin degree of freedom in various theoretical approaches.

The isospin-dependent quantum molecular dynamics *IQMD* model [22] is one of the major developments of the *QMD* model in which isospin degree of freedom has been incorporated. As we have discussed in chapter 1, the Bethe-Weizsäcker mass formula introduced the idea of isospin, where symmetry energy term has been added to incorporate the asymmetry between neutrons and protons. First, we give the details of isospin-dependent Boltzmann-Uehling-Uhlenbeck *(IBUU)* model [23, 24] which is also very successful in explaining role of isospin in reaction dynamics. Later, we discussed the *IQMD* model in detail.

2.4 Models used for the investigation of heavy-ion collisions with isospin effects

2.4.1 Isospin-dependent Boltzmann-Uehling-Uhlenbeck (IBUU) model

The *IBUU* model [23, 24], is a modification of the *BUU* model [159, 197], where the time evolution of the single particle phase-space distribution function is described by the

Boltzmann-Uehling-Uhlenbeck equation as:

$$\frac{\partial f_1}{\partial t} + v \cdot \nabla_r f_1 - \nabla_r U \cdot \nabla_p f_1 = \int \frac{d^3\acute{p_1} d^3 p_2 d^3\acute{p_2}}{(2\pi)^9} \sigma'_{12} v_{12} (2\pi)^3 \delta^3(p_1 + p_2 - \acute{p_1} - \acute{p_2}) \times \left[\acute{f_1}\acute{f_2}(1-f_1)(1-f_2) - f_1 f_2 (1-\acute{f_1})(1-\acute{f_2})\right]. \tag{2.32}$$

Here σ_{12} is the differential cross-section for a certain change of momentum $(p_1, p_2) \rightarrow (\acute{p_1}, \acute{p_2})$ and v_{12} is the relative velocity for the colliding nucleons. The isospin dependence has been added to the model by both the elementary nucleon-nucleon cross section $\sigma^{ibuu}(\sqrt{s})$ and the nuclear mean field U. *IBUU* model contains the experimental nucleon-nucleon cross sections with the explicit isospin dependence taken into account [216]. In the energy range 10 $MeV \leq E_{lab} \leq$ 1000 MeV the data for free space cross sections can be parameterized as [217]:

$$\begin{aligned} \sigma_{np}^{ibuu} &= -70.67 - 18.18(v/c)^{-1} + 15.26(v/c)^{-2} + 113.85(v/c)\ (mb) \\ \sigma_{pp}^{ibuu} &= -13.73 - 15.04(v/c)^{-1} + 8.76(v/c)^{-2} + 68.67(v/c)^4\ (mb) \end{aligned} \tag{2.33}$$

The relative strengths of various cross sections vary significantly at finite density and temperature which can be justified from the fact that isospin dependence of nucleon-nucleon cross-sections in free space disappears gradually as the bombarding energy and density increases [218]. The isospin dependence of cross section is incorporated in the model considering the fact, that the cross section of neutron-proton (σ_{np}) is about three times that of the neutron-neutron (σ_{nn}) or proton-proton (σ_{pp}) cross section. In this model, U is the mean field, which is function of the local density. It can be parameterized as an arbitrary function of density, making possible to model a variety of equations of state. Typically, it can be written as, the sum of three terms:

$$U = V^{Coul} + V^n + V^{sym}, \tag{2.34}$$

where V^{Coul}, V^n and V^{sym} are the Coulomb, iso-scalar nucleon potential and the symmetry energy, respectively. The nuclear mean field U including the isospin symmetry term is parameterized as:

$$U(\rho, \tau_z) = A\left(\frac{\rho}{\rho_0}\right) + B\left(\frac{\rho}{\rho_0}\right)^C + (1-\rho_z)V^{Coul} + c\left(\frac{\rho_n - \rho_p}{\rho_0}\right)\tau_z. \tag{2.35}$$

Here ρ_0 is the normal nuclear matter density, ρ, ρ_n and ρ_p are the nucleons, neutron and proton densities, respectively. τ_z equals to +1 or -1 for neutrons or protons, respectively. The V^{Coul} as discussed above represents the Coulomb potential. Other forms of the parametrization for mean fields which corresponds to probably more complete form of Skyrme forces are also possible [219]. The Skyrme term comes from averaging over the constituent two-body forces with Heisenberg component proportional to $(\tau_i,\ \tau_j)$ [220]. Its strength c can be deduced from experiments (e.g. nuclear symmetry energies, optical potentials for nucleon scatterings, excitation of analog states in (p,n) reactions). However, the extracted strength vary significantly from reaction to reaction and also depends on the energy of nucleon [220].

Recently, the momentum dependence of the symmetry energy has got a large attention of the nuclear physics community. For the exact measurement of the density dependence of symmetry energy $E_{sym}(\rho)$, one has to determine simultaneously both the density-dependence and momentum-dependence of the symmetry energy [30]. It has been concluded that the symmetry potentials with and without the momentum dependence but corresponding to the same density-dependent symmetry energy $E_{sym}(\rho)$ tends to give considerably different results on several $E_{sym}(\rho)-$sensitive experimental observables especially for energetic nucleons [221].

Experimentally, it is known that the strength of nuclear symmetry potential decreases linearly from about 28 $\pm$ 6 MeV with increasing kinetic energy with a slope of about 0.1 - 0.2 from optical model analysis of nucleon-nucleon scattering data [222]. However, the available data is limited only to nucleon energies less than 100 MeV. Guided by a Hartree-Fock calculation using the Gogny effective interaction, the single nucleon potential was recently parameterized with the momentum dependent symmetry energy in Refs. [221, 223].

This model provides an accurate description of the time dependence of the one-body distribution function. Accurate solution of the BUU equation average away fluctuations in the density that might lead to the formation of fragments in an individual collision. This is usually achieved by solving the BUU equation with a large number of test particles per nucleon N_{test}. The density fluctuations that lead to the fragment production are suppressed in the BUU equation, so the calculation of fragment yield directly via $IBUU$

model is not feasible. Therefore, alternate model such as, *Stochastic Mean Field (SMF)* model [176] and *Isospin Quantum Molecular Dynamics (IQMD)* model [22] has been developed to address the density fluctuations.

2.4.2 Isospin-dependent quantum molecular dynamics model (IQMD) model

The Vlasov-Uehling-Uhlenbeck *(VUU)* theory is actually the primary basis for all the microscopic models used for the understanding of HIC's. This theory, explicitly treats non-equilibrium and stochastic (quantum effects) in the framework of one particle quantities, as well as nuclear potential (nuclear EOS). One of the major motivations for the development of Quantum Molecular Dynamics *(QMD)* model was actually to study the certain fluctuations and correlations, such as the formation of fragments in heavy-ion collisions, which cannot be studied with transport model based on a single particles distribution function.

Isospin-dependent quantum molecular dynamics *(IQMD)* Model [22] (used for the N-body distribution) treats different charge states of nucleons, deltas and pions explicitly, as inherited from the *VUU* model [197, 224, 225]. In *IQMD* (improved version of *QMD*), the isospin is included explicitly via. symmetry potential (to achieve corrected distributions of protons and neutrons in the nucleus) and explicit Coulomb forces between the Z_P and Z_T protons. The isospin degree of freedom enters into the calculations via. both cross section and mean field [177-179]. This model constitutes three steps which are able to explain the dynamics of heavy-ion collisions: First, one has to generate the nuclei. This procedure is known as *initialization*. After the initialization, nuclei propagate under the influence of surrounding mean field. This is termed as *propagation*. The next step include the *collisions*, when nucleons are finally bounded to collide if they come too close to each other. The elastic and inelastic cross sections for proton-proton, neutron-neutron as well as proton-neutron are supposed to be affected in the presence of isospin.

In *IQMD* model, the centroids of the Gaussians are randomly distributed in a phase-space sphere ($r \leq RA'^{1/3}$ *and* $p \leq P_F$) corresponding to ground state density. However, the Fermi momentum in *QMD* model is determined by the local potential. In this model,

baryons are represented by Gaussian-shaped density distributions

$$f_i(r,p,t) = \frac{1}{\pi^2\hbar^2}\ e^{-(r-r_i(t))^2\frac{1}{2L}}\ e^{-(p-p_i(t))^2\frac{2L}{\hbar^2}}. \tag{2.36}$$

The uniform distribution of momenta affects the nucleons close to the surface which may unbound initially, As a result, the initialized nuclei have lesser binding energy. In *IQMD*, stronger stability is achieved due to lesser binding energy. Another difference between *IQMD* and *QMD* is the Gaussian width L, which is a measure of interaction range of nucleons. In the *IQMD* model, Gaussian width $L = 4.33\ fm^2$ is fixed, whereas, in the *IQMD* model, L varies with the size of the system. The system mass dependence of Gaussian width L is incorporated in order to obtain maximum stability of density profile. For the heavier system (e.g. $^{197}_{79}Au\ +\ ^{197}_{79}Au$), its value is chosen 8.66 fm^2 , while for lighter one (i.e. $^{40}_{20}Ca +^{40}_{20} Ca$), the value is 4.33 fm^2 and in between these two values for middle masses.

As stated above, the *IQMD* model contains isospin in the form of symmetry potential and Coulomb potential. In *QMD* model, the effective charge is used for all the nucleons (without distinguishing between protons and neutrons), in the contrary, the *IQMD* model constitutes the real charge, i.e., $Z_{proton} = 1$ and $Z_{neutron} = 0$, and thus the Coulomb potential becomes isospin-dependent. The Yukawa potential ($\mu = 0.4$ fm) is short ranged in the *IQMD* model, compared to the *QMD* where $\mu = 1.5$ fm. Though, remaining potentials Skyrme, Yukawa and momentum-dependent potentials are independent of isospin factor. The major ingredient of *IQMD* (added to the *QMD* model) is the symmetry potential between protons and neutrons which is described in chapter 1 in detail. The nuclear symmetry energy and its high density behavior has been regarded as a most uncertain property of the isospin-asymmetric neutron rich nuclear matter [226, 227]. In addition to the density dependence of the symmetry energy, the momentum dependence of the symmetry energy is also one of the hot topic in the present day nuclear physics research. The isospin momentum-dependent interaction given in the form practically usable in the *IQMD* model is proposed in Ref. [228]. It was concluded that the isospin-momentum dependent interaction yields an important isospin effect in the isospin fractionation ratio [228].

Considering the nucleus in its ground state, the expectation value of the total Hamiltonian should be equal to its binding energy. The Bethe-Weizsäcker mass formula con-

cludes that the kinetic energy, the Skyrme interaction and the momentum-dependent interactions contribute to the volume energy, the Yukawa interaction to the surface and volume energy, and the symmetry interactions to the volume symmetry energy. The above said facts results in the total baryon-baryon potential in *IQMD* model, which is shown below:

$$\begin{aligned} V_{ij} &= V_{ij}^{Skyrme} + V_{ij}^{Yukawa} + V_{ij}^{Coul} + V_{ij}^{MDI} + V_{ij}^{sym} \\ &= \left(t_1\delta(r_i - r_j) + t_2\delta(r_i - r_j)\rho^{\gamma-1}\left(\frac{r_i + r_j}{2}\right)\right) \\ &\quad + t_3\frac{exp(|r_i - r_j|/\mu)}{(|r_i - r_j|/\mu)} + \frac{Z_i Z_j e^2}{|r_i - r_j|} \\ &\quad + t_4 \ln^2[t_5(p_i - p_j)^2 + 1]\delta(r_i - r_j) \\ &\quad + t_6(1/\varrho_0)T_{3i}T_{3j}\delta(r_i - r_j) \end{aligned} \tag{2.37}$$

Here, Z_i and Z_j denote the charges of i^{th} and j^{th} baryon, and T_{3i}, T_{3j} are their respective T_3 components (i.e., 1/2 for protons and -1/2 for neutrons). The parameters μ and $t_1....t_6$ are adjusted to the real part of the nucleonic optical potential. For the density dependence of nucleonic optical potential, standard Skyrme-type parametrization is employed which is displayed in Eqn. 2.37. Similar to the *QMD*, two different types of nuclear EOS have been implemented. Also, the momentum dependence of the NN interactions V^{MDI}, which may optionally be used in *IQMD* is fitted to the experimental data [229] on the real part of nucleon optical potential [168, 230], which may yield:

$$V^{MDI} = \delta_M . \ln^2\left(\epsilon.(\triangle p)^2 + 1\right) . \left(\frac{\rho}{\rho_0}\right) \tag{2.38}$$

Here δ_M = 1.57 MeV and ϵ = 21.54. The strength of symmetry energy is found to be equal to 32 MeV at normal nuclear matter density. Similarly, in the *IQMD* model the symmetry energy as a function of density becomes:

$$E_{sym}(\rho) = 32.\left(\frac{\rho}{\rho_0}\right)^{\gamma} \; MeV \; . \tag{2.39}$$

The term gamma (γ) determine the strength of the symmetry energy at densities away from normal nuclear matter density. In Fig. 2.3, we display the symmetry energy variation with the $\frac{\rho}{\rho_o}$ using *IQMD* model for the different values of γ.

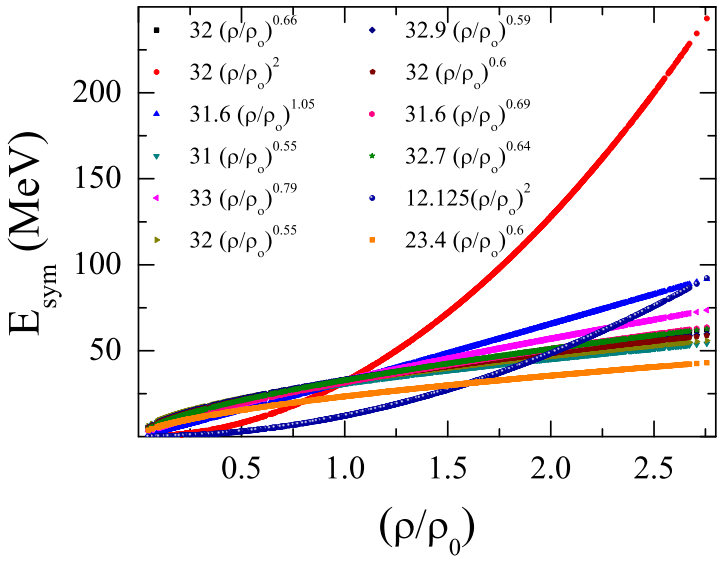

Figure 2.3: The various forms of density dependences of symmetry energy.

In case of the stiff dependence, symmetry energy tends to increase at supra-densities ($\rho > \rho_o$), and in case of the soft dependence, symmetry energy decreases above the normal nuclear matter density. In chapter 3, we use different forms of density dependent symmetry energy to study the multifragmentation. Also, the role of MDI in fragment production have been analyzed subjected to the different forms of density dependent symmetry energy. The term symmetry energy, which accounts for the isospin dependence of the nuclear EOS, has also an impact on the momentum dependent interactions.

Another difference between the *QMD* and *IQMD* models is the parameterizations of nucleon-nucleon scattering cross section. In the *QMD* model, Cugnon parametrization has been taken into account (without distinguishing between isospin), here parameterizations of VerWest and Arndt have been taken [178]. For elastic NN collisions, the experimental parametrization has been taken into account. For details, see Ref. [177-179]. Though, the treatment of collisions is done in the same way as in the *QMD* model, the Pauli blocking becomes isospin-dependent, i.e., occupancy of phase space of scattering partners is checked for the particles having same isospin as that of the scattered one. During the propagation, two nucleons are supposed to suffer a binary collision if the distance between their centroids is:

$$|r_i - r_j| \leq \sqrt{\frac{\sigma_{tot}}{\pi}}, \sigma_{tot} = \sigma(\sqrt{s}, type), \tag{2.40}$$

"type" denotes the ingoing collision partners (N-N, N-Δ, N-π,..). In addition, Pauli blocking (of the final state) of baryons is taken into account by checking the phase space densities in the final states. The final phase space fractions P_1 and P_2 which are already occupied by other nucleons are determined for each of the scattering baryons. Furthermore, parameterized free *pn* and *pp* cross-sections are used instead of an averaged nucleon-nucleon cross sections. The pictorial representation of elastic and inelastic cross-sections for proton-proton (pp) and proton-neutron (nn) used in *IQMD* model [22] are shown in Fig. 2.4.

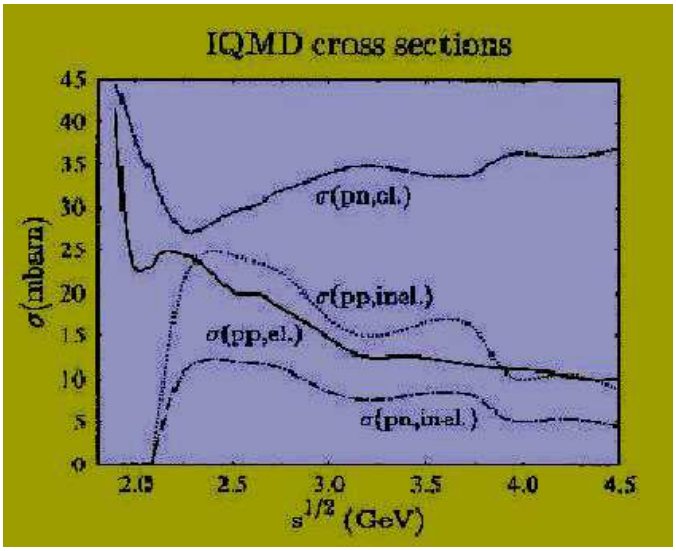

Figure 2.4: The elastic and inelastic cross sections for proton-proton (pp) and proton-neutron (pn) used in *IQMD*. The neutron-neutron (nn) cross section is assumed to be equal to pp. The total cross-section is equal to sum of elastic and inelastic cross sections. This figure is taken from Ref. [22].

It is well known that the scattering cross section between two nucleons depends on their isospin. Because of the differences in the transition matrices of the isospin $T = 1$ and $T = 0$ channels, and the fact that both the iso-singlet and iso-triplet channels contribute to neutron-proton (np) scattering, their cross sections (σ_{np}^{free}) in free space are higher in free space are higher than those for proton-proton (pp) or neutron-neutron

(nn) scatterings (σ_{pp}^{free}) where only iso-triplet channels are involved [18]. It is seen from the figure that neutron-proton cross section is about a factor of 2 to 3 larger that the proton-proton or neutron-neutron cross section.

In addition to nucleons and deltas (as in *QMD* model), the production of pions is also included via. the decay of delta resonances. The following inelastic reactions that might influence the dynamics of a collision are explicitly taken into account:

$$\begin{aligned} N\ N &\rightarrow\ \Delta\ N\ (hard-delta\ production) \quad (a),\\ \Delta &\rightarrow\ N\ \pi\ (delta\ decay) \qquad\qquad\qquad (b),\\ \Delta\ N &\rightarrow\ N\ N\ (delta\ absorption) \qquad\quad (c),\\ N\ \pi &\rightarrow\ \Delta\ (soft-delta\ production) \qquad (d). \end{aligned} \tag{2.41}$$

Elastic $\pi\ -\ \pi, \pi\ -\ N, \pi\ -\ \Delta, \Delta\ -\ \Delta, \Delta\ -\ N$ scattering is not taken into account. Experimental cross sections are used for processes (a) and (d) [177, 178], as well as for the elastic NN collisions. Inaccessible reactions like ΔN$\rightarrow\ NN$ are calculated from their reverse reactions (here $NN\ \rightarrow\ \Delta N$) using modified detailed balance formula [231]. The conventional detailed balance formula is only correct for particles with infinite lifetimes (zero width). The elastic nucleon-nucleon scattering angular distribution is taken to be [200]:

$$\frac{d\sigma_{el}}{d\Omega}\ \approx\ exp\left[A(s)t\right], \tag{2.42}$$

where t is $-q^2$, the transverse momentum transfer and

$$A(s)\ =\ 6\frac{\left[3.65\left(\sqrt{s}-1.8766\right)\right]^6}{1+\left[3.65\left(\sqrt{s}-1.8766\right)\right]^6}. \tag{2.43}$$

$\sqrt{s}$ is the c.m. energy in GeV.

The isospin degree of freedom play an important role especially for the particle production. The employed inelastic channels $NN\ \rightarrow\ NN^*,\ N\Delta\ and\ \Delta\Delta$ are treated in an analogous fashion. The parametrization suggested by Huber and Aichelin [232] is used: fitted differential cross sections are extracted from one-boson- exchange (OBE)

$x' = \sqrt{s}\ (GeV)$	$a\ (fm)$	b
2.104 - 2.12	$294.6(x'-2.014)^{2.578}$	$19.71(x'-2.014)^{1.551}$
2.12 - 2.43	$\frac{0.01224}{(x'-2.225)^2\ +\ 0.004112}$	$19.71(x'-2.014)^{1.551}$
2.43 - 4.50	$\left(\frac{2.343}{x'}\right)^{43.17}$	$33.14\ arctan(0.5404(x'-2.146)^{0.9784})$

Table 2.2: a(s) and b(s) as a function of the c.m. energy

calculations:

$$\frac{d\sigma_{in}}{d\Omega} \approx a(s)exp\left[b(s)cos\theta\right]. \tag{2.44}$$

The $a(s)$ and $b(s)$ are functions of $\sqrt{s}$ and vary in their definition for different intervals of $\sqrt{s}$ (see Table 2.4.2). θ is the polar angle.

In the following, the importance of *IQMD* over *QMD* model is discussed.

Advantage of IQMD approach over QMD

1. The *IQMD*-model offers rather stable density distributions and good energy conservation, however for the price of nucleon evaporation and improper binding energies ($E_{bind} \approx 4-5\ MeV/nucleon$ for heavy nuclei instead of 8 MeV/nucleon).

2. In addition to the use of the explicit charge states of all baryons and mesons a symmetry potential between protons and neutrons corresponding to the Bethe-Weizsäcker mass formulae have been included.

3. In *QMD* model, the effective charge is used for all the nucleons (without distinguishing between protons and neutrons), in the contrary, the *IQMD* model constitutes the real charge, i.e., $Z_{proton} = 1$ and $Z_{neutron} = 0$, and thus the Coulomb potential becomes isospin-dependent.

The above mentioned models are "primary models" that are used to generate the phase-space of nucleons. Further, we need to have "secondary models" to clusterize the nucleons into fragments. These clusterization methods are discussed briefly in the following section.

2.5 Secondary models for clusterization

2.5.1 Minimum spanning tree (MST) method

The Minimum Spanning Tree (MST) method is the most extensively used phenomenology to clusterize the nucleons [166, 169, 180-182]. In *MST* method, two nucleons share the same fragment if their centroids are closer than a certain distance d_{min}.

$$| \vec{r}_i - \vec{r}_j | \leq d_{min} \tag{2.45}$$

where $\vec{r}_i$ and $\vec{r}_j$ are the spatial positions of both nucleons. The value of d_{min} can vary between $2 - 4$ fm. As reported, it has small effect on multifragmentation [180-183]. However, this method cannot address the question of time scale as it yields big fragments during the early stage of the reaction. It is worth to mention that this method can only be used to analyze asymptotic configurations in which the fragmenting system can be viewed as a very dilute mixture of free particles and almost equilibrated fragments. To study the time of fragment formation, one needs to device a method which should be able to detect the overlapping fragments.

2.5.2 Minimum spanning tree method with momentum cut (MSTM)

An improvement over the *MST* algorithm, is to put additional cut in momentum space [185, 186]. This method is dubbed as *MSTM*. It helps to get rid of fragments that although close in position, but far in momentum space. The *MSTM* method also takes care of the relative momentum of nucleons. Along with the restriction in the spatial space of nucleons, another restriction is put on the relative momentum of nucleons i.e.,

$$| \vec{p}_i - \vec{p}_j | \leq p_{min} \tag{2.46}$$

The value of cut (in the relative momentum of two nucleons) is about the average Fermi momentum (p_{min}) of nucleons as reported in [22].

The transport models can provide time evolution of single nucleons. The phase space thus obtained can be used to study various phenomenon such as multi-fragmentation, collective flow and nuclear stopping which can shed light on the form and strength of

symmetry energy at densities away from the normal matter density. In the next chapters, we will shed light on multifragmentation, elliptical flow and nuclear stopping subjected to different forms of symmetry energy.

Chapter 3

Fragmentation around the transition energy

3.1 Introduction

Among the various phenomena, collective flow and its disappearance, the breaking of colliding nuclei into pieces (i.e., multifragmentation), as well as formation of the hot and dense nuclear matter has been a topic of wider interest for nuclear physics community since the last few decades. Another emerging area in the recent times is the isospin physics, particularly the symmetry energy and its density dependence. At low incident energies, directed transverse flow is attractive, but turns repulsive at higher incident energies. At a particular incident energy, flow disappears, and this is known as the balance energy. Another form of the flow, i.e., elliptical flow, also shows the switch-over from in-plane to out-of-plane. The incident energy of this switch-over is known as the transition energy, which is shown in Fig. 3.1. The different positive (or negative) values of the elliptical flow are related to the shape of the colliding matter. The elliptical flow describes the eccentricity of an ellipse-like distribution. The positive value of the elliptical flow reflects an in-plane emission, whereas an out-of-plane emission is reflected by its negative value.

It is found that the transition energy depends on the participant expansion and shadowing of the spectator matter, apart from the nucleons dominating the binary nucleonic collisions. Obviously, the fragment flow constitutes various complex phenomenon which are also inter-related. Different flows represent collective velocity in a particular direction.

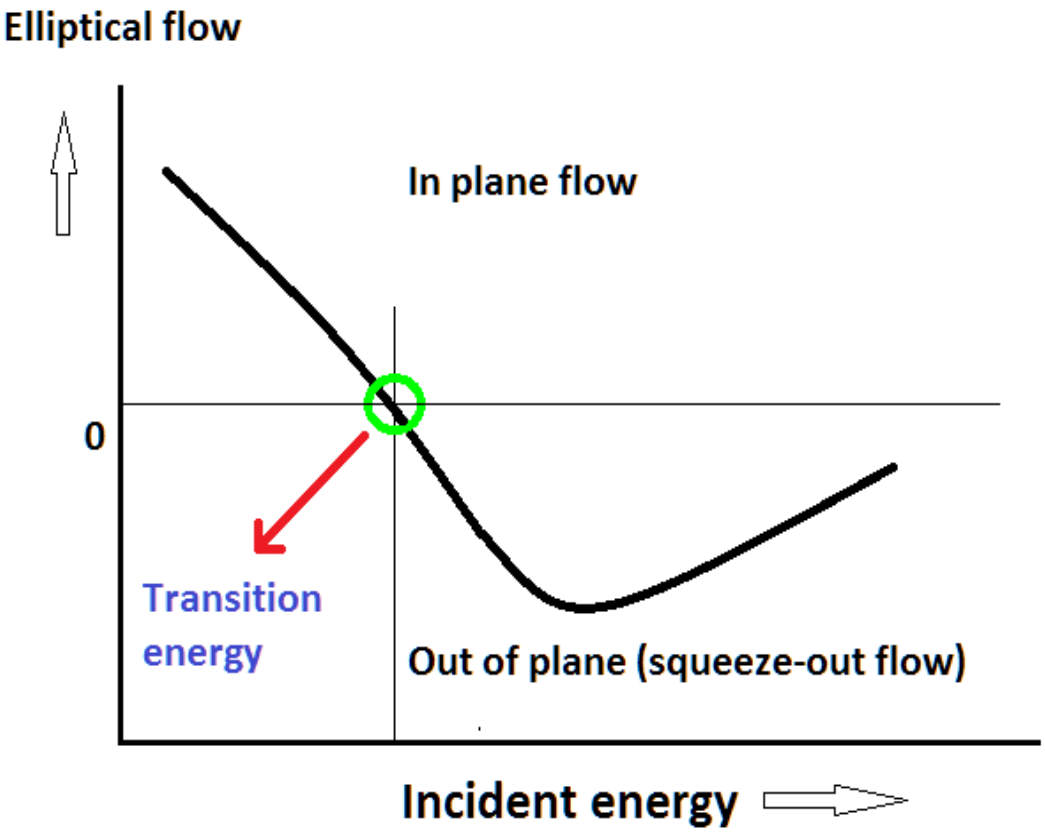

Figure 3.1: Pictorial representation of the transition energy.

3.2 Significance of multifragmentation around transition energy

Transition energy corresponds to the isotropic distribution of nuclear matter in the transverse reaction plane [186, 233-237]. In such a case, the values of elliptical flow becomes zero. Although independent studies of various phenomena are available in the literature, no correlated study is available in the literature that shows fragment structure at the transition energy of the elliptical flow. It is of the interest to know whether this structure differs from the multifragmentation obtained below or above the transition energy. Since transition energy is known for shape transition, one needs to investigate whether any non-trivial structure is obtained at the transition energy. In earlier times, Puri and coworkers studied the fragmentation structure at the balance energy and no particular pattern was observed there [238].

3.3 Results and discussion

In this chapter, we analyze the fragment production around transition energy. We have performed a complete systematic study of multifragmentation at the transition energy and compare the outcome at the incident energies below and above the transition energy. Results are spanned over the entire periodic table and, in particular, we simulate the reactions of $^{40}_{20}Ca + {}^{40}_{20}Ca$, $^{131}_{54}Xe + {}^{131}_{54}Xe$, and $^{197}_{79}Au + {}^{197}_{79}Au$. For the analysis, a hard equation of state has been employed, along with an isospin-dependent free nucleon-nucleon cross section.

The phase space generated by the *IQMD* model has been analyzed using the minimum spanning tree (MST) method and analysis packages discusssed in chapter 2. Phase space is analyzed at 200 fm/c. As reported in Ref. [186], the transition energies for the reactions $^{40}_{20}Ca + {}^{40}_{20}Ca$, $^{131}_{54}Xe + {}^{131}_{54}Xe$, and $^{197}_{79}Au + {}^{197}_{79}Au$, are 325, 150, and 140 MeV/nucleon, respectively, for free nucleons, and 210, 140, and 135 MeV/nucleon for LCP's, respectively. Therefore, these reactions have been simulated at their corresponding transition energies, as well as at the incident energies below and above the transition energies.

3.3.1 Time evolution of light fragments

In Fig. 3.2, the time evolution of FN's as well as LCP's is displayed, corresponding to the reactions of $^{40}_{20}Ca +^{40}_{20} Ca$, $^{131}_{54}Xe +^{131}_{54} Xe$, and $^{197}_{79}Au +^{197}_{79} Au$. We also display the results at the incident energies of 100 MeV/nucleon (below the transition energy) as well as 400 MeV/nucleon (above the transition energy). A steady increase is observed in the production of FN's as well as LCP's with an increase in incident energy. We do not see a particular behavior at the corresponding transition energies. One can see that the reaction is over quite early in lighter colliding nuclei compared to heavier, where nucleonic interactions keep going for longer times. No typical behavior is observed at the transition energies. In addition to the mean-field and NN collisions, other effects like the expansion of matter above the transition energy and shadowing of the spectator below the transition energy take place. One should note that FN's result from the binary collisions, whereas for the production of LCP's, mean field plays a dominant role.

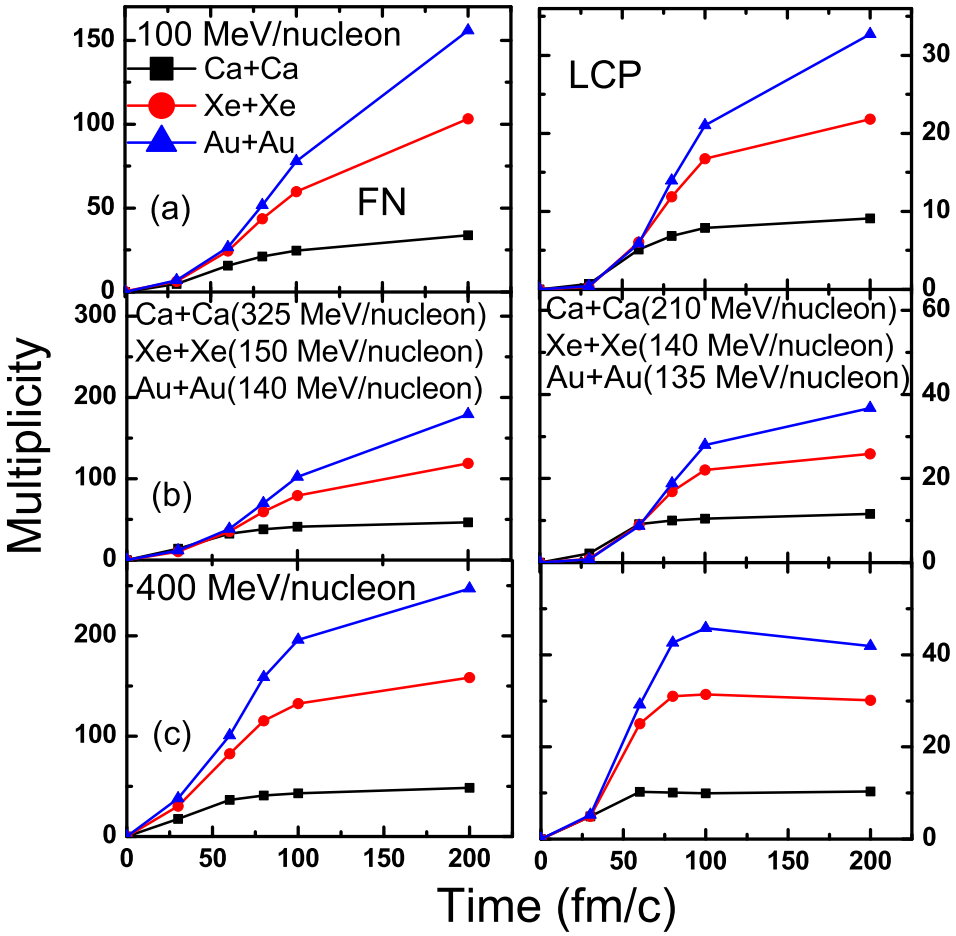

Figure 3.2: The time evolution of multiplicity for FN's (left panels) and LCP's (right panels). (a) Top, (b) middle, and (c) bottom panels represent three different incident beam energies, i.e., below transition, at transition, and above transition energy, respectively.

3.3.2 Variation of number of particles with transverse momentum

In Fig. 3.3, we display the number of particles in a particular transverse-momentum region. The transverse momentum is a factor that is used in the denominator of the elliptical flow. The transverse momentum is equal to the sum of the squares of momentum in x and y directions, assuming the reaction plane to be the xz plane. Again, it is clear from the figure that, with an increase in the incident energy from below to above the transition energy, the nucleon with larger transverse momentum starts dominating the physics. Nucleons with a high p_t tail start emerging, indicating that highly energetic nucleons appear at the incident energies above the transition energy.

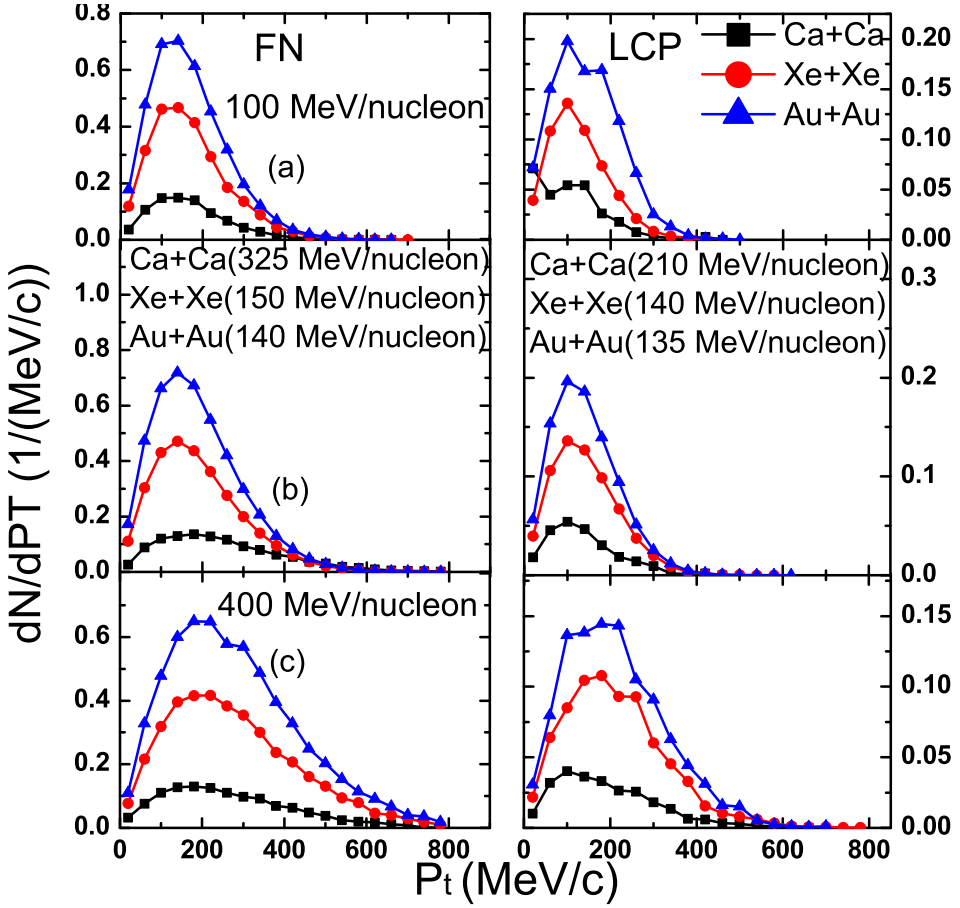

Figure 3.3: Transverse momentum spectra as a function of P_t for FN's (left panels) and LCP's (right panels). The different panels have the same meaning as those of Fig. 3.2.

3.3.3 Rapidity distribution of fragments

To observe nucleonic stopping, we plot the rapidity distribution in Fig. 3.4. It is observed that fragments are insensitive toward the nuclear stopping. This is in agreement with Ref. [239]. Moreover, nuclear stopping is found to vary above and below the transition energy. The rapidity distribution denotes the nuclear stopping in terms of Gaussians. The narrower the Gaussian, the more nuclear stopping occurs. From the graph, it is also clear that the Gaussian is narrower for the energy at which the elliptical flow is at its maximum, and starts becoming broader below and above this particular energy of maximum elliptical flow. One can further say that, for nuclear stopping, the energy at which the elliptical flow is at its maximum is more important compared to the values at which the transition from positive to negative values takes place, i.e., changing from

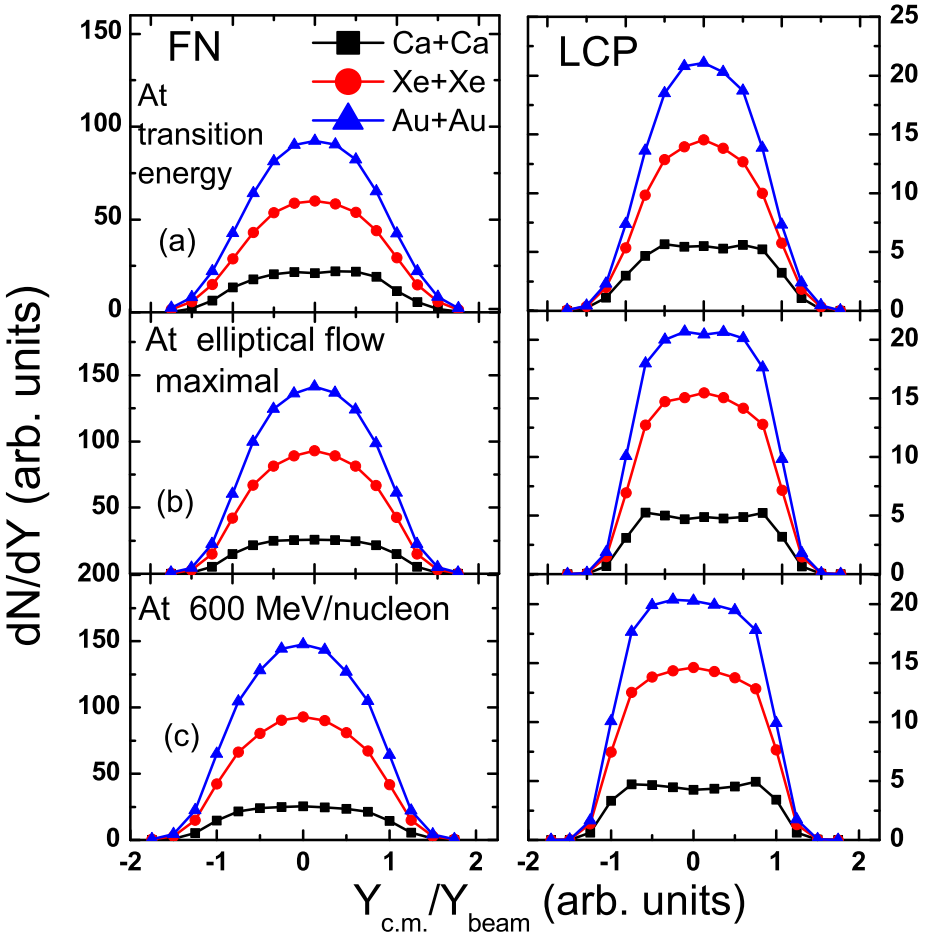

Figure 3.4: Rapidity distribution of FN's (left panels) and LCP's (right panels). The (b) middle panels represent the rapidity distribution at the energy at which there is maximal elliptical flow. The (a) top and (c) bottom panels represent rapidity distribution at the transition energy and at 600 MeV/nucleon, respectively

rotational to expansion behavior. Interestingly, Gaussians are narrower for free particles compared to LCP's. Kumar *et al.* [239] showed that free particles fail to explain some of the properties of nuclear stopping, while all properties can be explained by the LCP's in a reasonable manner.

3.3.4 Incident energy dependence of fragment multiplicity

From the above discussion for Figs. 3.2 and 3.3, it is quite important to see the incident-energy dependence of the multifragmentation (i.e., for FN's and LCP's). Once again, different behavior of fragments observed at different incident energies (as shown in Fig. 3.5). The free particles are found to increase with the incident energy while LCP's are

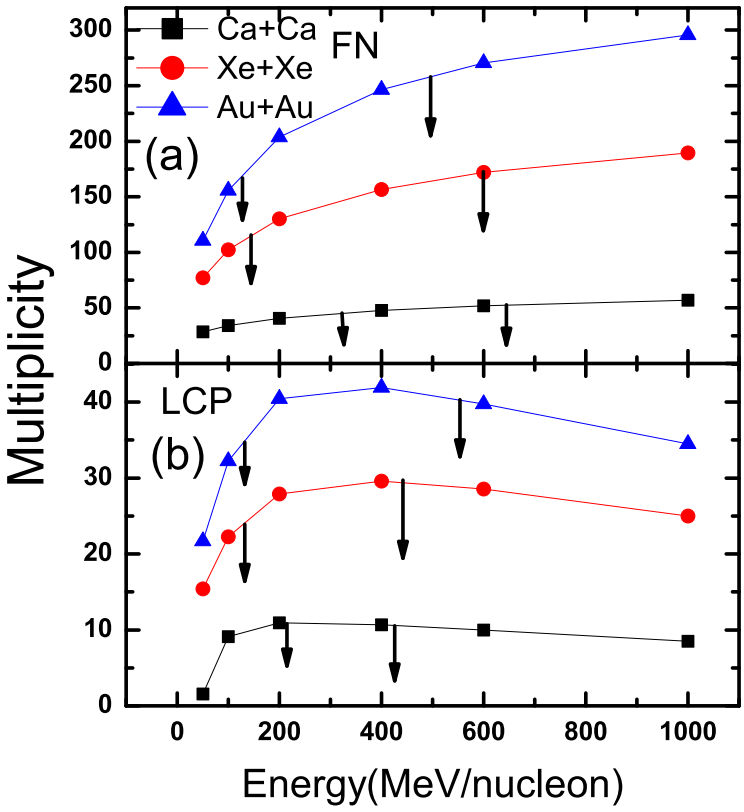

Figure 3.5: Incident-energy dependence of the multiplicities for different symmetric systems for (a) FN's and (b) LCP's. The first point is the transition point of elliptic flow and the second arrow is the energy, where the elliptical flow reaches its maximum value.

found to decrease after a certain incident energy. The change in the behavior is also true for the elliptical flow and nuclear stopping. This indicates that the study of LCP's, below, at, and above the transition energy, is more important compared to the study of free particles. The arrows in Fig. 3.5 indicate the values for different systems at which the transition takes place, as well as values corresponding to the maximal elliptical flow. From the lower panel, it is observed that as soon as the elliptical flow reaches its maximum, the production of the LCP's starts varying drastically. From here, it is clear that there is a resemblance in the behavior of LCP's, nuclear stopping, and elliptical flow, which can be the backbone of heavy-ion physics.

3.3.5 Mass dependence of fragment multiplicity

Finally, we have tried to fit the multiplicity of FN's and LCP's with the total mass of the system at the corresponding transition energies, as well as at the incident energies

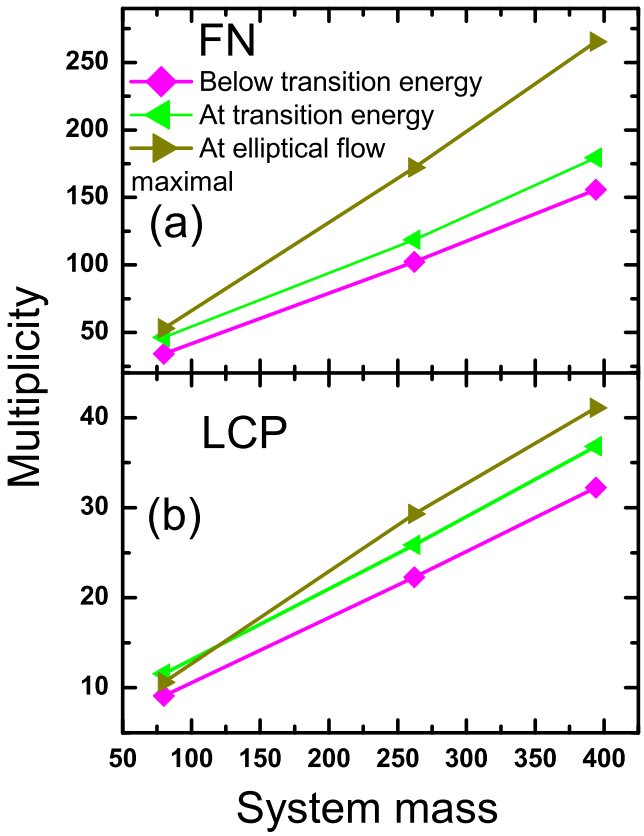

Figure 3.6: Multiplicity as a function of the composite mass of the system for (a) FN's and (b) LCP's.

below and above the transition energies in Fig. 3.6. The free particles and LCP's are found to increase with an increase in the mass number of the system. The main point to be noted is that the variation in the free particles with the variation in the energy is greater compared to LCP's. This is one of the important points in the present study. The reason for larger variation is that, the free nucleons originate from the participant zone, which keeps increasing with the increase in incident energy. On the other hand, LCP's also have some contributions from the spectator matter, in contrast to the free nucleons that emerge from the participant region only. For this reason, the difference in the production of LCP's is less compared to the production of the free particles. We also fit the multiplicity in terms of the mass number. The multiplicity is parameterized as the power law of the form A^{τ}. The values of τ in the case of free nucleons at different incident energies, i.e., below, at, and above the transition energy, are 0.97, 0.88, and 1.02, respectively. Similarly, the values of τ in the case of LCP's are 0.81, 0.74, and 0.84 at the three

different incident energies, i.e., below, at, and above the transition energy, respectively. The variation in the values of τ is greater in the case of FN's compared to LCP's.

3.4 Summary

Various properties of multifragmentation for different reacting systems at incident energies between 50 and 1000 MeV/nucleon has been investigated. Our detailed study over a wide range of incident energies showed no typical structure at the transition energies. We observed a continuous homogeneous change in the production of light charged particles and free nucleons.

Chapter 4

Effect of density-dependent symmetry energy on fragmentation

4.1 Introduction

After the collision phase, the compressed nuclear matter shatters into a large number of fragments, where the size and multiplicity of these fragments scale with reaction conditions like incident energy, impact parameter and the mass of colliding nuclei. The multifragmentation has been recognized as an extremely important phenomenon to understand the methodology of the phase transition and nuclear matter equation of state. One of the prominent question is the cause of this breakup, where one is interested to know that whether it is a statistical process, making micro-canonical phase space model a proper tool or is it driven by the fluctuations during the collision [79, 80, 83, 240].

The observations deduced from the measurement of particles in the detector depend on the size of the colliding nuclei, on the beam energy as well as on the impact parameter, which is the distance between the centers of the two nuclei as depicted in Fig. 4.1. For details see [166, 230]. The impact parameter b characterizes the centrality of the collision. Ideally, only the nucleons in the overlapping zone, called fireball, participate in the collision. Other nucleons are called spectators which keep moving with unchanged velocities.

In addition to this, reaction dynamics driven by the asymmetric colliding nuclei are quite different compared to that of symmetric colliding nuclei. Also, the equation of state, nucleonic cross section, the density profiles of colliding nuclei, momentum dependence of the equation of state, and Gaussian width of nucleons have a considerable effect on the formation of fragments [180-185, 241]. The dissociation of the nuclear matter after the

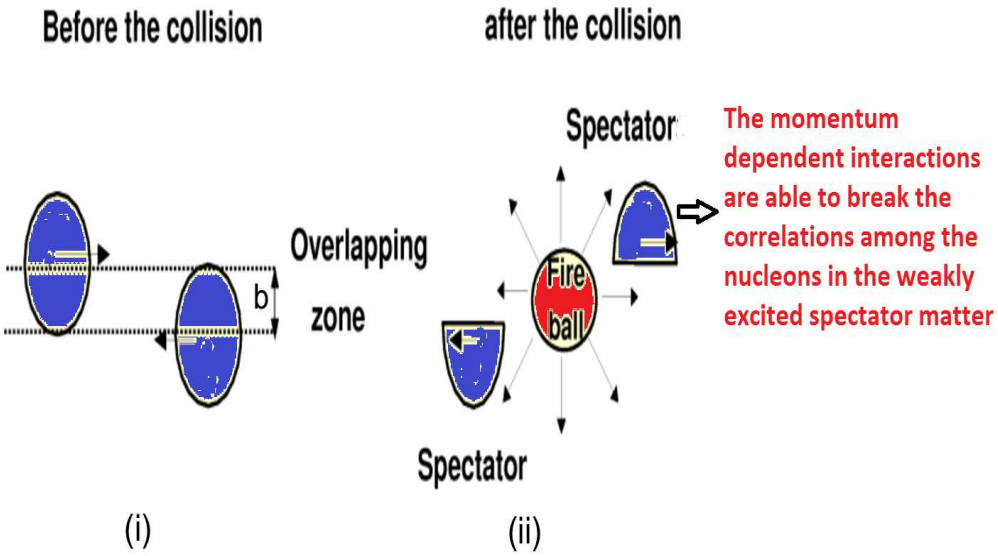

Figure 4.1: (i) The impact parameter b decides the overlapping zone; (ii) Spectator and fireball (participant) region formed after NN collision.

overlapping stage depends upon the compression generated during the collision, where the nuclei gets condensed with the emission of free nucleons and fragments. In addition to density, the compression generated during the collision is also influenced by the whole momentum plane of the reaction.

The momentum dependence of the nuclear EOS has been reported to affect the collective flow and particle production on a large scale [30, 242-245]. It is reported in the literature, [166, 168] that the pion yield was suppressed by 30 % once momentum dependent interactions were included in the evolution of the reaction. Moreover, the MDI's also suppress the nucleon-nucleon collisions/density by the same amount. Similarly, if one goes from soft to hard equation of state, the decrease in the pion yield is about 10 percent. Interestingly, a soft equation of state with momentum dependent interactions (SMD) yields the same transverse momentum as static hard equation of state [166, 168, 242, 243]. It was also concluded that SMD explains the data better than the hard equation of state

[246].

At the same time, compression generated during the collisions affect the strength of symmetry energy. The abrupt rise in the density during the overlapping of target and projectile results in a sizable variation of symmetry energy and similarly during the dissociation phase. The isospin content of the system and momentum dependence of the EOS affects the fate of the nucleons emitted from the fireball zone. We provide the details in the next section.

4.1.1 Exploring density dependence of symmetry energy with multifragmentation

As discussed earlier in chapter 1, the symmetry energy as well as its density dependence plays a crucial role in the dynamics of HIC's at intermediate and relativistic energies. Eqn. 1.7 provides the parametrization for the density dependence of symmetry energy. The outcome of the HIC's in the intermediate energy range is highly specific to the neutron content (or isospin-asymmetry) of the system. The hot and compressed nuclear matter gets condensed with the emission of large number of light and heavy mass fragments. The multiplicity of the light and heavy mass fragments scale with the incident energy and impact parameter of the reaction. As stated above, the phenomenon of multifragmentation takes place during the dissociation stage when the collision phase is over and the density of system is less than the normal nuclear matter density. Therefore, one is interested to carry out the investigation for the fragment formation for various forms of density dependent symmetry energy to probe the behavior of symmetry energy at sub-saturation densities. It has been stated in Chapter 1, that the various studies performed on fragmentation and particle production indicates the soft density dependence of symmetry energy in the low density region.

The different forms of symmetry energy leads to the different strengths of the symmetry potential at densities away from normal nuclear matter density. Here, one is interested to know that how much is the fragment formation affected by the density dependence of the symmetry energy. The investigation of the density dependence of symmetry energy was stimulated by the work performed in Refs. [86, 247]. The multifragmentation (dissociation of the nuclear matter after the overlapping phase) has always attracted the theoreticians as well as experimentalists [81, 99, 103, 166, 100, 230, 248, 249]. The reason

behind this is the several hidden phenomena can be explored only if we have an in-depth knowledge of the fragmentation. The rare astronomical phenomenon such as bing bang and the environment created just after that is similar to the freeze-out stage of HIC's. Hereby, to extract the essential physics via. multifragmentation, we have also included the momentum dependent interactions, which are favorable to explain the reaction dynamics compared to the static equation of state. Need for the momentum dependent interactions in HIC's is discussed in next section.

4.1.2 Need for the momentum dependent mean field

The ultimate motivation for the momentum dependent equation of state is the better understanding of the nuclear reactions, especially at peripheral collisions. It is acknowledged that the compressibility of the nuclear matter in HIC's does not depend only on the density but also on the entire momentum plane. This can be justified from the optical potential where strong momentum dependence was reported in the literature [168]. At different colliding geometries, there is a change in the size of the participant fireball and the spectator fragment region [250]. Also, it has a direct impact on the density and the compression reached during the collision. It has been reported that the peripheral collisions are more helpful in pinning down the role of MDI [251]. This is due to the fact that the EOS is also influenced by the relative velocities of the nucleons. At peripheral collisions, the nuclear matter is mildly excited. The momentum dependent interactions are able to break the correlation among the nucleons in the weakly excited spectator matter. However, the violent phase of reaction in central collisions witness larger participant zone, where the nucleon-nucleon correlations are already broken.

No doubt, equation of state apart from the population of nucleons also depends upon their relative velocities. The momentum dependence of EOS has a significant impact on the fragment production [119, 245, 252, 253]. The inclusion of MDI results in the larger emission of free nucleons and light complex fragments. The repulsive nature of MDI and its effect on the reaction dynamics is also sensitive to the system size (mass of colliding partners). Kumar *et al.* [182] analyzed the role of system size and momentum dependent effects on the multifragmentation for the symmetric reactions of ${}^{40}_{20}Ca + {}^{40}_{20}Ca$, ${}^{58}_{28}Ni + {}^{58}_{28}Ni$, ${}^{93}_{41}Nb + {}^{93}_{41}Nb$, ${}^{131}_{54}Xe + {}^{131}_{54}Xe$, ${}^{167}_{68}Er + {}^{167}_{68}Er$, ${}^{197}_{79}Au + {}^{197}_{79}Au$, and

$^{238}_{92}U$ + $^{238}_{92}U$, at beam energies between 50 MeV/nucleon and 1000 MeV/nucleon for the whole colliding geometry. The study of system size effects in the presence of repulsive MDI yields a mass power law behavior. For the clear understanding of momentum dependent interactions, we provide a critical review of the role of momentum dependent interactions during nucleon-nucleon collisions.

4.1.3 Interplay of momentum dependent interactions during nucleon-nucleon collision

The static interactions represented by V^{Skyrme} depend solely on the density ρ, where the parameter C leads to different incompressibility which refers to the different equations of state. The static equation of state ($\propto \ \rho$) is not sufficient to describe the exact reaction picture because the Skyrme parametrization being an oversimplified prescription does not include the exchange effects on nucleon-nucleon interactions. In the frame work of G-matrix, which is a solution of Bethe-Goldstone equation, the momentum dependence comes in a natural way [174]. However, one cannot solve the Bethe-Goldstone equation numerically at each point in phase-space and time. The concept of momentum dependence of the mean field arises from the optical model potential fitted to NN scattering data [166, 168]. Here, the parameterized momentum dependent potential takes care of the momentum dependence. This parametrization includes the density- and momentum-dependent G-matrix elements in terms of two-body interaction. First of all, a density- and momentum-dependent two-body potential between two particles, V $(\rho, \mid \mathbf{p} - \mathbf{p}' \mid)$ is defined, which is parameterized in the form:

$$V(\rho, \mathbf{p}) = \sum_{i=0}^{3} \sum_{j=1}^{3} a_{ij} (\rho/\rho_0)^j p^i \tag{4.1}$$

The momentum-dependent interactions (MDI) are obtained by parameterizing the term taken from the measured energy dependence of the nucleon-nucleus optical potential. Its parametrization is explained in Eqn. 2.38.

A parameterized form of the local plus momentum-dependent potential ($V^{loc} + V^{MDI}$) is given by:

$$U = V^{loc} \ + \ V^{MDI} \ = \ A\left(\frac{\rho}{\rho_0}\right) + B\left(\frac{\rho}{\rho_0}\right)^C + \delta_M . \ln^2\left(\epsilon.(\triangle p)^2 + 1\right) . \left(\frac{\rho}{\rho_0}\right) \tag{4.2}$$

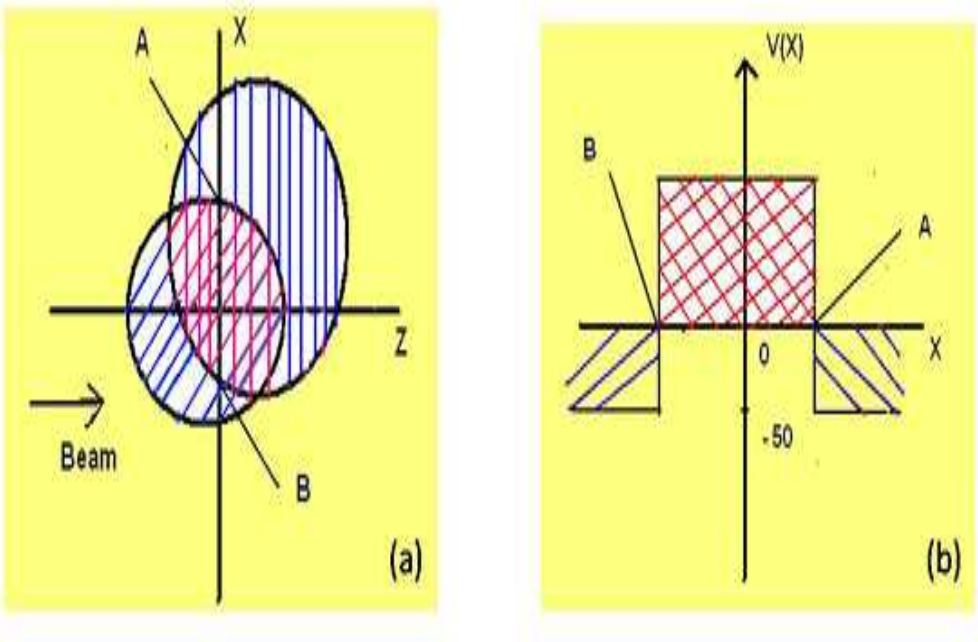

Figure 4.2: The transverse momentum caused by the momentum-dependent forces. (a) The reaction in the beam-impact parameter plane. (b) The potential along the x-axis. We see in the overlap region a strong repulsive and outside it, an attractive potential. The figure is taken from Ref. [166].

It can be used to compute the corresponding density dependence of the compressional energy per nucleon. The soft (S) and hard (H) equations of state along with momentum-dependent interactions are dubbed as soft momentum dependent (SMD) and hard momentum dependent (HMD) EOS, respectively. During the Covariant formulation of *BUU* approach, an another implementation of momentum-dependent interactions can be achieved. For details, please see Ref. [254, 255].

During the reaction, the relative momentum between the interacting nucleons is very small as long as the projectile and target do not overlap. Therefore, momentum-dependent interactions play a negligible role at that time. As soon as the projectile and target begin to overlap (see Fig. 4.2 (a)), nucleons of very large relative momenta are close to each other. Due to such large relative momentum, projectile nucleons feel a very strong repulsion to target nucleons and vice versa. On the other hand, outside the overlap zone,

nucleons in spectator zone are either from the projectile or target. Thus, the potential is still attractive in that region (see Fig. 4.2 (b)). Thus there is a strong potential gradient perpendicular to the beam direction, i.e. along the impact parameter. This causes the larger scattering of nucleons outside the overlap zone in the transverse direction quite early during the reaction. This also leads to decrease in density as well as number of collisions. Thus, observables which are connected to NN collisions should reflect this behavior of momentum-dependent interactions. The compressional energy per particle for static (soft and hard EOS) and momentum-dependent interactions (SMD and HMD EOS) as a function of density is shown in Fig. 2.1. From the figure, it is clear that there is no difference between static and momentum-dependent EOS at normal nuclear matter density. On the contrary, as we go above normal nuclear matter density, the difference between different equations of state goes on increasing. Thus, the momentum-dependent interactions govern the dynamics of heavy-ion collisions.

At different colliding geometries, the density and compression generated by the overlapping nuclei gets affected to a large extent. This variation in the density will affect the strength of symmetry energy during the whole time span of the reaction. For the better theoretical interpretation of HIC's, we investigate the collective effect of density dependent symmetry energy and MDI on the fragmentation. In addition to that, we study the effect of Coulomb interactions on the fragment formation. The charge distribution of nuclear matter in HIC's is analyzed and the theoretical predictions have been compared with experimental data.

4.2 Results and discussion

For the present analysis, we simulate the reaction of ${}^{197}_{79}Au + {}^{197}_{79}Au$ for the whole colliding geometry at various incident energies. In addition, we simulated the reactions of ${}^{58}_{28}Ni + {}^{58}_{28}Ni$, ${}^{124}_{54}Xe + {}^{124}_{54}Xe$, ${}^{20}_{10}Ne + {}^{27}_{13}Al$, ${}^{40}_{18}Ar + {}^{45}_{21}Sc$, ${}^{84}_{36}Kr + {}^{93}_{41}Nb$, ${}^{129}_{54}Xe + {}^{139}_{57}La$, and ${}^{129}_{54}Xe + {}^{119}_{50}Sn$ and compared the theoretical results with experimental findings. The phase space generated by the *IQMD* model has been analyzed using the minimum spanning tree *(MST)* method and *MST(M)* method.

4.2.1 Time evolution of fragment multiplicity

In view of the findings of Chen *et al.* [53], it is believed that the best estimate of the density dependence of the symmetry energy can be extracted from the heavy-ion reaction studies using Eqn. 1.7. It has been reported that the stiffness parameter $\gamma = 0.69$ is among the best candidates to study the density dependent symmetry energy in theoretical calculations [26]. This form of the density dependence of the symmetry energy is consistent with the parametrization adopted by the Heiselberg and Hjorth-Jensen in their study on neutron stars [37].

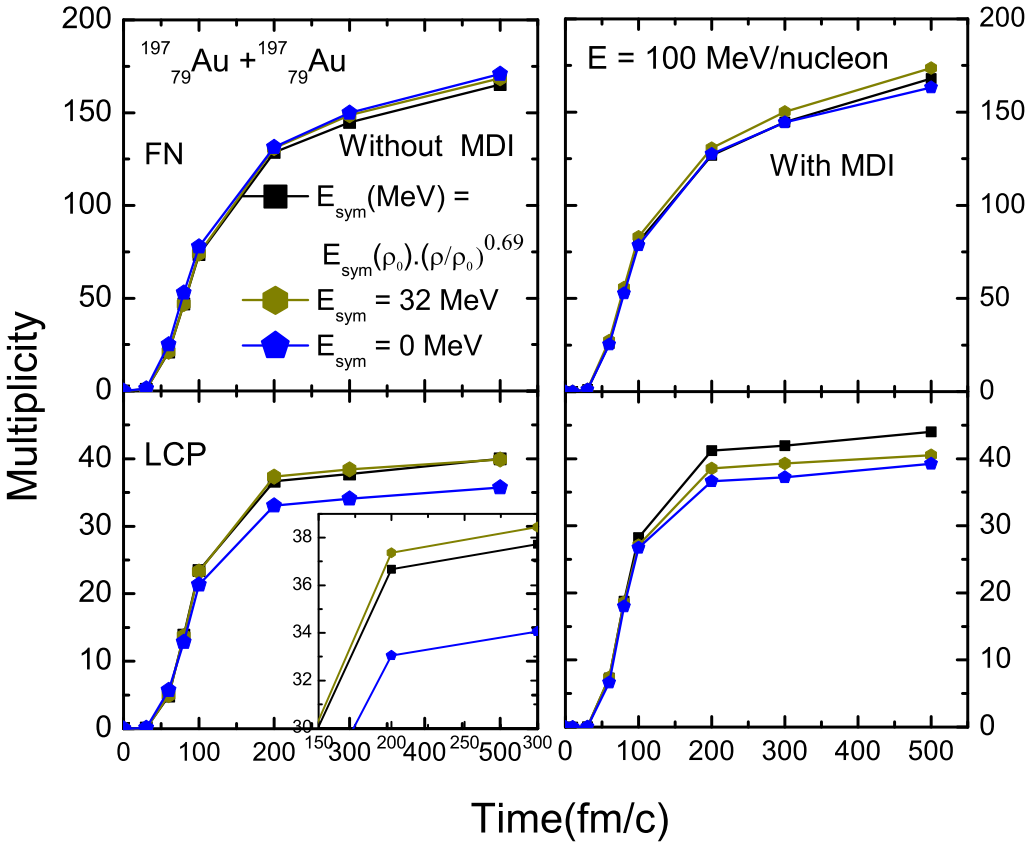

Figure 4.3: The time evolution of the FN's (upper panel) and LCP's (bottom panel) for the reaction of $^{197}_{79}Au + ^{197}_{79}Au$ at E = 100 MeV/nucleon.

In Fig. 4.3, we display the time evolution of FN's and LCP's for symmetry energy 32 MeV, 0 MeV and for $32(\rho/\rho_0)^{0.69}$ MeV to study the effect of symmetry energy on fragmentation, without MDI (left panel) and with MDI (right panel). The trends observed through simulations shows more sensitivity of LCP's towards symmetry energy. In contrary, to the FN's, LCP's are more affected by the different forms of the symmetry

energy. The larger sensitivity of LCP's towards symmetry energy is due to the pairing nature of LCP's, because the symmetry energy term $\propto\ (N-Z)^2$ contributes considerably. With zero symmetry energy, we see that fewer LCP's are produced, whereas the maximum production scale with the symmetry energy. The reduced value of γ leads to mild effect compared to full symmetry energy strength. The inclusion of MDI results in larger variation of fragment production for $\gamma = 0.69$. Its worth to carry out the investigation for the density dependence of symmetry energy for the different values of γ, i.e., the forms of symmetry energy. Therefore, we perform a comparative study by parameterizing the percentage change in the FN's and LCP's multiplicity for the different values of γ.

4.2.2 Charge distribution of nuclear matter

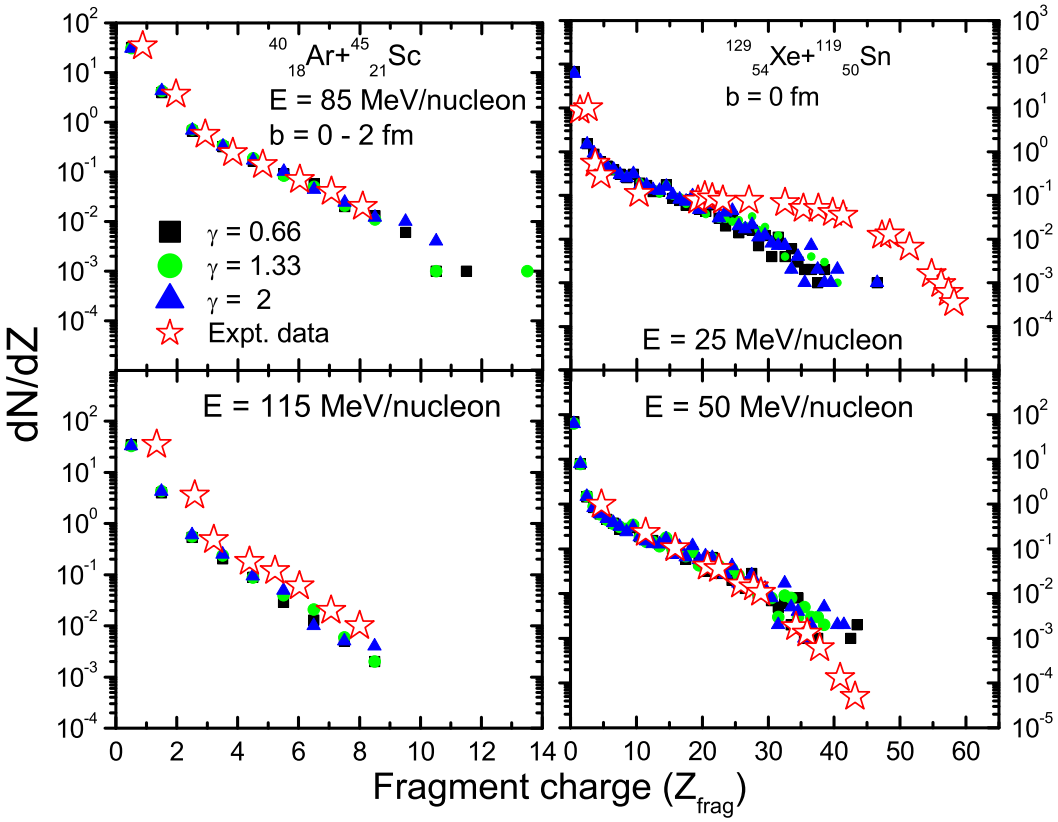

Figure 4.4: The charge distribution for the reaction $^{40}_{18}Ar\ +\ ^{45}_{21}Sc_{21}$ at the incident energy of 85 MeV/nucleon & 115 MeV/nucleon (left panels) and $^{129}_{54}Xe\ +\ ^{119}_{50}Sn$ at the incident energy of 25 MeV/nucleon & 50 MeV/nucleon (right panels) and a comparison with experimental data [256-260].

In addition to the fragmentation, the distribution of the nuclear matter after collision

can also be studied through the charge distribution corresponding to the nuclear matter. In Fig. 4.4, we display the charge distribution (dN/dZ) as a function of fragment's charge (Z_{frag}) for the reaction of $^{40}_{18}Ar + ^{45}_{21}Sc$ (left panels) and $^{129}_{54}Xe + ^{119}_{50}Sn$ (right panels) and comparison with the experimental data [256-260]. The charge distribution (dN/dZ) as a function of charge gives us a clear picture of the nuclear matter dissociation. A linear dependence of the charge distribution can be seen. The negative slope of the charge distribution indicates a gradual transition of the spectator matter towards total disassembly. A very mild effect of density dependent symmetry energy on the charge distribution is observed. The increase in the incident energy corresponds to more steeper slope. For both the cases, the theoretical results are in good agreement with the experimental data [256-260].

4.2.3 Fragment production with different strength of symmetry energy

In Fig. 4.5, we display the percentage change in the production of FN's and LCP's at different colliding geometries for the reaction $^{197}_{79}Au + ^{197}_{79}Au$ for the different parameterizations of the density dependence of symmetry energy i.e., γ = 0.66, 0.7, 0.9, 1.33 and 2, without MDI (left panel) & with MDI (right panel). The FN's and LCP's multiplicity seems to be sensitive towards the different forms of the symmetry energy. Fig. 4.5 (left panel) shows that the effect of the symmetry energy is more at the semi-central collisions (i.e. $\hat{b} = 0.5$) for all the parameterizations of the density dependence of the symmetry energy. The percentage change in multiplicity is more in case of the LCP's as compared to the FN's for all the parameterizations of the density dependence of the symmetry energy. We see that, without MDI, the symmetry energy affect the fragment production within 2.7 % for FN's and 4.6 % for LCP's on an average. LCP's seems to be more sensitive towards the symmetry energy as concluded above in Fig. 4.3. However, in Fig. 4.5 (left panel), the multiplicity of FN's as a function of scaled impact parameter shows the larger change in the multiplicity for lesser values of gamma. After achieving a saturation value at $\gamma = 0.7$, the peak value tends to decrease for the value of γ above and below it. The findings of Shetty *et al.* [26] and Heiselberg *et al.* [37] indicates that for $\gamma = 0.69$ the symmetry energy provides a better description of the nuclear matter equation of state at sub nuclear densities. The maximum change is said to be observed for the $\gamma = 0.7$ and

$\gamma = 0.66$ for the FN's and the LCP's respectively. In central collisions, nearly no effect is seen. This happens due to the violent phase of collision for central geometry.

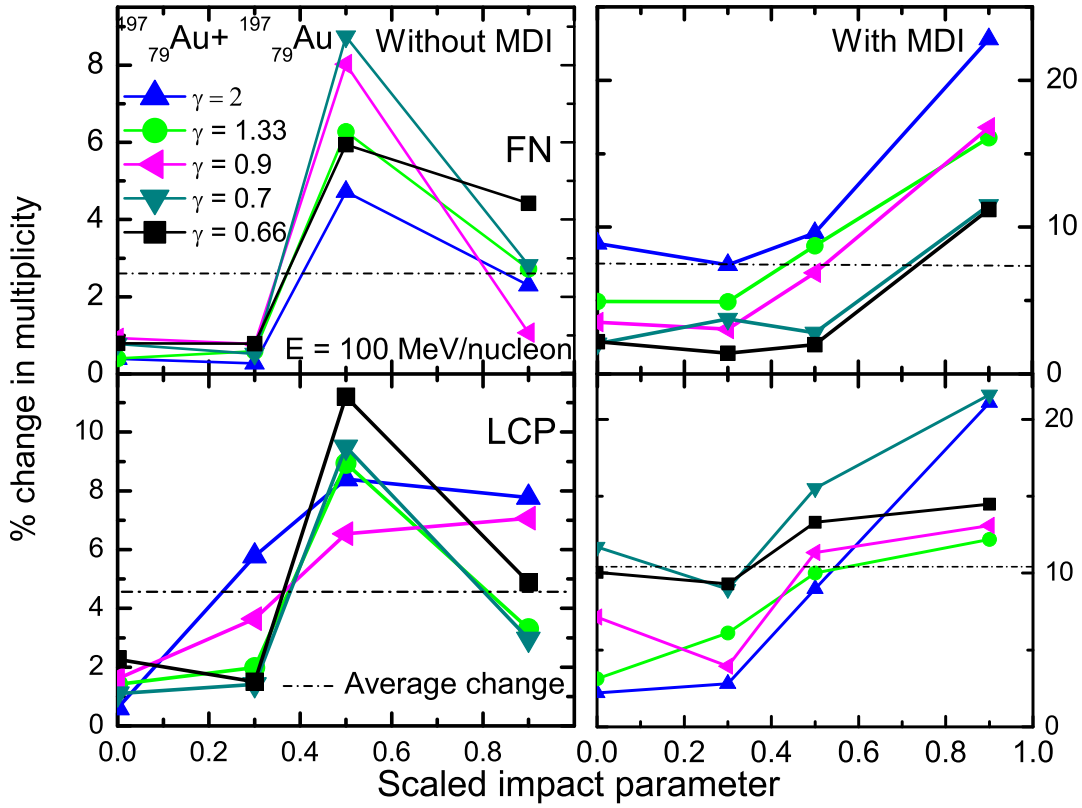

Figure 4.5: Percentage change in the multiplicity as a function of scaled impact parameter for different parameterizations of the density dependence of the symmetry energy for the system $^{197}_{79}Au + {}^{197}_{79}Au$.

In all cases, the effect of drastic variation in the form and strength of symmetry energy is less than 10 %. However, our findings are based at the incident energy of 100 MeV/nucleon. This energy is not large enough to see the huge variation in the production of fragments because the density achieved in collision is not so large. This is in agreement with the findings of the Lehaut *et al.* [148] where it was concluded that isospin content of the system has no major influence at low incident energies. In a major contribution, Dutt *et al.* [261] provides an evidence that at low incident energies, which belong to smaller baryonic densities, the isospin dependence of mean field potential was shown to yield same result obtained with potentials that has no isospin. The sensitivity of the fragment production can be easily observed for the different values of γ. We hereby, wants to probe the phenomenon of density dependence of symmetry energy through fragmentation.

However, the detected fragments corresponds to the sub-saturation density, therefore, it is not possible to see a huge variation in the fragment production w.r.t. density dependent symmetry energy. We observe that the inclusion of MDI results in the larger variation of the fragment production for the various forms of density dependent symmetry energy. The MDI and symmetry energy affects the fragment production within 7.5 % for FN's and 10.3 % for LCP's on an average for $\gamma = 0.66$ to 2. Therefore, our findings gives a clear indication of the role of MDI in multifragmentation and the momentum dependence of the symmetry energy. In Ref. [262], it has been reported that the momentum dependence of the symmetry potential has a significant role in nuclear reactions.

4.2.4 Excitation energy dependence of mean IMF multiplicity

In Fig. 4.6, we show the incident energy dependence of the mean IMF multiplicity and comparison with the *ALADIN* data [82, 100] for the central collisions. The momentum dependent interactions and symmetry energy seems to be less sensitive at low incident energies. The IMF multiplicity seems to be least sensitive at the incident energy of 100 MeV/nucleon. This is due to the less density achieved during the collision which is not sufficient to produce the effect of density dependent symmetry energy.

As the incident energy increases, the MDI and symmetry energy seems to affect the IMF production. At higher incident energies, the mean field does not plays any role. Though, MDI destabilizes the nuclei, a careful analysis is made by Puri *et al.,* [263] and found that upto 200 fm/c, emission of the nucleons with MDI is quite small. The repulsion produced due to MDI and symmetry energy tends to reduce the IMF production. The maximum effect can be observed around the incident energy of 400 MeV/nucleon. Therefore, the larger role of the symmetry energy can be observed at higher incident energies due to the larger variation in density. The effect of the symmetry energy and MDI seems to decrease at the incident energy above 400 MeV/nucleon because of the lesser overlapping time of the target and projectile due to the violent collision. The results obtained with the inclusion of MDI & $\gamma = 0.69$ favors the data.

In Fig. 4.7, we display the mean multiplicity of IMF's as a function of incident energy for the various systems and compared the results with the *NSCL* experimental data [264]. We here imply the momentum cut of the order of 150 MeV/c. The confrontation of the

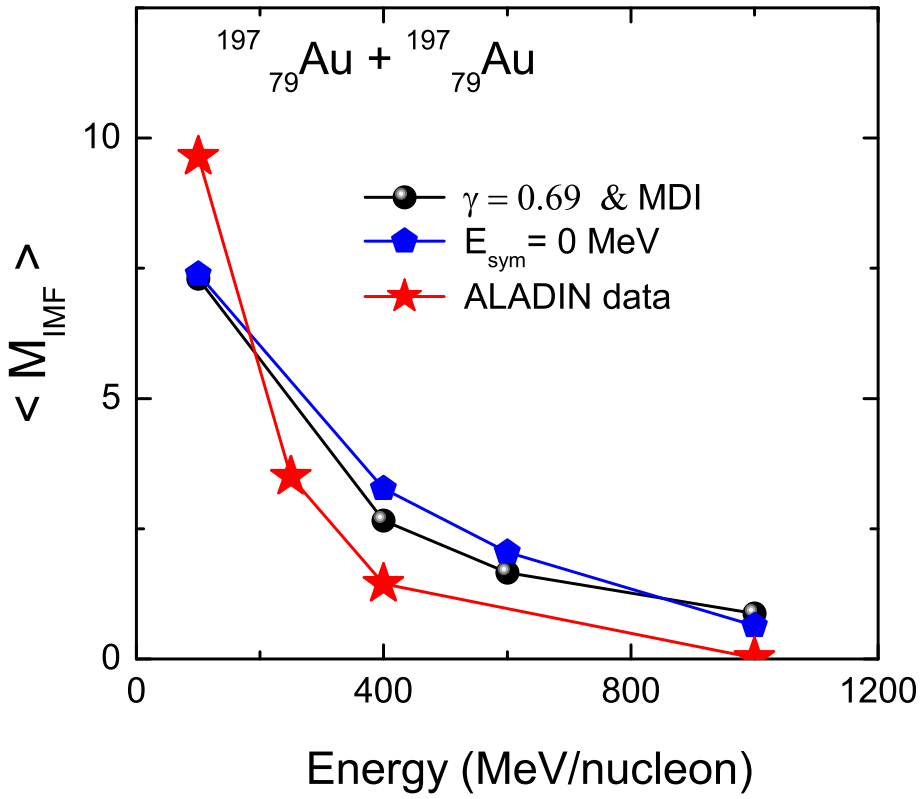

Figure 4.6: The incident energy dependence of the mean IMF multiplicity for the reaction of ${}^{197}_{79}Au + {}^{197}_{79}Au$ and comparison with *ALADIN* data [82, 100].

theoretical results with experimental findings can explain the complex processes which happen during the NN collisions. The theoretical predictions give similar trends those of the *NSCL* experimental data. For the reactions of ${}^{20}_{10}Ne + {}^{27}_{13}Al$ and ${}^{40}_{18}Ar + {}^{45}_{21}Sc$, the mean IMF multiplicity decreases with an increase in incident energy. However, for the reactions of ${}^{84}_{36}Kr + {}^{93}_{41}Nb$ and ${}^{131}_{54}Xe + {}^{139}_{57}La$, the mean IMF multiplicity increases with an increase in incident energy. Although, in these two reactions the incident energy is much less than the first two reactions. The dynamics at low incident energies is marked by the attractive mean field. At low incident energies, of the order of 20 MeV/nucleon we observed that the effect of symmetry energy vanishes, except ${}^{131}_{54}Xe + {}^{139}_{57}La$, which can be due to the large interplay of Coulomb interactions.

The stiffer form of symmetry energy, yields lesser symmetry energy repulsion in the low density region. That is why, the lesser neutrons are bound inside the bigger fragments in case of soft symmetry energy which decreases the IMF production. Similar findings are

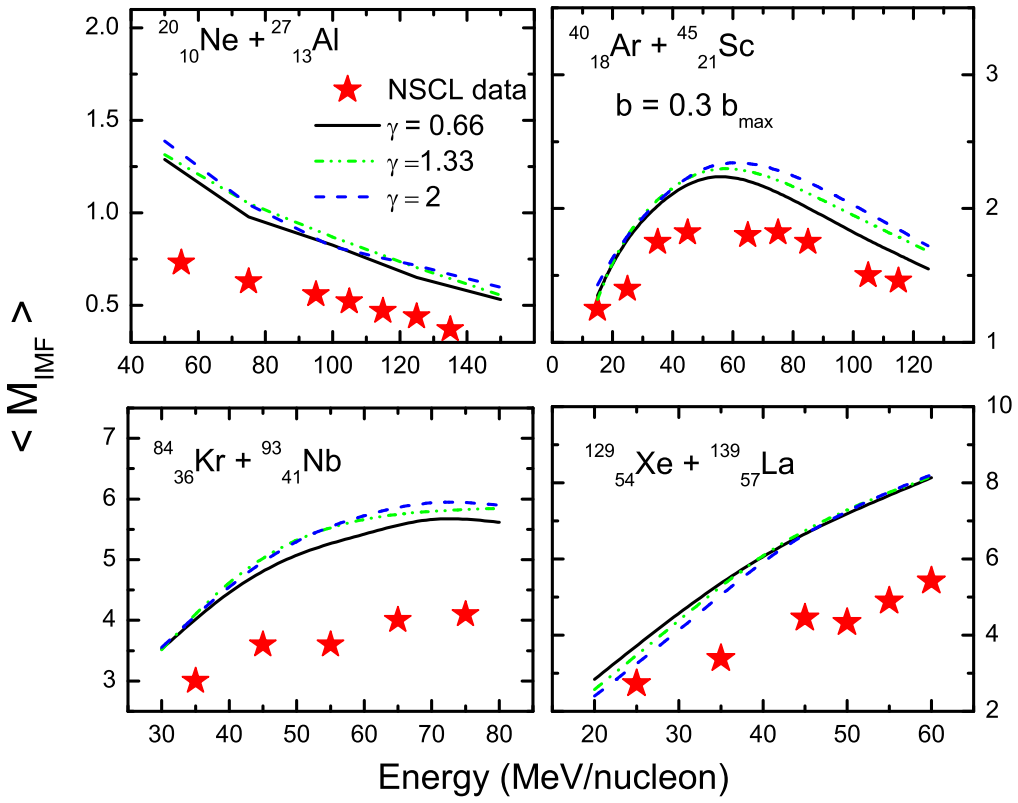

Figure 4.7: Mean multiplicities of IMF as a function of incident energy and comparison with the NSCL data [264].

also observed in Ref. [47], where the neutron (proton) yield was affected by the different forms of the density dependence of the symmetry energy. In case of system $^{131}_{54}Xe + ^{139}_{57}La$, Coulomb forces are more dominant. Overall, the symmetry energy with $\gamma = 0.66$ is more compatible with the NSCL data [264] compared to other forms ($\gamma = 1.33, 2$). Generally, soft density dependence of symmetry energy is recommended in the low density region [26, 47]. The present observations are also compatible with those findings.

4.2.5 Impact parameter dependence of IMF production

The impact parameter has a significant impact on the production of fragments. We display the mean IMF multiplicity for the whole colliding geometry in the Fig. 4.8. The fragment production is subjected to the *MST(M)* method. One can clearly observe the larger value of $< M_{IMF} >$, for the larger value of γ. The IMF production decreases with an increase in impact parameter of the reaction. At peripheral collisions, the overlapping of target and projectile is very less, which results in the formation of heavy mass fragments.

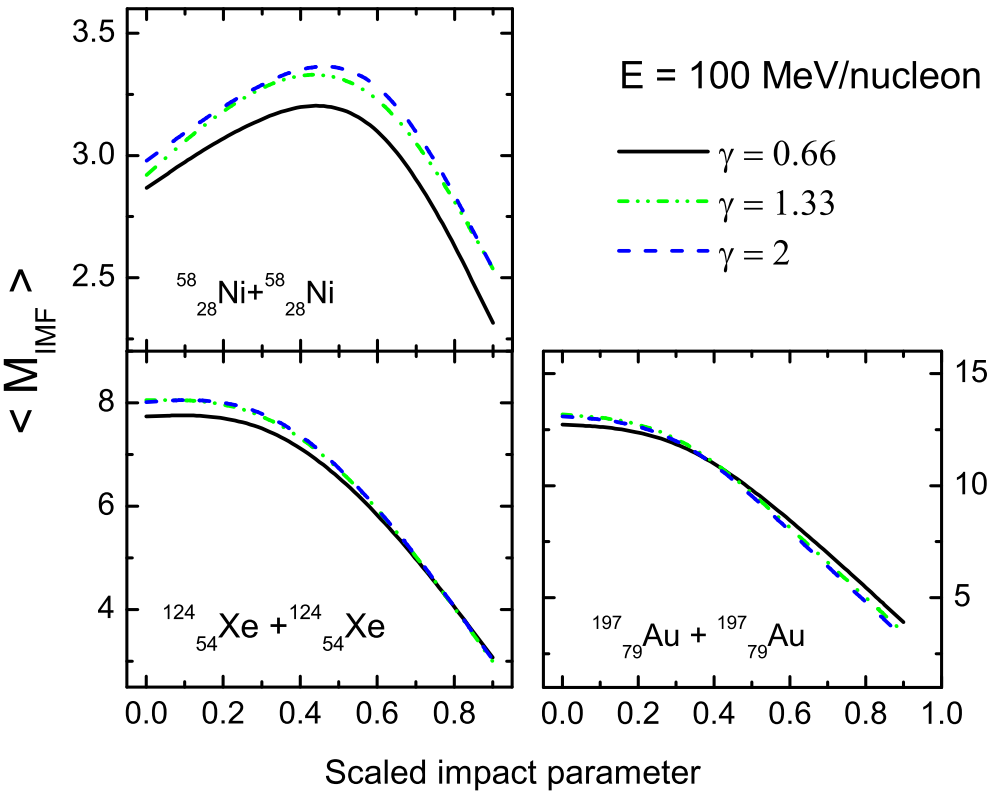

Figure 4.8: The impact parameter dependence of the mean IMF multiplicity at the incident energy of 100 MeV/nucleon.

However, for the heavier systems, $^{124}_{54}Xe + ^{124}_{54}Xe$ and $^{197}_{79}Au + ^{197}_{79}Au$, mild effect of symmetry energy is observed. The effect nearly diminishes at peripheral collisions. Interestingly, the IMF production for the system $^{58}_{28}Ni + ^{58}_{28}Ni$, shows a somehow rise and fall behavior, which is not observed in case of other two systems. In case of lighter system, the multiplicity of IMF decreases in central collisions compared to semi-central collisions. In heavier systems, the bigger size constitutes more mean field due to the larger nucleonic content and hence the IMF production is highest at central collisions. Here, the mean field dominates which suppress the production of FN's and LCP's.

Coulomb effect is more dominant in case of heavier systems. The larger proton content in the heavier systems increase the impact of Coulomb interactions. In such a case, the Coulomb interactions overcome the strength of symmetry energy. That is why, the IMF multiplicity is least affected in case of system $^{197}_{79}Au + ^{197}_{79}Au$. The pressure created due to Coulomb repulsion affects the IMF production due to the early boiling of the system

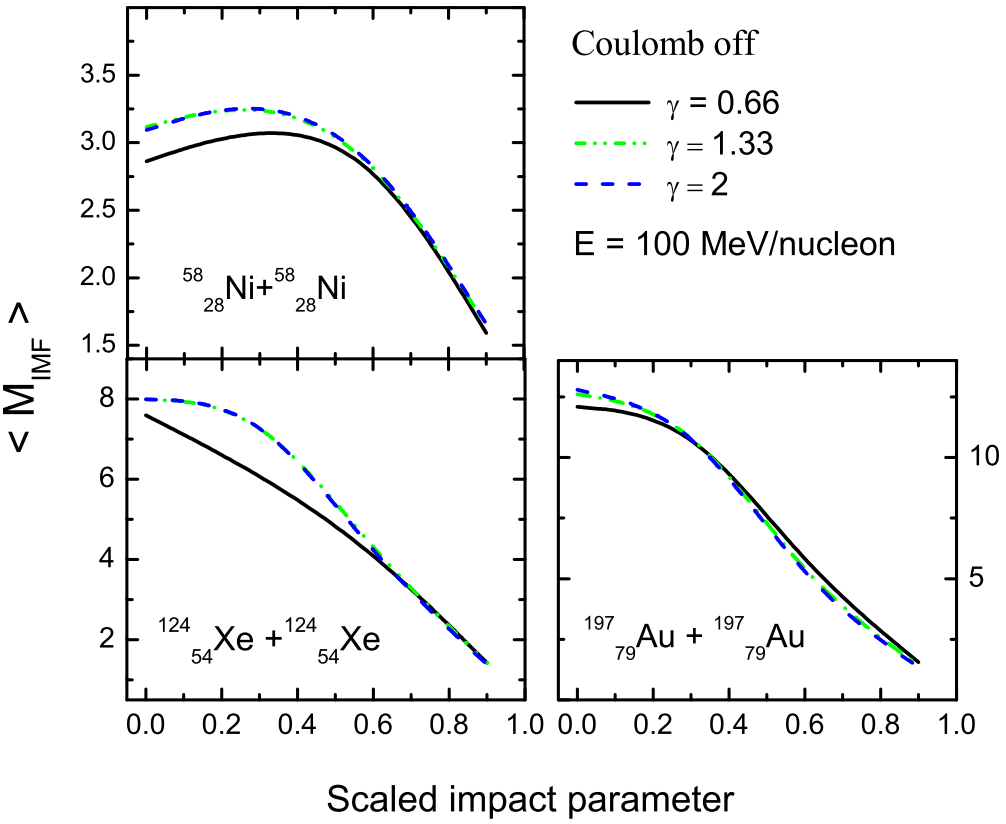

Figure 4.9: The impact parameter dependence of IMF multiplicity exhibiting the Coulomb interactions. The incident energy is 100 MeV/nucleon.

during the dissociation phase. The Coulomb interactions have more influence on the reaction dynamics in case of heavier systems (systems having larger proton content). One can see that the Coulomb interactions affect the IMF production drastically at peripheral collisions.

To study the effect of density dependent symmetry energy, we plot the impact parameter dependence of mean IMF multiplicity by excluding the Coulomb interactions in Fig. 4.9. We observed that in the absence of Coulomb interactions the effect of symmetry energy diminishes totally at the peripheral collisions. This is due to the fact that dissociation of nuclear matter is very less at larger impact parameters.

To understand the direct role of Coulomb interactions, we display the mean IMF multiplicity for the whole colliding geometry, in the absence of symmetry energy in Fig. 4.10. Overall, the IMF production increases with the inclusion of Coulomb interactions. This is due to the repulsion generated by the protons after the collision phase which

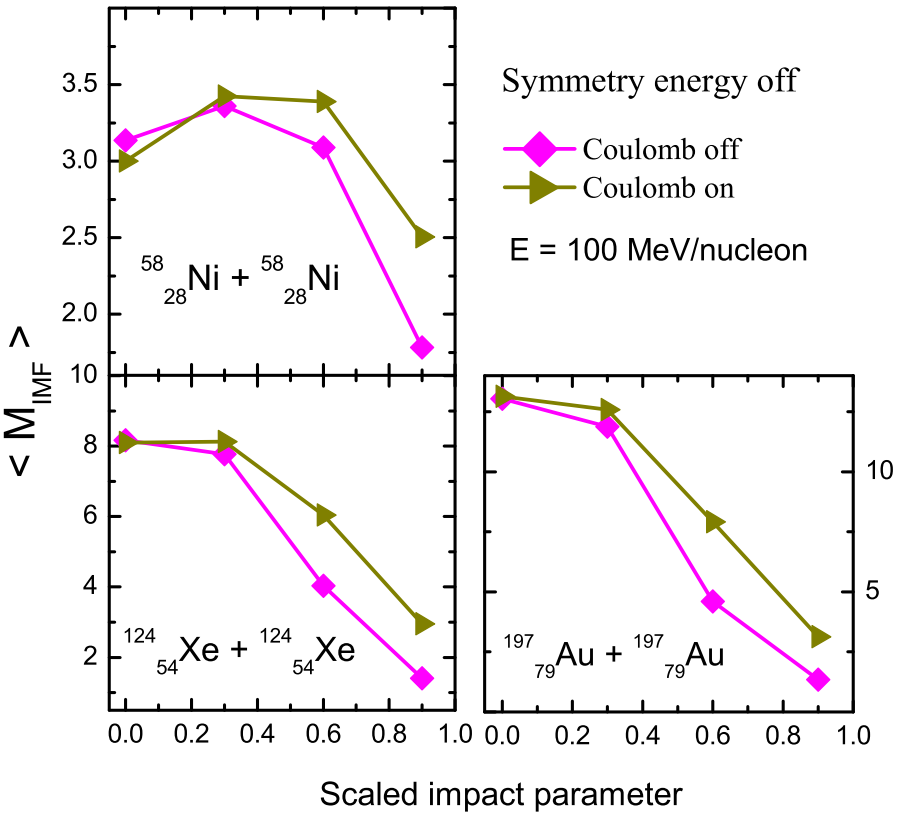

Figure 4.10: The impact parameter dependence of mean IMF multiplicity with the exclusion of symmetry energy. The incident energy is 100 MeV/nucleon.

enhance the production of IMF's due to the break-up of nuclei. One can clearly observe the larger effect of Coulomb interactions in the IMF production at peripheral geometries. This is due to the fact that violent collisions decrease the impact of Coulomb interactions. A significant role of Coulomb interactions in IMF production, especially at the peripheral collisions, tends to reduce the role of various forms of symmetry energy.

In Fig. 4.11, we display the mass of the heaviest fragment $< A_{max} >$ along the whole colliding geometry without symmetry energy. The value of $< A_{max} >$ increases with the impact parameter of the reaction. This happens due to the less violent phase of the reaction at peripheral collisions. The inclusion of Coulomb interactions results in the smaller value of $< A_{max} >$. The size of the largest fragment $< A_{max} >$ decreases due to the repulsion generated by the Coulomb interactions, which results in the formation of other smaller fragments.

In Fig. 4.12, we display the $< Z_{bound} >$ along the whole colliding geometry with and

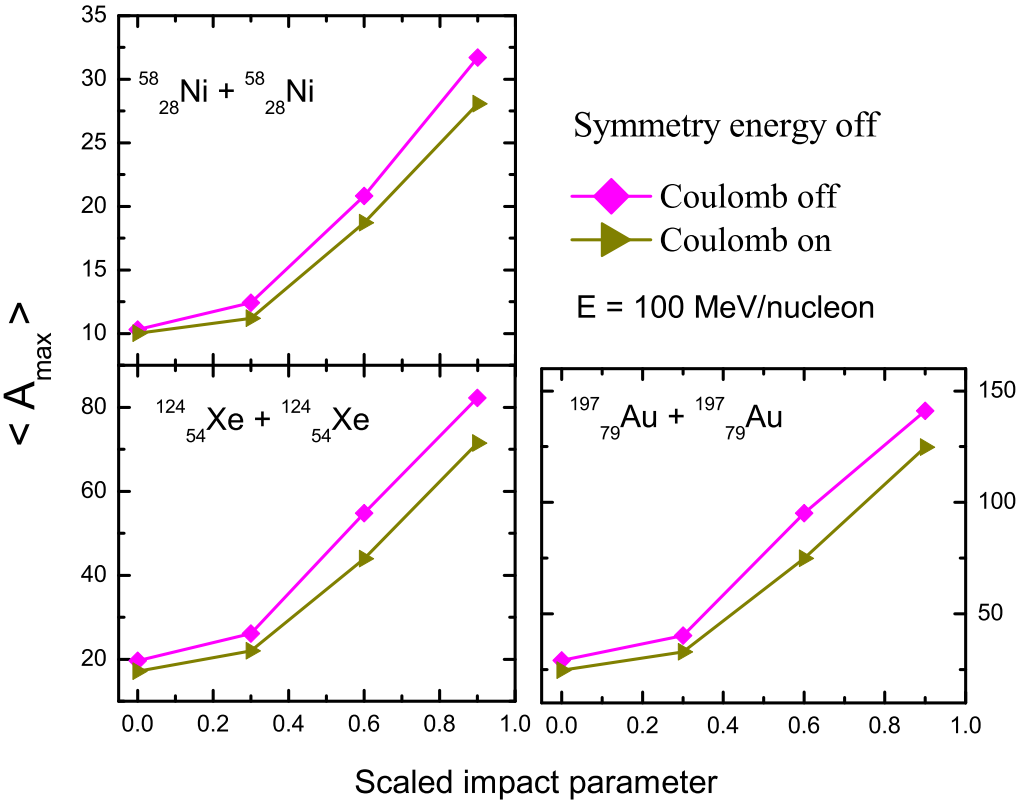

Figure 4.11: The variation in the mass of heaviest fragment $< A_{max} >$ along the whole colliding geometry and excluding symmetry energy. The incident energy is 100 MeV/nucleon.

without Coulomb interactions (exhibiting the symmetry energy). The quantity $< Z_{bound} >$ is defined as the sum of all atomic numbers (Z_i) of all projectile fragment with $Z_i \geq 2$. $< Z_{bound} >$ is a good parameter to measure the violence of the collision and of the energy deposited in the excited spectator. $< Z_{bound} >$ shows the similar behavior as that of $< A_{max} >$. This reflects the disintegration of $< Z_{bound} >$ with the inclusion of Coulomb interactions.

The correlation between the mean IMF multiplicity with scaled impact parameter is plotted for the system $^{197}_{79}Au + ^{197}_{79}Au$ in Fig. 4.13. The theoretical trends are in accordance with the data of *ALADIN* set up [82, 100]. The momentum cut of the order of 150 MeV/c have been applied to analyze the phase space. The maxima of IMF multiplicity is reached at semi-peripheral collisions. In case of central collisions, the violent collisions reduce the fragment production. While in case of peripheral collisions, the IMF production again decreases due to the lesser overlapping of the target and projectile. The inclusion of MDI

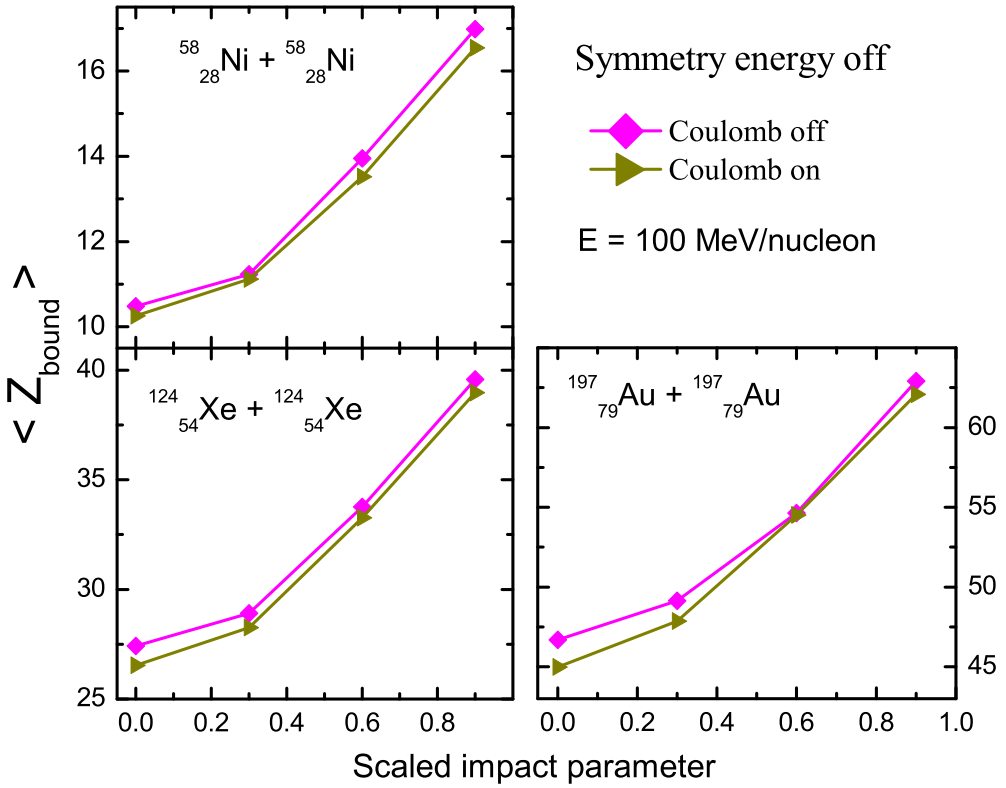

Figure 4.12: $< Z_{bound} >$ as a function of the scaled impact parameter for various systems at 100 MeV/nucleon.

& $\gamma = 0.69$, concludes a significant shift in the peak IMF multiplicity.

For further analysis, we have compared the theoretical predictions for the impact parameter dependence of IMF multiplicity for the system $^{197}_{79}Au + ^{197}_{79}Au$ with the data of *ALADIN* Collaboration [82, 100] at the incident energy of 400 MeV/nucleon as shown in Fig. 4.14. At the incident energy of 400 MeV/nucleon, repulsive nucleon-nucleon scattering dominates the reaction dynamics. Theoretical trends are in good agreement with the data of *ALADIN* set up [82, 100]. Indeed, the maximum IMF multiplicity is reached at semi-peripheral collisions. The peak of maximum production is shifted w.r.t. data in case we consider symmetry energy as a function of the density with MDI. The peak of maximum production is reached for central collisions in case we do not include the MDI. In case of central collisions, at the incident energy of 400 MeV/nucleon, the violent collision reduces the fragment production. While in case of the peripheral collisions, the IMF production again decreases due to the lesser overlapping of target and projectile.

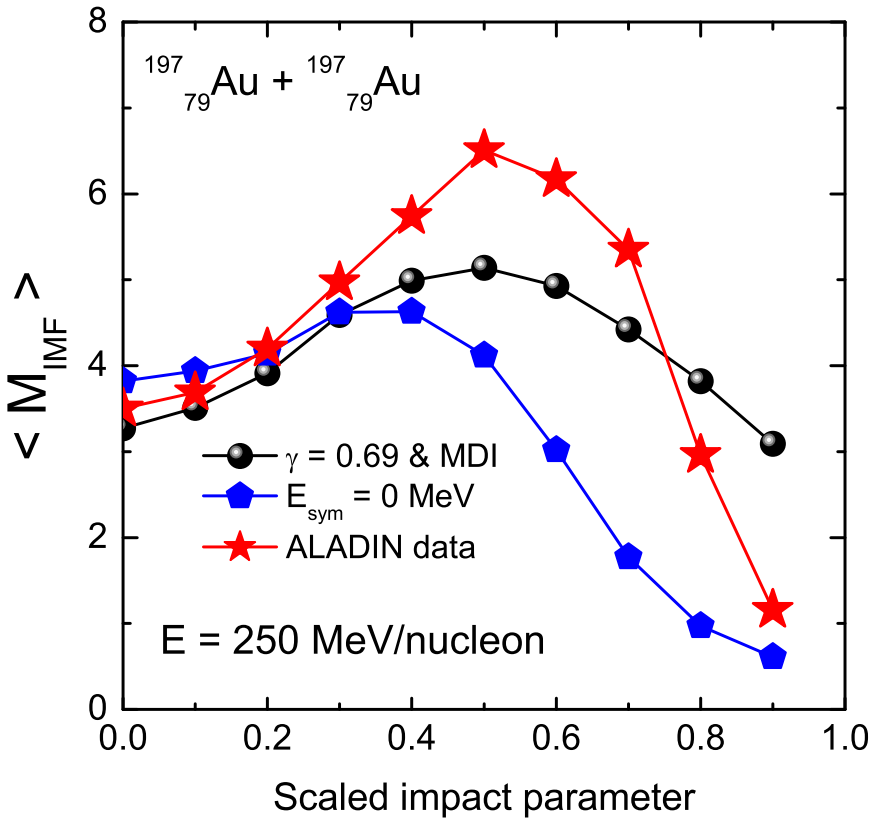

Figure 4.13: Impact parameter dependence of the mean IMF multiplicity at E = 250 MeV/nucleon for the system $^{197}_{79}Au + ^{197}_{79}Au$ and comparison with the ALADIN data [82, 100].

In such a case, heavy mass fragments are produced. The difference of theoretical results from experimental data is due to our no access to experimental filters under which data is taken.

4.3 Summary

We have investigated the effect of density dependent symmetry energy and momentum dependent interactions on the multiplicity of fragments. Our calculations shows larger sensitivity of LCP's towards symmetry energy. The fragment multiplicity seems to be affected by the symmetry energy at semi-peripheral and peripheral collisions. Overall, we see that symmetry energy affect the fragment production within 2.7 % for FN's and 4.6 % for LCP's on an average. This mild sensitivity can be attributed to the fact that the density at which the fragmentation takes place is not high enough to see the role of

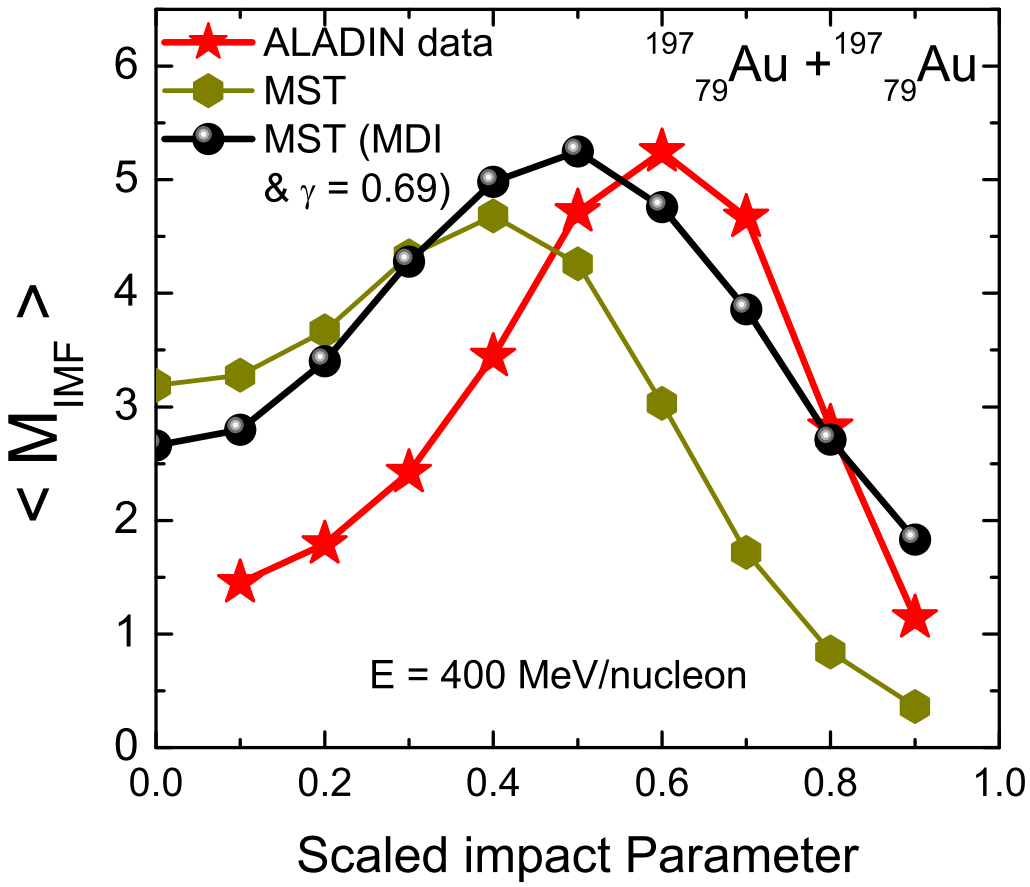

Figure 4.14: Impact parameter dependence of the mean IMF multiplicity at E = 400 MeV/nucleon for the reaction of $^{197}_{79}Au$ + $^{197}_{79}Au$.

various forms of symmetry energy. Also, the inclusion of MDI concludes larger variation, i.e. 7.5 % for FN's and 10.3 % for LCP's on an average. The momentum dependence of symmetry energy plays a significant role in multifragmentation.

Moreover, the IMF production and charge distribution shows a mild but considerable sensitivity towards the various forms of density dependent symmetry energy. This is due to the fact that the phenomenon of fragment production occurs after the collision phase is over, when the density of the system is below normal density. The IMF multiplicity increases with the stiffness of symmetry energy. As far as the fragment production of IMF's is concerned, the impact of density dependent symmetry energy reduces due to the early boiling of the system by Coulomb interactions in the heavier systems. The inclusion of Coulomb interaction results in the disintegration of heaviest fragment and increases the yield of intermediate mass fragments. The theoretical trends are in good agreement

with the experimental data.

Chapter 5

Effect of symmetry energy on the elliptical flow of fragments

5.1 Introduction

In the last chapter, the effect of density dependence of symmetry energy on multifragmentation is studied in detail. It is the need of the time to study the other aspects like collective flow and nuclear stopping parameters with respect to the different forms of density dependence of symmetry energy. In this chapter, we will deal with the elliptical flow of the fragments. Information about nuclear matter under extreme conditions of temperature and density and the role of symmetry energy under these conditions are still topics of crucial importance in the present day nuclear physics research. Among different observables, collective flow and its various forms enjoys a special status, due to its sensitivity towards the model ingredients that define an equation of state. The collective flow, especially the elliptical one, is highly sensitive to the isospin content of the system and can act as a good probe for the symmetry energy at sub-supra saturation densities.

Recently, many efforts have been made to study the collective flow both theoretically and experimentally in the heavy-ion collisions [50, 133, 139-141, 265-269]. The collective flow is a motion characterized by the space-momentum correlations of dynamic origin. The directed flow and elliptical flow are the two parameters available in the heavy-ion collisions to study the collective flow. The directed flow seems to be constrained only along the reaction plane which is due to the bounce-off of the compressed nuclear matter. However, the elliptical flow is more suited to study the collective flow which represents the complex interplay between the shadowing of the spectator matter and the expansion of hot compressed nuclei [186, 233-236]. Generally, the elliptical flow is the difference between

the major and minor axes. It describes the eccentricity of an ellipse like distribution. Elliptical flow is a fundamental observable since it directly reflects the initial spatial anisotropy, of the nuclear overlap region in the transverse plane, directly translated into the observed momentum distribution of identified particles. The spatial anisotropy is largest at the beginning of the reaction. That is why, the elliptical flow can give an overview of the early stages of system evolution during the overlapping of target and projectile. The details are discussed in next section.

5.2 Evolution of elliptical flow

The elliptical flow (or squeeze-out flow) is generated due to the anisotropic distribution of the nuclear matter, which is produced due to the non-central collisions resulting in an orthogonal asymmetry in the configuration space and re-scattering. Assuming x-z as the reaction plane, the initial "ellipticity" of the overlap zone is usually characterized by a quantity $\epsilon = \frac{y^2-x^2}{y^2+x^2}$. As the system expands, spatial anisotropy decreases. The orientation of the major axes is confined to the azimuthal angle ϕ; while $\phi + \frac{\pi}{2}$ indicates that the orientation of the ellipse is perpendicular to the reaction plane [270]. The out-of-plane enhancement of particles is observed clearly at the mid-rapidity.

Mathematically, elliptical flow can be written as;

$$v_2 \;=\; \langle \frac{p_x^2 - p_y^2}{p_x^2 + p_y^2} \rangle. \tag{5.1}$$

where p_x and p_y represents the x and y components of the momentum. The p_x is the component of momentum in the reaction plane, while p_y is perpendicular to the reaction plane. A positive (negative) value of the elliptical flow v_2 indicates in-plane (out-of plane) enhancement of the particle emission. The zero value of elliptical flow corresponds to an isotropic distribution of nuclear matter in the transverse plane. The highly stopped and compressed nuclear matter around the mid-rapidity region ($\mid Y_{red.} \mid = \mid \frac{Y_{c.m.}}{Y_{beam}} \mid \;\leq\; 0.1$) is seen directly in the squeeze-out. Here $Y_{c.m.}$ can be expressed as [238, 271];

$$Y_{c.m.} \;=\; \frac{1}{2} ln \, \frac{[\; E(i) \;+\; p_z(i) \;]}{[\; E(i) \;-\; p_z(i) \;]}. \tag{5.2}$$

where *E(i)* and $p_z(i)$ are the total energy and the longitudinal momentum of the i^{th} particle respectively.

The elliptical flow is basically generated from the participant zone due to the squeeze-out of nucleons during the projectile and target overlap. The elliptical flow is defined by the second-order Fourier coefficient from the azimuthal distribution of detected particles at mid-rapidity. Mathematically,

$$\frac{dN}{d\phi} = p_0(1 + 2v_1 Cos\phi + 2v_2 Cos2\phi + ...). \tag{5.3}$$

Here ϕ stands for the azimuthal angle of the emitted particles. The parameter $Cos2\phi$ represents the term elliptical flow. The phenomenon of elliptical flow is a complex interplay between the expansion of the highly excited nuclear matter, rotation and shadowing of the spectators, apart from the incident energy.

Fig. 5.1, gives a 3D representation of a non-central collision [272]. The reaction plane is determined by the beam direction and impact parameter (the z and x axes respectively) of the reaction. The almond shape formed is the reaction volume, where the participating nucleons take part due to the interaction, the two half spheres represent the spectator nucleons.

During the collision phase, the density becomes few times the normal nuclear matter density resulting in a drastic variation in the strength of symmetry energy which affects the reaction dynamics significantly. The elliptical flow being generated from the high density region (participant zone), is helpful in exploring the behavior of symmetry energy at high densities. From the above said facts, one can conclude that the second order flow (elliptical flow) is a better candidate for determining the isospin dependence of nuclear equation of state compared to first order sideward flow (directed flow).

The elliptical flow is shaped by the interplay between the geometry and the mean field and, when gated by the transverse momentum, reveals the momentum dependence of the mean field, especially along the participant zone. The pulsating sign of elliptical flow, observed at intermediate energies has received particular attention which represents the pressure build-up in the non-isotropic collision zone. The *Diogene collaboration* at the Saturne synchrotron in Saclay observed the glimpse of azimuthal distribution of particles at mid-rapidity [129]. In 1997, H. Sorge [234], introduced the term "elliptical flow" which signifies the anisotropy of the ϕ distribution at mid-rapidity. The analysis of the transverse momentum dependence of elliptical flow has also been put forwarded in Refs. [50, 139-141, 273]. In recent years, several experimental groups have measured the elliptical flow. The

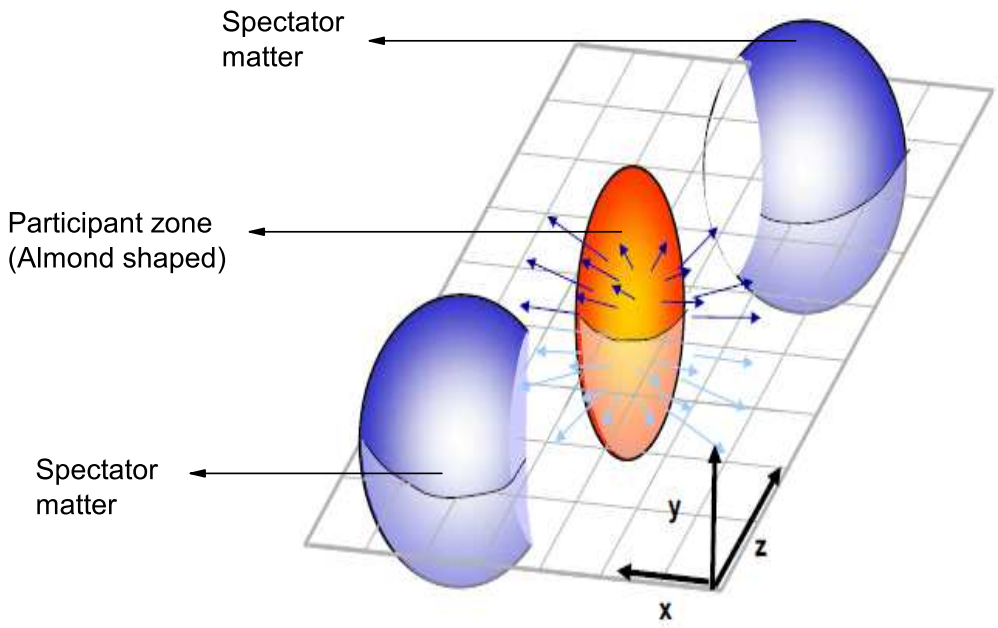

Figure 5.1: Non-central collision of two nuclei results in the formation of almond shaped volume. The spatial anisotropy with respect to the x-z plane (reaction plane) translates into a momentum anisotropy of the produced particles (anisotropic flow). Figure is taken from Ref. [272].

FOPI, INDRA and *PLASTIC BALL* collaborations [50, 139-141] are actively involved in measuring the excitation function of elliptical flow from Fermi energies to relativistic energies. In most of these studies, reaction of ${}^{197}_{79}Au + {}^{197}_{79}Au$ has been taken [50, 139-141]. Interestingly, a change in the elliptical flow was reported from positive to negative values around 100 MeV/nucleon. Both the mean field and two-body binary collisions play an important role in this energy domain. The mean field is supposed to play a dominant role at low incident energies. At high energies, binary collisions starts dominating the physics gradually. A detailed study of the excitation function of elliptical flow in entire energy region can provide a useful information about the nucleon-nucleon interactions related to the nuclear EOS.

5.2.1 Transition energy

One of the pertinent and useful feature of the elliptical flow is the existence of transitions between two forms of the observable. These transitions corresponds to measuring "zeros" in the flow excitation functions, or the energy. The particular energy at which elliptical flow vanishes is termed as the transition energy which corresponds to the isotropic distribution of nuclear matter in the transverse plane. At this particular energy, the expansion of the compressed participant zone is counter-balanced by the shadowing of the spectator matter. The schematic behavior of the elliptical flow as a function of the beam energy is shown in Fig. 3.1. The transition energy is recognized as a crucial parameter which can shed light on the complex interactions among the neutrons & protons in highly thermalized state. In the present analysis, we show the variation of transition energy with the stiffness factor γ (different parameterizations of the density dependence of the symmetry energy).

5.2.2 Elliptical flow as a probe for symmetry energy

One needs to understand that the high-density symmetry energy term can be probed from the isospin effects in HIC's. The elliptical flow, which provides us an opportunity to study the pressure that is generated very early during the reaction [234, 235], is highly sensitive to the symmetry energy [18, 53, 66, 183, 186]. Transport model calculations concluded that the squeeze-out of nucleons with high transverse momenta perpendicular to the reaction plane, i.e. the elliptical flow, has probably the highest sensitivity to the symmetry energy [18, 53, 66]. Recently, an attempt was made by Kumar *et al.,* [186] to correlate the elliptical flow with isospin content of the reacting nuclei. However, those calculations were silent about the density dependence of the symmetry energy.

Different techniques are being employed to study the role of symmetry energy at sub-saturation densities and supra-saturation densities. Danielewicz *et al.* [15] made an attempt to determine the equation of state of dense nuclear matter, by analyzing the flow of matter to extract the pressure generated in the compressed nuclear matter. Results obtained from the iso-scalar collective vibrations, collective flow and kaon production in energetic nucleus-nucleus collisions have constrained the equation of state for symmetric matter for densities ranging from saturation density to five times saturation density [15,

274]. Experimentally, symmetry energy is not a directly measurable quantity and has to be extracted from the observables which can shed light on the symmetry energy. Some authors from the *FOPI* Collaboration concluded that the symmetry energy at supra-densities is very soft [70]. However, others got an opposite finding [33].

In a recent communication, it was advocated that at high baryon densities, large symmetry energy repulsion affects the transverse in-plane flow [275] of a neutron rich matter in HIC's. A large sensitivity for the transverse in-plane flow was detected by assuming the symmetry potential as a function of density [275]. However, it could be of interest to carry out a meaningful investigation for the elliptical flow associated to the various fragments, by including the density dependence of the symmetry energy. We investigated the effect of density dependent symmetry energy on elliptical flow via. transition energy of the light and heavy fragments.

5.3 Results and discussion

We here perform a complete systematic study for the reaction $^{197}_{79}Au + ^{197}_{79}Au$, using different parameterizations of the density dependence of the symmetry energy. Many studies concluded the matter to be soft, whereas many more believe the matter to be harder in nature [197, 224, 225, 237]. In the present analysis, we use the hard equation of state, along with the reduced isospin-dependent cross section (0.9 of σ_{NN}). It has been revealed in many previous investigations that the energy transferred in the *IQMD* events is governed by the elementary nucleon-nucleon cross section, that was assumed to be independent of the nuclear environment [105, 267, 276, 277]. In a contribution, [267, 276, 277] the demand for a reduced isospin-dependent cross section has been advocated for a better explanation of the experimental data. In addition, the reactions of $^{124}_{50}Sn + ^{124}_{50}Sn$ and $^{197}_{79}Au + ^{197}_{79}Au$ are simulated using soft EOS, to see the effect of momentum dependent equation of state & isospin dependent cross section on the neutron-proton P_t-differential elliptical flow subjected to the density dependence of symmetry energy $E_{sym}(\rho) = E_{sym}(\rho_0).\left(\frac{\rho}{\rho_0}\right)^{0.66}$ MeV.

5.3.1 Transverse momentum dependence of elliptical flow

The symmetry energy acts directly on the squeeze-out of nucleons, that mostly originate from the high-density region, formed during an early stage of the reaction and are not affected by the spectator nucleons [18, 53, 66]. The pressure created during a collision can be revealed by studying the elliptical flow with respect to the transverse momenta. The study of collective flow in HIC's, where nuclear matter undergoes a huge compression and expansion, can shed light on the various aspects of symmetry energy. Also, the nucleon-nucleon scattering cross section has a considerable dependence on the isospin-content of the system. The transition matrices of the isospin $T = 1$ and $T = 0$ channels made the neutron-proton cross section (σ_{np}^{free}) in free space higher than the proton-proton (σ_{pp}^{free})/neutron-neutron (σ_{np}^{free}) cross section [18]. In addition to the cross section, the momentum dependent interactions has a significant impact on the nuclear dynamics, which affects the particle production and collective flow on a large scale [166, 243]. For a better understanding of the nuclear equation of state, via. collective flow, it becomes essential, to understand the role of momentum dependent EOS and isospin-dependent cross section on the elliptical flow of nuclear matter in heavy-ion reactions.

The isospin effect basically generates from the mid-rapidity region or in other words from the participant zone. To study the effect of symmetry energy, we parameterized v_2 as a function of P_t at mid-rapidity ($\mid Y \mid = \mid \frac{Y_{c.m.}}{Y_{beam}} \mid \leq 0.1$) in Fig. 5.2. We display the FN's (top panel), LCP's (middle panel) and IMF's (bottom panel) for the various forms of the density dependence of the symmetry energy. The incident energy is 100 MeV/nucleon. At the incident energy of 100 MeV/nucleon, the mean field and binary collisions both contribute towards the dynamics of the reaction. In such a case, larger effect of isospin can be observed. Gaussian-type, behavior is observed for all the forms of the density dependence of the symmetry energy, i.e., for the different values of gamma. The effect of symmetry energy is clearly visible in the figure. The elliptical flow seems to be sensitive towards the various forms of the density dependence of the symmetry energy. The trends observed through our simulations shows the weaker squeeze-out flow for the larger values of gamma. The very stiff forms of the symmetry energy, i.e. $\gamma = 2$, corresponds to the maximum positive value of elliptical flow. Indeed, the very stiff form of symmetry energy, i.e. $\gamma = 1.33$ and 2, does not seem to affect the squeeze-out flow on a large scale. We see

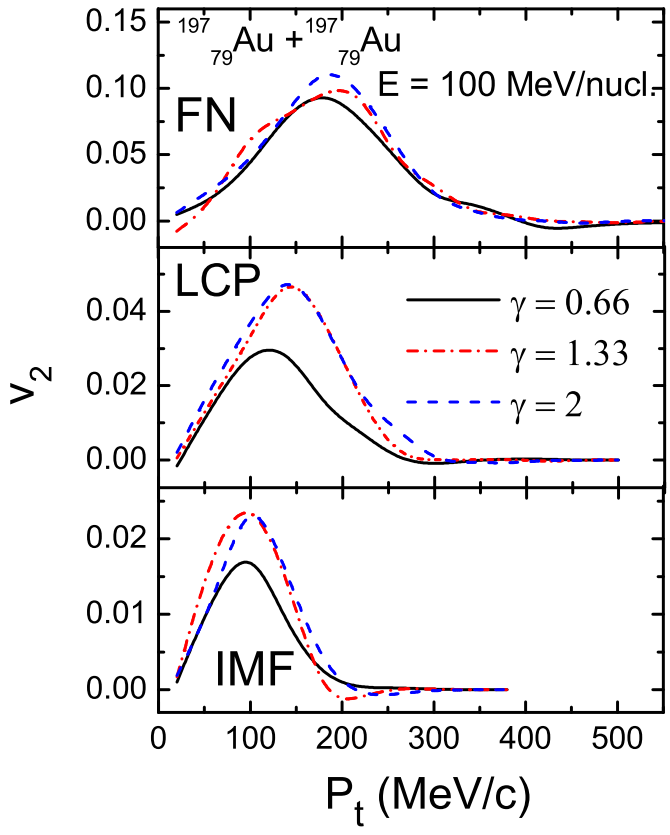

Figure 5.2: Transverse momentum dependence of the elliptical flow, for mid rapidity ($|Y| = |\frac{Y_{c.m.}}{Y_{beam}}| \leq 1$), at b = 5 fm for the reaction of $^{197}_{79}Au + ^{197}_{79}Au$ using different forms of density dependence of symmetry energy, at 100 MeV/nucleon. The top, middle, and bottom panels represent the FN's, LCP's, and IMF's, respectively.

that the squeeze-out is affected more in case of LCP's as compared to other fragments. Although, the heavier fragments have weaker sensitivity to the symmetry energy. The different forms of the symmetry energy tends to affect the elliptical flow considerably.

In Fig. 5.3, we display the final state elliptical flow v_2 for the protons and neutrons as a function of transverse momentum (P_t), over the entire rapidity region. The Figure reveals the Gaussian-type behavior for both the protons and neutrons. The maximum value of v_2 is larger for the protons as compared to the neutrons for both the cases. This happens due to the crucial role of symmetry energy in the nuclear dynamics, especially at higher densities, which arises due to compression along the participant zone, from where the elliptical flow is actually generated. This observation is of significant importance in order to extract the behavior of the symmetry energy at sub-supra saturation densities.

As stated above, the symmetry energy effect is more pronounced for the squeeze-out

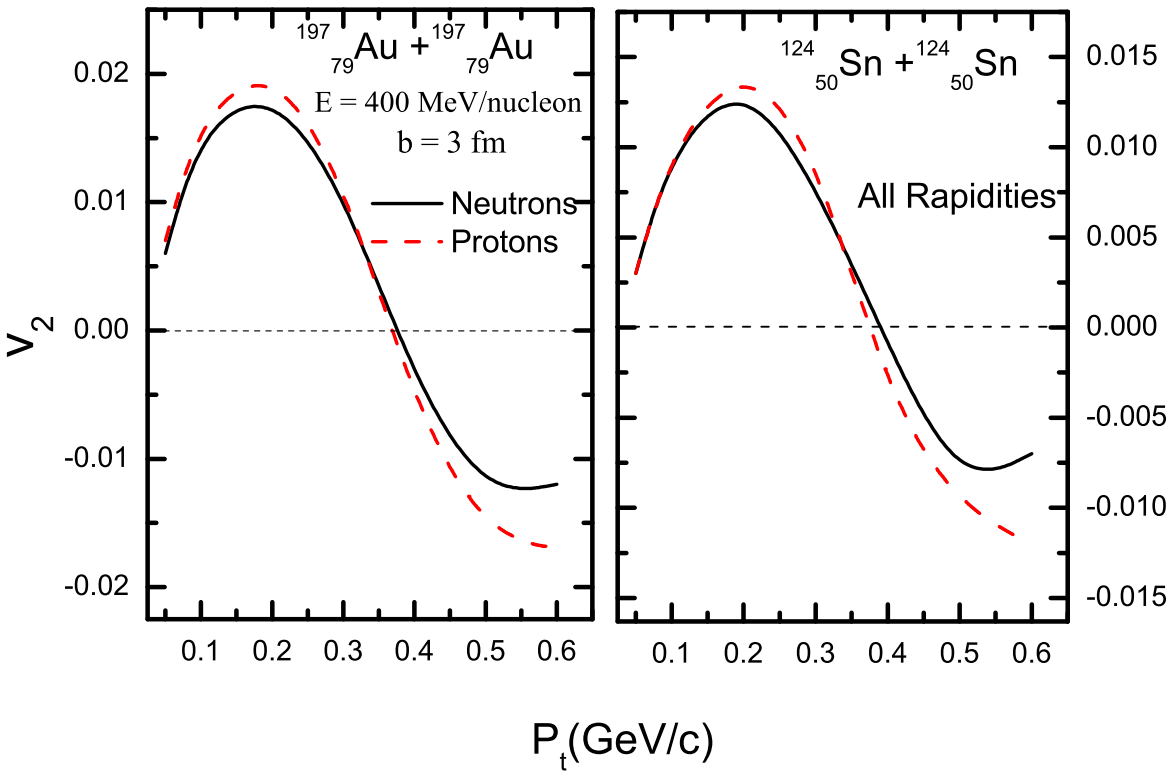

Figure 5.3: Transverse momentum dependence of elliptical flow (v_2) for the neutrons and protons, summed over the entire rapidity region. The incident energy is 400 MeV/nucleon and impact parameter b = 3 fm.

nucleons, that are mostly from the high-density region, formed during an early stage of the reaction. To obtain a more realistic view, we parameterize v_2 as a function of P_t at mid-rapidity in Fig. 5.4. We observed the negative value of v_2 along the whole P_t range. This is due to the fact that the out-of plane or squeezed-out nuclear matter is observed only in the mid-rapidity region [50, 139-141, 186, 236]. The larger out-of plane deflection of protons in mid-rapidity region indicates the weaker squeeze-out of neutrons along the participant zone [186, 236]. This is due to the fact, that the symmetry energy offers highly repulsive (attractive) potential to the neutrons (protons) in the participant zone [35, 36]. Therefore, it is clear that the strength of symmetry energy can be predicted from the nucleons emitted in the early stages of the reaction from the participant zone.

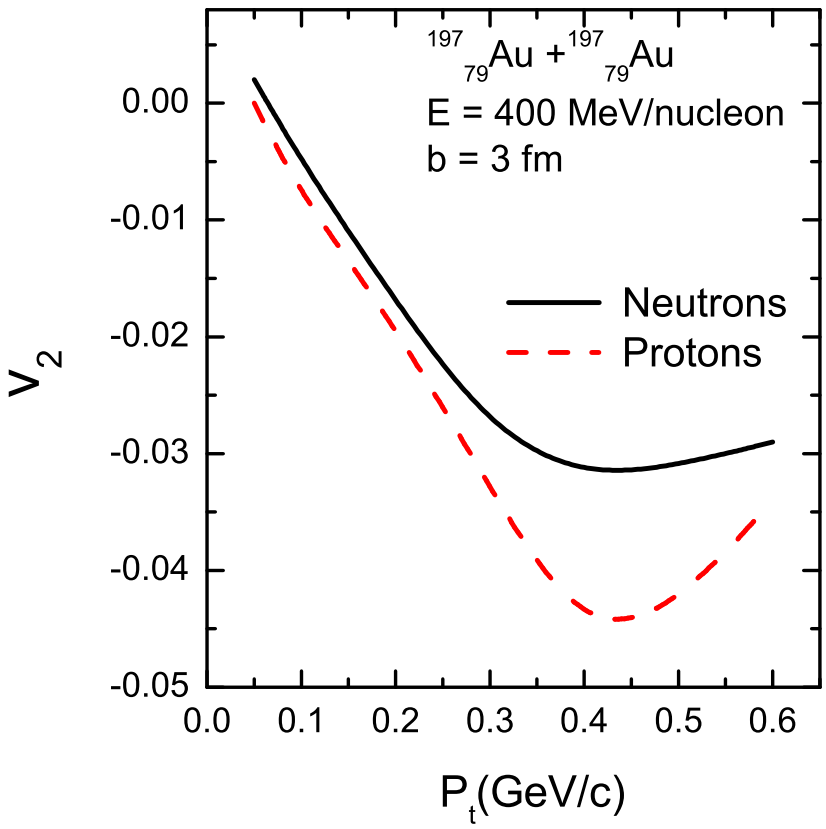

Figure 5.4: Transverse momentum dependence of $\langle v_2 \rangle$, for protons and neutrons at mid rapidity ($|Y| = |\frac{Y_{c.m.}}{Y_{beam}}| \leq 0.1$). The incident energy is 400 MeV/nucleon and impact parameter b = 3 fm.

In chapter 3, we described the role of MDI in multifragmentation. We showed that, how much the density dependent symmetry energy and MDI collectively affect the fragment production. To study the effect of momentum dependent interactions on the elliptical flow, we parameterize v_2 as a function of P_t, for the various equations of state (i.e. with and without MDI) in Fig. 5.5. The momentum dependent interactions are found to affect the v_2 of both neutrons and protons. The inclusion of momentum dependent interactions results in larger positive value of v_2. This is due to the repulsive nature of the MDI at the beam energies for which the present analysis is performed. The relative velocities of the neutrons and protons will support the deflection of particles around the reaction zone.

We have provided the details regarding the cross section (isospin-dependent and

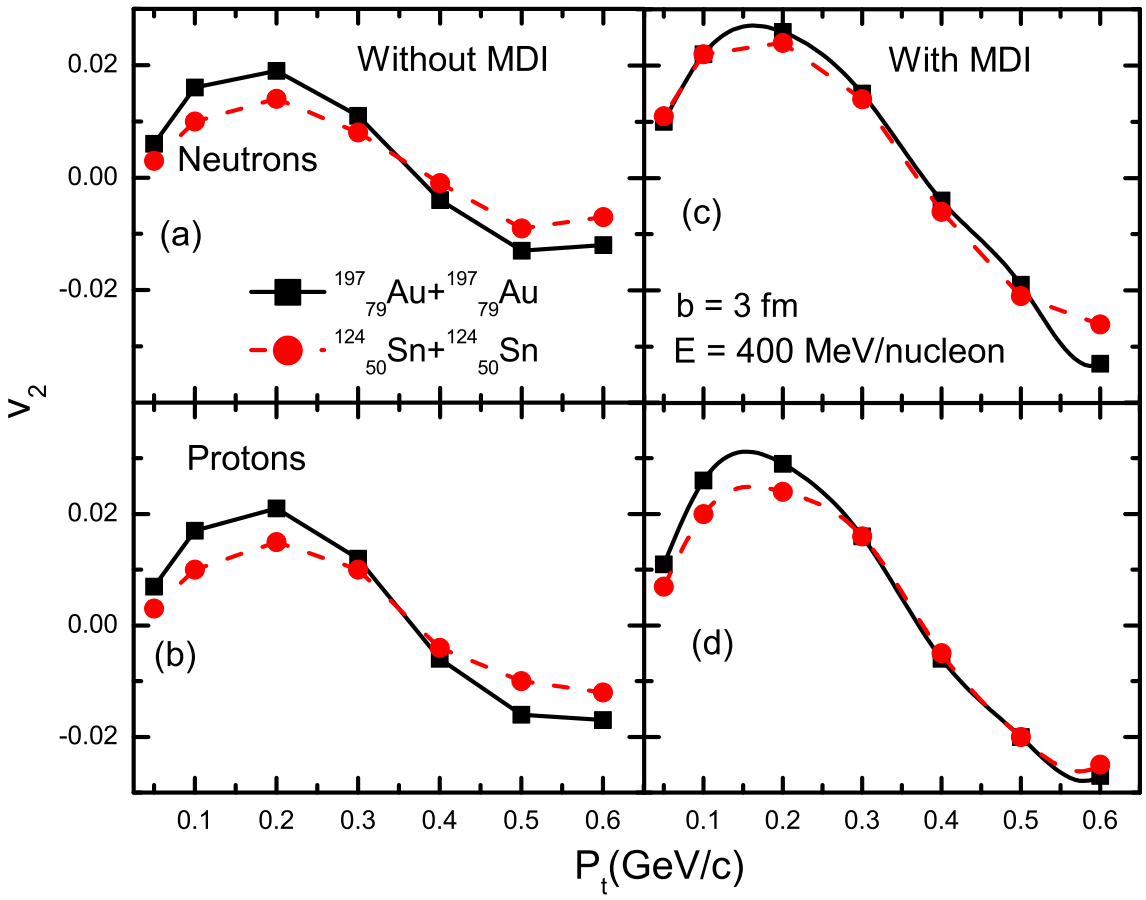

Figure 5.5: Elliptical flow v_2 as a function of P_t for neutrons [panels (a) & (c)] and protons [panels (b) & (d)] without MDI (left panels) and with MDI (right panels) for the entire rapidity region. The incident energy is 400 MeV/nucleon and impact parameter b = 3 fm.

independent) in chapter 2. Here, we shed light on the role of isospin-dependence of cross section in elliptical flow. For the better understanding of the isospin effect, we display, in Fig. 5.6, the transverse momentum dependence of v_2 for neutrons [panels (a) & (c)] and protons [panels (b) & (d)], for the isospin-dependent (σ_{iso}) (left panels) and isospin-independent cross section (σ_{noiso}) (right panels). One can clearly see the larger positive value of v_2 for the isospin dependent cross section in all the cases. This happens because in the case of isospin dependent cross section, neutron-proton cross section is three times larger compared to the neutron-neutron and proton-proton cross section (i.e. $\sigma_{np} = 3\sigma_{nn} = 3\sigma_{pp}$) [22, 207, 279] that will enhance binary collisions and will result in the larger scattering of nucleons.

The most interesting aspect in this case can be the variation of the transition energy

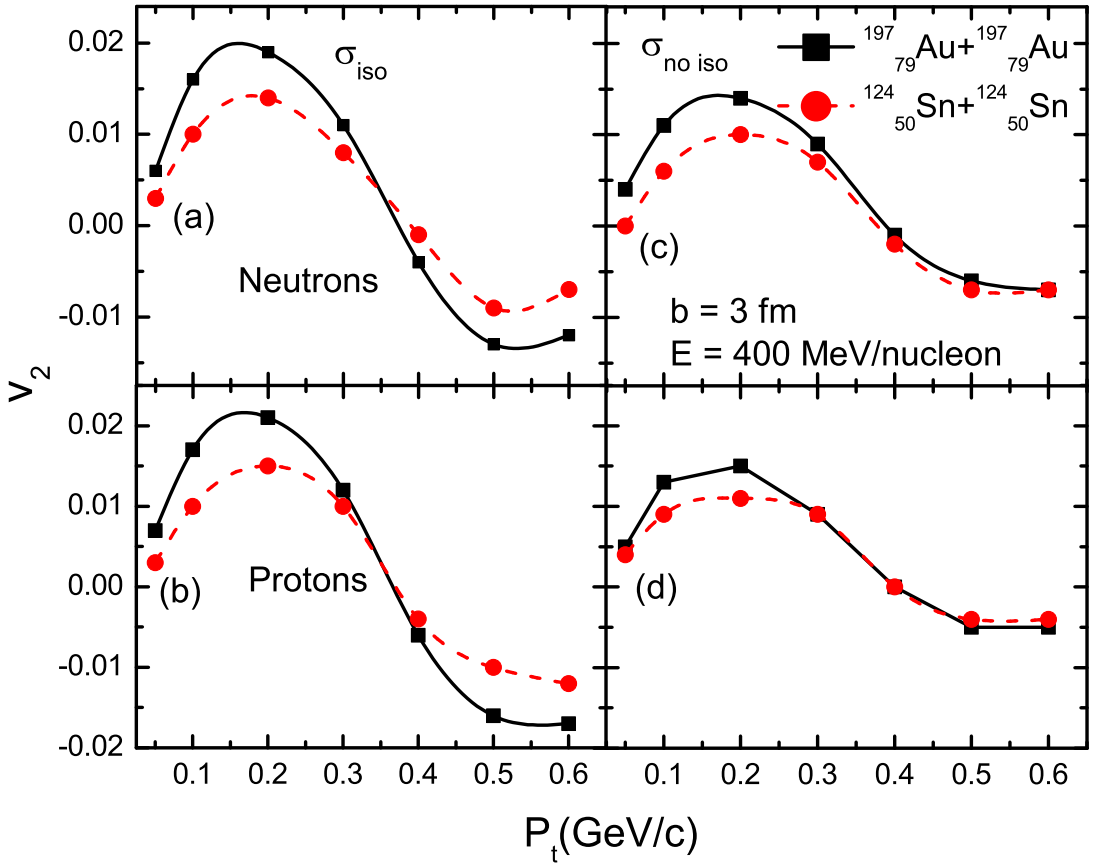

Figure 5.6: Elliptical flow v_2 as a function of P_t for neutrons [panels (a) & (c)] and protons [panels (b) & (d)] using isospin-dependent cross section (σ_{iso}) (left panels) and isospin-independent cross section (σ_{noiso}) (right panels) for the entire rapidity region. The incident energy is 400 MeV/nucleon and impact parameter b = 3 fm.

(E_{Trans}) with different forms of the density dependent symmetry energy. Although, the variation in the squeeze-out of nuclear matter due to the various forms of the symmetry energy can be understood with the transition energy.

5.3.2 Transition energy as a function of stiffness parameter (γ)

In Fig. 5.7, we have parameterized the transition energy with the stiffness parameter γ. The transition energy tends to increase with an increase in the value of γ. The light charged particles however tends to behave in a different manner compared to the intermediate mass fragments. As the FN's and LCP's originate from the participant zone. The larger sensitivity of FN's and LCP's tends to increase the transition energy upto a certain level. E_{Trans} tends to decrease for very stiff forms of the symmetry energy.

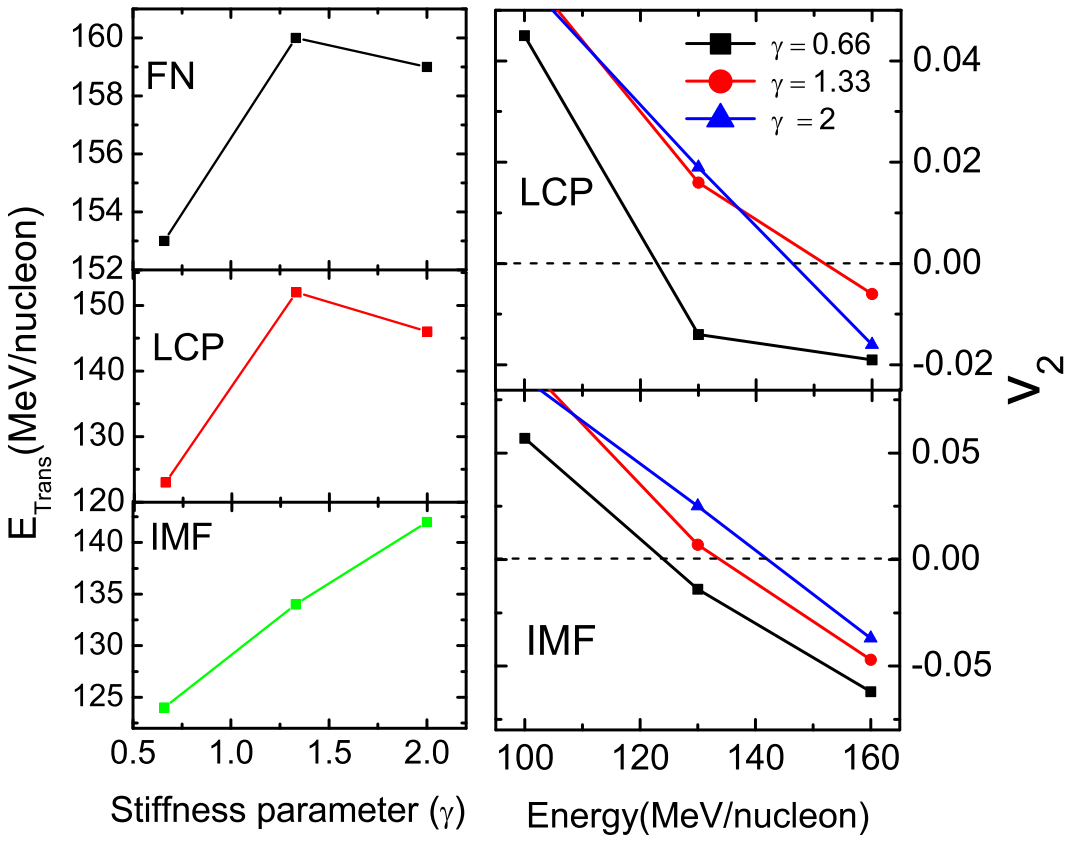

Figure 5.7: Transition energy dependence of stiffness parameter (γ) for the reaction of $^{197}_{79}Au + {}^{197}_{79}Au$.

Nevertheless, the IMF's are generated solely from the spectator zone. The transition energy for the IMF's increases with γ. The IMF's being heavy particles move slowly as compared to FN's and LCP's. The symmetry energy tends to play a role at later stages in case of heavy fragments (IMF's). Therefore, in case of FN's and LCP's the transition energy tends to decrease with stiffness of density dependent symmetry energy, which is not so in case of IMF's. The elliptical flow which is generated due to the compression in the participant zone, tends to give different behavior for the heavy fragments (generated from the spectator zone) as compared to the light fragments (generated from the participant zone).

5.3.3 Comparison with experimental data

In Fig. 5.8, we show the elliptical flow, v_2 at mid rapidity for $Z = 2$ (left panel) and for protons (right panel) as a function of the incident energy. The rapidity cut is in accordance

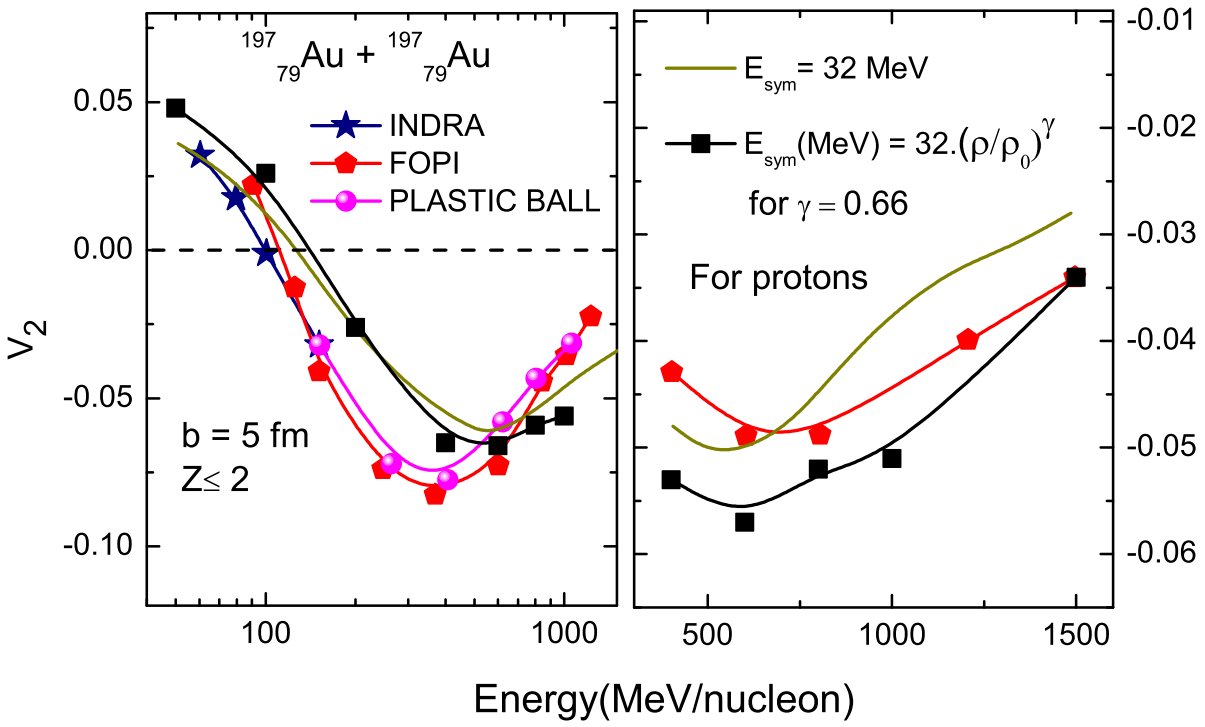

Figure 5.8: Variation of the elliptical flow, summed over the entire transverse momentum, with beam energy at mid-rapidity ($|Y| = |\frac{Y_{c.m.}}{Y_{beam}}| \leq 0.1$) for the reaction $^{197}_{79}Au + ^{197}_{79}Au$. Here comparison is shown with the full symmetry energy strength (32 MeV) and the density dependent symmetry energy for gamma = 0.66, with the experimental findings of the *INDRA, FOPI,* and *PLASTIC BALL* Collaborations [50, 139-141].

with the experimental findings. We compare the theoretical results with constant form of the symmetry energy and the density dependent symmetry energy for $\gamma = 0.66$, with the experimental data extracted by *INDRA, FOPI,* and *PLASTIC BALL* collaborations [50, 139-141]. The elliptical flow shows a transition from in-plane to out-of-plane with an increase in the incident energy. The elliptical flow is found to become more negative with an increase in incident energy. This is because the mean field, which contributes to the formation of a rotating compound system, becomes less important, and the collective expansion process based on nucleon-nucleon scattering starts to be predominant. The out-of-plane emission decreases again toward higher incident energies. This happens due to the faster movement of the spectator matter after v_2 reaches a maximal negative value. The density dependent symmetry energy tends to give a greater squeeze-out of the nuclear matter as compared to the constant form.

For $\gamma = 0.66$, the symmetry energy tends to play a more important role across

the high-density region. The repulsion produced due to the symmetry energy tends to give the larger squeeze-out flow, which is evolved due to the pressure generated in the participant zone. However, no such effect is observed in case of low incident energies. At low incident energies, the density of the system is not so large to see a huge variation in the symmetry energy. As in the case of higher incident energies of the order of 800 - 1000 MeV/nucleon, the density of the system is 2 - 3 times the normal nuclear matter density. The mid-rapidity region corresponds to the participant zone. The high density achieved in the participant zone, due to the target and projectile collisions, tends to produce the effect of density-dependent symmetry energy. A larger squeeze-out is also observed in case of protons.

5.4 Summary

We have checked the sensitivity of the elliptical flow towards the various forms of density dependent symmetry energy. We found that the elliptical flow is highly sensitive to the different forms of density dependent symmetry energy. The transition energy tends to give different behavior for the lighter particles compared to the heavy fragments. However, a larger squeeze-out is observed with density dependent symmetry energy (for $\gamma = 0.66$), compared to the full symmetry energy strength, i.e. 32 MeV. The elliptical flow is significantly influenced by the momentum dependent interactions and isospin-dependent cross section. The mid-rapidity region observes a larger squeeze-out for the protons compared to the neutrons due to the interplay of symmetry energy. The $[v_2(neutrons) - v_2(protons)]$ can give an estimate for the strength of symmetry energy at sub-supra saturation densities. The transverse momentum dependence of neutron-proton elliptical flow can give a good understanding of the complex nuclear matter interactions and can shed light on the density dependence of the symmetry energy.

Chapter 6

Effect of symmetry energy on nuclear stopping

6.1 Introduction

In the previous chapters, we explored the various aspects of multi-fragmentation and elliptical flow, when subjected to the different forms of density dependent symmetry energy. Now, we shall concentrate on the reaction dynamics (density & temperature) and nuclear stopping in heavy-ion collisions. We have correlated temperature and nuclear stopping, as the global stopping in HIC's can give a good estimation of the degree of thermalization reached during the collision.

The compression generated due to the reaction tends to increase the density and temperature of the colliding nuclei which acts as a true testing ground for the nuclear EOS. The maximum density and temperature are basically determined by the incident energy and impact parameter of the reaction. The highly dense and thermalized nuclear matter tends to expand, providing crucial information regarding the supernova explosion and the cooling rate of neutron stars. The study of the temperature and densities reached in HIC's can be useful to understand the rare conditions when QGP and hadron gas (HG) existed during the early stages of the formation of the universe. Experiments have been performed at the relativistic heavy-ion collider *(RHIC)* and the large hadron collider *(LHC)* to probe the picture which existed during the evolution of the universe [280].

Earlier, we have emphasized on the fact that the extraction of the exact form and strength of the symmetry energy is necessary to understand the isospin-dependent part of the nuclear EOS. Information about the nuclear reaction dynamics (density and temperature) is of the great physical importance in order to understand the nuclear matter

properties in compressed phase. It could be of further interest to study the role of density dependent symmetry energy in the nuclear reaction dynamics, which is also found to affect various observables, which shed light on the nuclear matter EOS, as discussed in previous chapters. We here present the density and temperature reached in HIC's for various systems having different isotopic composition, for different parameterizations of the density dependence of the symmetry energy. The description of temperature and density has been taken from Refs. [207, 278, 281, 282]. In addition, an analysis is carried out for the nuclear stopping for the various forms of the density dependent symmetry energy. Nuclear stopping has gained a lot of interest because it provides the possibility of examining the degree of thermalization or equilibration achieved during the collision. It has been stated earlier also that the understanding of transport properties is of crucial importance that can be critical to describe the process of supernova collapse and the formation of neutron stars [6, 148].

The recent advances in radioactive nuclear beam (RNB) physics have provided an opportunity to the scientific world for the investigation of isospin effects in HIC's [14, 283, 284, 285]. The radio-active beam facilities are able to produce nuclear collisions for the neutron rich matter at high incident energies. Nuclear stopping has been reported to be determined by both the mean field and the in-medium NN cross sections [286]. Various findings concluded the nuclear stopping, to be explored in reference to the isospin degree of freedom [143, 179, 183, 287, 288]. It has been recently explored that the isospin via symmetry energy can play an important role in probing the nuclear stopping in HIC's [287, 289].

The iso-scalar giant resonances in the Sn nuclei and implications for the asymmetry term in nuclear-matter incompressibility are acknowledged in Refs. [48, 290, 291]. Correlations between the behavior of the nuclear symmetry energy, the neutron skins, and the percentage of energy-weighted sum rule (EWSR) exhausted by the pygmy dipole resonance (PDR) in $^{68}_{28}Ni$ and $^{132}_{50}Sn$ were investigated, which were found to be helpful in determining the neutron radii and the parameters which govern the density dependence of symmetry energy [6, 48]. The term symmetry energy is linked to the giant monopole resonance (GMR) and giant dipole resonance (GDR) of exotic nuclei [48, 290-292]. Symmetry energy influences the organization of the pasta structures in the proton-neutron

star crust [293]. Therefore, it seems essential, in this situation, to carry out a meaningful investigation for global nuclear stopping for different forms of the symmetry energy. The present study includes a descriptive analysis of global nuclear stopping and explanation for its correlation to the temperature reached in HIC's.

The rapidity distribution is a crucial parameter for the analysis of participant-spectator contribution in HIC's [294]. Here, a systematic study regarding the role of participant matter and spectator matter in nuclear stopping using isospin-dependent quantum molecular dynamics model is presented with the inclusion of density dependence of symmetry energy ($\gamma = 0.66$). The simulations have been carried out with soft equation of state along with the reduced isospin-dependent cross section to study the effect of different types and size of rapidity distributions on the nuclear stopping for the whole colliding geometry.

6.2 Interpretation of density and temperature

When the nuclear matter is subjected to high compression, large density built up during the collision tends to affect the symmetry energy. In such a case we tend to study the nuclear dynamics subjected to various forms of the symmetry energy. However, we start with the normal density, which tends to vary (both increases and decreases) during collision. In an approach [207, 278, 281, 282], the density can be defined as,

$$\rho(r,t) = \sum_{i=1}^{A_T+A_P} \frac{1}{2\pi L}.exp[-(r - r_i(t))^2/2L]. \tag{6.1}$$

Where L is the Gaussian width of the wave packet. A_P and A_T corresponds to the projectile and target mass, respectively The density is calculated in the central sphere of radius 2 fm. This procedure of density calculation give us two possibilities (i) one can look at the maximum density $< \rho^{max} >$ reached anywhere in this sphere or (ii) take an average value over the whole sphere $< \rho^{avg} >$. The uniform distribution of dense nuclear matter will result in almost similar values of $< \rho^{max} >$ and $< \rho^{avg} >$.

Another quantity associated with the compressed nuclear matter is temperature. In general, a true temperature can be assigned only for a thermalized and equilibrated matter. Since the nuclear matter is said to be non equilibrated in case of heavy-ion

collision. One cannot take the temperature into consideration, unless, we opt for the local environment. In the present case, we follow the description of the temperature given in the references [207, 278, 281, 282]. The extraction of the temperature T is based on the local density approximation, that is, one deduces the temperature in a volume element surrounding the position of each particle at a given time step [207, 278, 281, 282]. It is possible to extend the definition of "temperature" to non-equilibrium situations from the heavy-ion simulations. The local temperature can be extracted using a local density approximation associated with the hot Thomas-Fermi approach generalized for the case of two Fermi spheres [278].

Each local volume element of nuclear matter in coordinate space and time has some 'temperature' defined by the diffused edge of the deformed Fermi distribution consisting of two colliding Fermi spheres, which is typical for non-equilibrium momentum distribution in HIC's. The temperature and density both depend significantly on the colliding geometry of the reaction. The peripheral collisions result in smaller overlap of the colliding nuclei and hence a lower density and temperature.

With the formalism (dubbed the hot Thomas-Fermi approach [278]), it is possible to determine the extensive quantities such as density, kinetic energy and entropy with the help of momentum distributions at a given temperature. The above said parameters can give us the value of local temperature. In Refs. [207, 281, 282], a clear representation for the local temperature is given with the help of local density.

In this formalism, the momentum distribution of nucleons in a hot nuclear matter at a temperature T is given by the Fermi dirac distribution as,

$$n(k,t) = \frac{1}{1 + exp\{[\epsilon(k) - \mu]/T\}} \tag{6.2}$$

Here $\epsilon(k)$ is the energy of the nucleon with momentum k and μ is the chemical potential which is determined by the normalization to a given density of nuclear matter ρ

$$\rho = \frac{g}{(2\pi)^3} \int n(k) dk, \tag{6.3}$$

where g (=4) is the spin-isospin degeneracy of a nucleon with momentum k.

When one uses the effective mass approximation for the single particle energies ϵ (k) as,

$$\epsilon(k) = \frac{\hbar^2 k^2}{2m} \; + \; U(k) \simeq \frac{\hbar^2 k^2}{2m^*} \; + \; U(0), \tag{6.4}$$

then equation 6.2 becomes

$$n(k,t) = \{1 + exp[\frac{\hbar^2 k^2}{2m^* T} - \eta]\}^{-1} \tag{6.5}$$

with η = (μ - U(0))/T we can use the nuclear matter to tabulate the kinetic energy and entropy densities for different temperatures and nuclear matter densities. The kinetic energy density ($\hbar^2\tau$/2m) and the entropy σ can be defined as

$$\tau = \frac{g}{(2\pi)^3} \int k^2 n(k) dk, \tag{6.6}$$

$$\sigma = -\frac{g}{(2\pi)^3} \int \{n(k) \; ln \; n(k) + [1 - n(k)] \; ln[1 - n(k)]\}. \tag{6.7}$$

For the case of single nuclear matter limit, the integration in Eqns. 6.3, 6.6 and 6.7 can be performed in a standard way [295]. In case the limit T $\longrightarrow$ 0, $\sigma \longrightarrow 0$, ρ and τ go to the results of the Thomas-Fermi formalism at zero temperature.

As the collision proceeds, the target and projectile starts to overlap, and during the reaction the area in momentum space between the two original Fermi-spheres will be occupied. The relative momentum (k_R) becomes very less and differs significantly from zero, at the decomposition stage of the reaction. Therefore, it becomes necessary to consider the deformed momentum distribution consisting of two interpenetrating Fermi spheres at each time step. The nuclear matter densities in the two fermi spheres is given by:

$$\rho_i = \frac{g}{(2\pi)^3} \int_{V_i} n(k) dk, \tag{6.8}$$

where indices i = 1, 2 represent the nucleons in first (F_1) and second (F_2) fermi spheres, respectively. V_1 and V_2 are the volumes in momentum space. Considering the normalization to the nuclear matter densities in the two Fermi spheres F_1 & F_2 the kinetic energy density ($\hbar^2\tau/2$m) and the entropy density σ are defined as:

$$\tau_i = \frac{g}{(2\pi)^3}\int_{V_i} k^2 n(k) dk, \tag{6.9}$$

$$\sigma_i = -\frac{g}{(2\pi)^3}\int_{V_i}\{n(k)\ ln\ n(k) + [1-n(k)] \\ ln[1-n(k)]\} \tag{6.10}$$

All integrations must be performed over the cylindrical co-ordinates k_r and k_z with the center chosen as that of the big sphere (F_1). To calculate the local temperature at each point r in each time step, we require the matter density and kinetic energy densities of the target and the projectile which are given as [207, 281, 282],

$$\rho_T(r,t) = \sum_{i=1}^{A_T}\rho_i(r,t), \qquad \rho_P(r,t) = \sum_{i=1}^{A_P}\rho_i(r,t) \tag{6.11}$$

$$\tau_T(r,t) = \sum_{i=1}^{A_T}\frac{p_i^2}{2m}\rho_i(r,t),\ \tau_P(r,t) = \sum_{i=1}^{A_P}\frac{p_i^2}{2m}\rho_i(r,t) \tag{6.12}$$

where $\rho_i(r,t)$ has been stated above in equation 6.1.

The nuclear matter densities and kinetic-energy densities are calculated with respect to the position of each particle in each time step. Using these four values, one can determine the Fermi energies, the local temperature T and the relative momentum k_R. This methodology made the extraction of local temperature in heavy-ion collisions as simple as the density calculation. Using this formulation, we have extracted the average and maximum temperature within a central sphere of 2 fm radius as described in the case of the density.

6.3 Results and discussion

For the present analysis, simulations are carried out at the incident energies of 100 MeV/nucleon and 400 MeV/nucleon, for the systems ${}^{40}_{20}Ca + {}^{40}_{20}Ca(\frac{N}{Z} = 1)$, ${}^{48}_{20}Ca + {}^{48}_{20}Ca(\frac{N}{Z} \approx 1.5)$, ${}^{60}_{20}Ca + {}^{60}_{20}Ca(\frac{N}{Z} = 2)$, ${}^{80}_{40}Zr + {}^{80}_{40}Zr(\frac{N}{Z} = 1)$, ${}^{100}_{40}Zr + {}^{100}_{40}Zr(\frac{N}{Z} = 1.5)$, ${}^{120}_{40}Zr + {}^{120}_{40}Zr(\frac{N}{Z} = 2)$, ${}^{58}_{28}Ni + {}^{58}_{28}Ni(\frac{N}{Z} = 1.07)$, ${}^{72}_{28}Ni + {}^{72}_{28}Ni(\frac{N}{Z} = 1.5)$, ${}^{84}_{28}Ni + {}^{84}_{28}Ni(\frac{N}{Z} = 2)$, ${}^{100}_{50}Sn + {}^{100}_{50}Sn(\frac{N}{Z} = 1)$, ${}^{124}_{50}Sn + {}^{124}_{50}Sn(\frac{N}{Z} = 1.5)$ and ${}^{150}_{50}Sn + {}^{150}_{50}Sn(\frac{N}{Z} = 2)$, having different isotopic composition. In addition, we have simulated the reactions of ${}^{124}_{54}Xe + {}^{124}_{50}Sn$ at different incident energies to probe the relation between the global nuclear stopping and the temperature evolved during the collision. The colliding geometry is fixed for the whole analysis, i.e., $\hat{b} = 0.3$, where $\hat{b} = \frac{b}{b_{max}}$, for $b_{max} = 1.12\ (A_P^{1/3} + A_T^{1/3})$ fm.

6.3.1 Time evolution of density and temperature

In Fig. 6.1, we display the time evolution of the maximum density $\langle \frac{\rho^{max}}{\rho_0} \rangle$ and average density $\langle \frac{\rho^{avg}}{\rho_0} \rangle$ for the neutron rich systems ${}^{84}_{28}Ni + {}^{84}_{28}Ni$ (left panels), and ${}^{150}_{50}Sn + {}^{150}_{50}Sn$ (right panels) at the incident energy of 100 MeV/nucleon, for the symmetry energies of $32.(\rho/\rho_o)^{\gamma}$ MeV for $\gamma = 0.66$, 1.33 and 2, respectively. Here, $\langle ... \rangle$ denotes average over the number of events. It can be easily observed that for both the systems, $< \frac{\rho^{max}}{\rho_0} >$ is slightly higher than the $< \frac{\rho^{avg}}{\rho_0} >$, which shows that the dense matter is not uniformly distributed in the system. The variation in the density is due to the target and projectile collisions, which exhibit the effect of density dependent symmetry energy. The peak value of density increases with the stiffness of the symmetry energy. The larger value of γ corresponds to a larger symmetry energy strength at higher densities. Our simulations gives a clear picture of increase in the peak value for the maximum and average densities for the larger values of gamma.

In order to clarify our approach, we here present the maximum temperature and average temperature for the whole time span of the reaction in Fig. 6.2. The maximum values of the maximum temperature and the average temperature is reached around 10 - 20 fm/c. The temperature is found to give similar behavior as that of density. The variation in the temperatures (maximum & average) for the different forms of symmetry energy is due to the variation in the density which affects the density dependent symmetry energy.

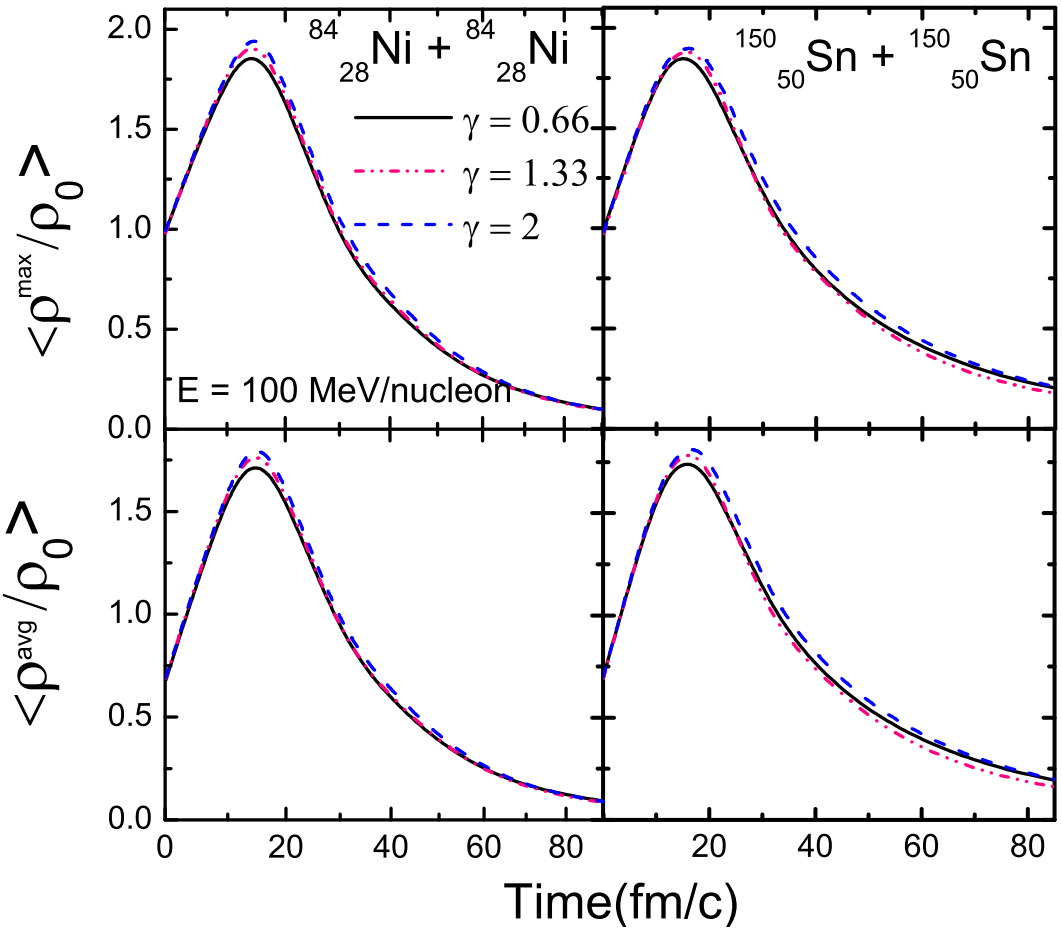

Figure 6.1: Time evolution of the maximum density (upper panel) and average density (lower panel), for the reactions of ${}^{84}_{28}Ni + {}^{84}_{28}Ni$, and ${}^{150}_{50}Sn + {}^{150}_{50}Sn$ at an incident energy of 100 MeV/nucleon.

6.3.2 Isospin dependence of maximum/average density

To understand the isospin effects on maximum and average density, we display the N/Z dependence of the maximum value of the maximum density $\langle\frac{\rho^{max}}{\rho_0}\rangle$ and average density $\langle\frac{\rho^{avg}}{\rho_0}\rangle$, for the different parameterizations of the density dependence of the symmetry energy, for the above said systems in Fig. 6.3. The maximum of the density and temperature corresponds to the maximum value of these observables reached during the whole time span of the reaction. The systems having N/Z = 1, does not seem to feel the strength of various forms of the symmetry energy. However, the role of symmetry energy is found to increase with the isospin asymmetry of the nuclear matter. Considerable effect can be observed for the systems having N/Z = 1.5 and 2. This indicates that the role of symmetry energy tends to increase as we move away from the charge symmetric nuclear

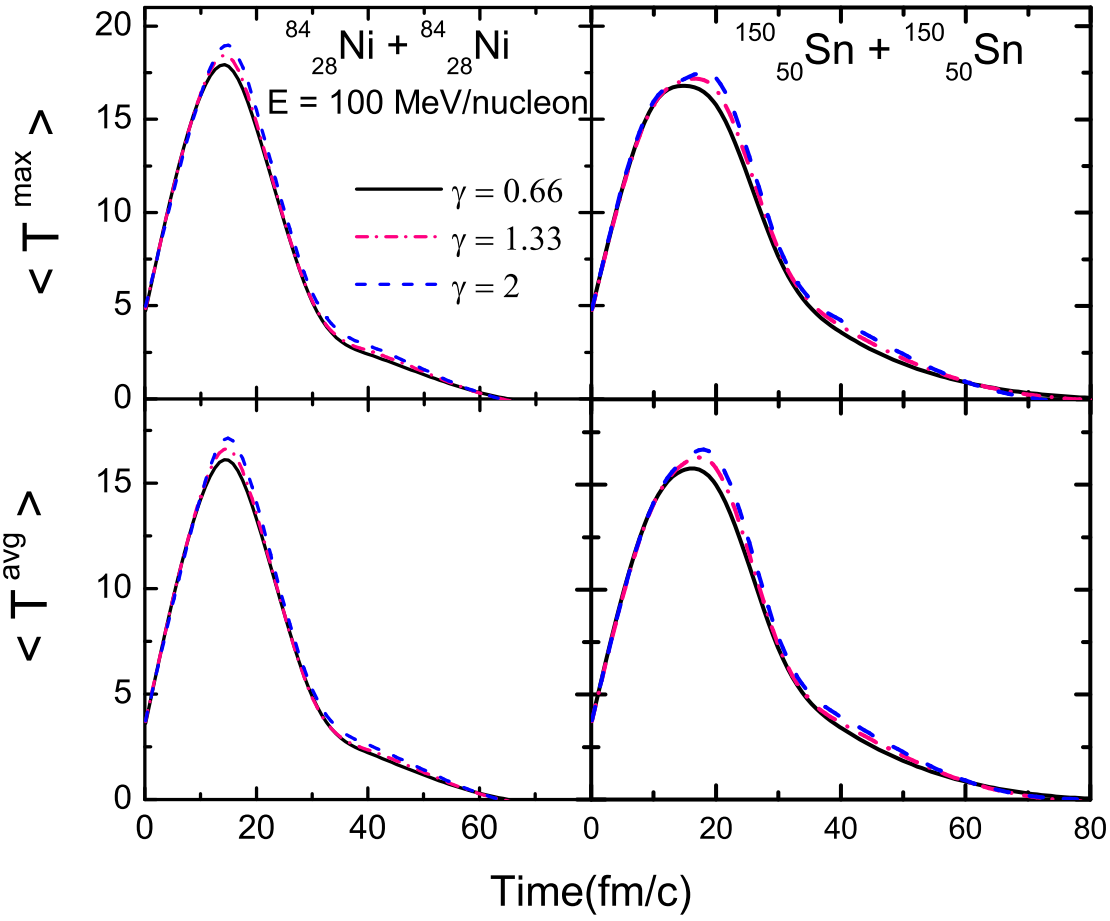

Figure 6.2: The variation of maximum temperature (upper panel) and average temperature (lower panel) with time for the reaction of $^{84}_{28}Ni + ^{84}_{28}Ni$ and $^{150}_{50}Sn + ^{150}_{50}Sn$. The incident energy is 100 MeV/nucleon.

matter. Also the density (average and maximum) achieved during the collision is more for the stiffer form of the symmetry energy.

6.3.3 Density and temperature as a function of system mass

We display the maximum value of the $< \frac{\rho^{max}}{\rho_0} >$ and the $< \frac{\rho^{avg}}{\rho_0} >$ achieved during the collision as a function of composite mass of the system in Fig. 6.4. The density (average and maximum) reached in a heavy-ion collision is sensitive towards the density dependent symmetry energy. The larger variation is observed for the systems having N/Z = 2, which is also observed in Fig. 6.3.

In Fig. 6.5, we have displayed the maximal values of $< T^{max} >$ and $< T^{avg} >$ as a

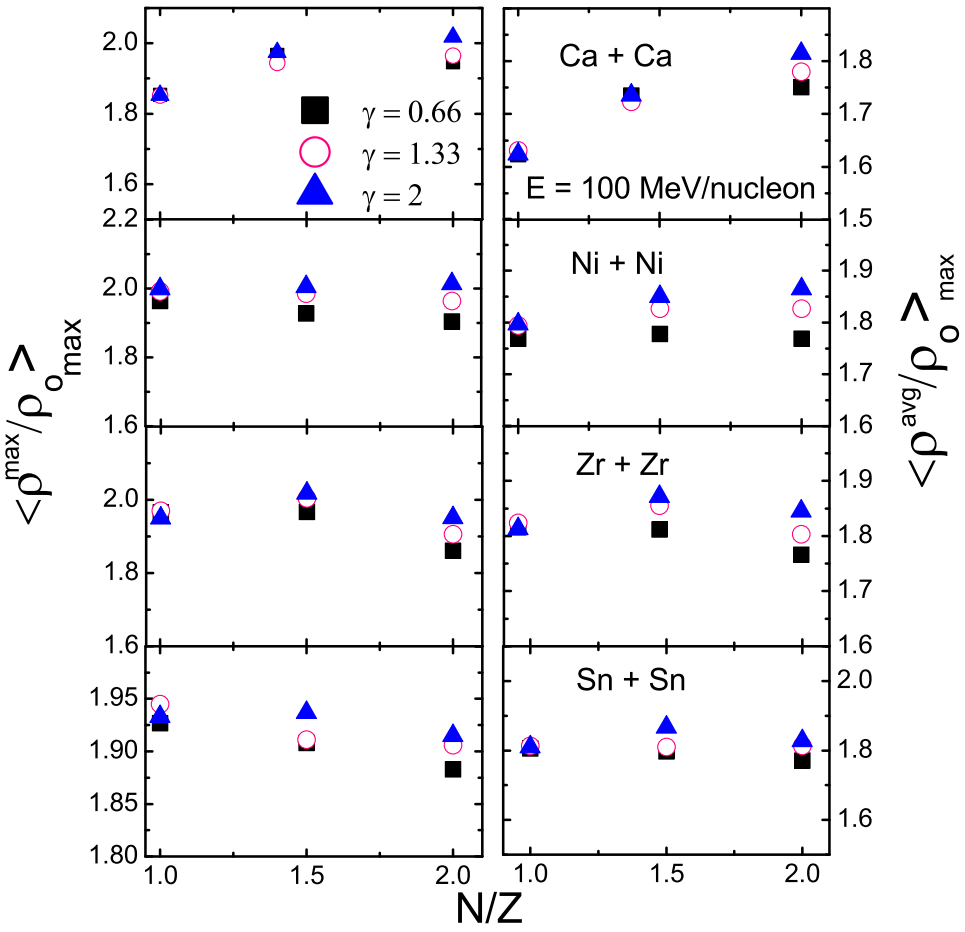

Figure 6.3: The N/Z dependence of the maximal value of maximum density and average density for various reactions at the incident energy of 100 MeV/nucleon.

function of the composite mass of the system with N/Z = 1.5 and 2. The temperature reached in heavy-ion collision is found to vary for different values of γ. A larger variation is observed for N/Z = 2, which is due to the larger interplay of symmetry energy as we move away from the isospin symmetric nuclear matter. The different forms of symmetry energy affect the density and temperature achieved during the reaction, as the stiff density dependence tend to increase the density and temperature. Further, we carry out an analysis for the nuclear stopping when subjected to different forms of the density dependent symmetry energy.

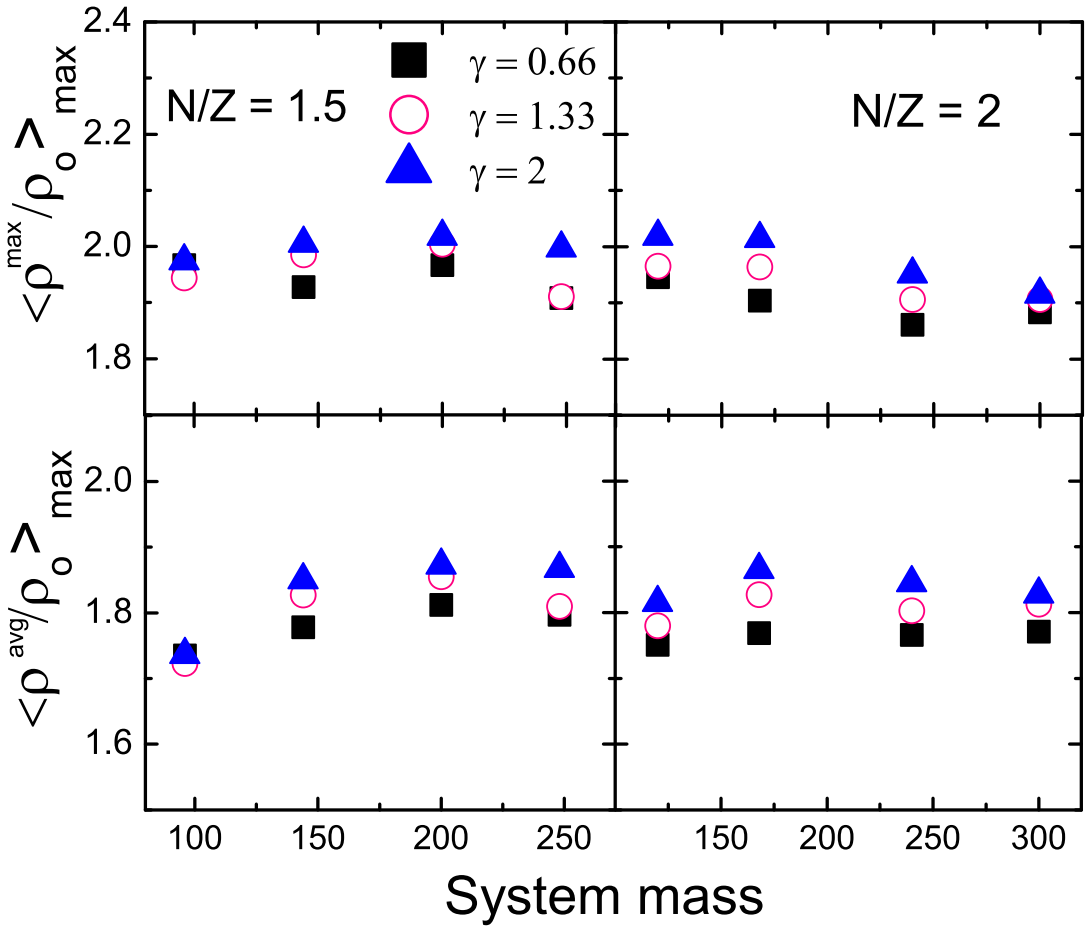

Figure 6.4: The system size dependence of the maximum value of the maximum density and average density for different N/Z ratios

6.3.4 Time evolution of global nuclear stopping

One can use the anisotropy ratio (R_P) as a probe for the degree of stopping [148, 179, 183].

$$< R_P > \;=\; \frac{2}{\pi}\,\frac{[\ \sum_i p_\perp(i)\ ]}{[\ \sum_i p_{||}(i)\ ]}. \tag{6.13}$$

where $p_\perp(i) = \sqrt{p_x^2(i) + p_y^2(i)}$ and $p_{||}(i) = p_z(i)$. Another quantity, which is an indicator of the nuclear stopping is the quadrupole moment Q_{zz}, defined as [179],

$$< Q_{zz} > \;=\; \sum_i [2\ p_z^2(i) - p_x^2(i) - p_y^2(i)\ ]. \tag{6.14}$$

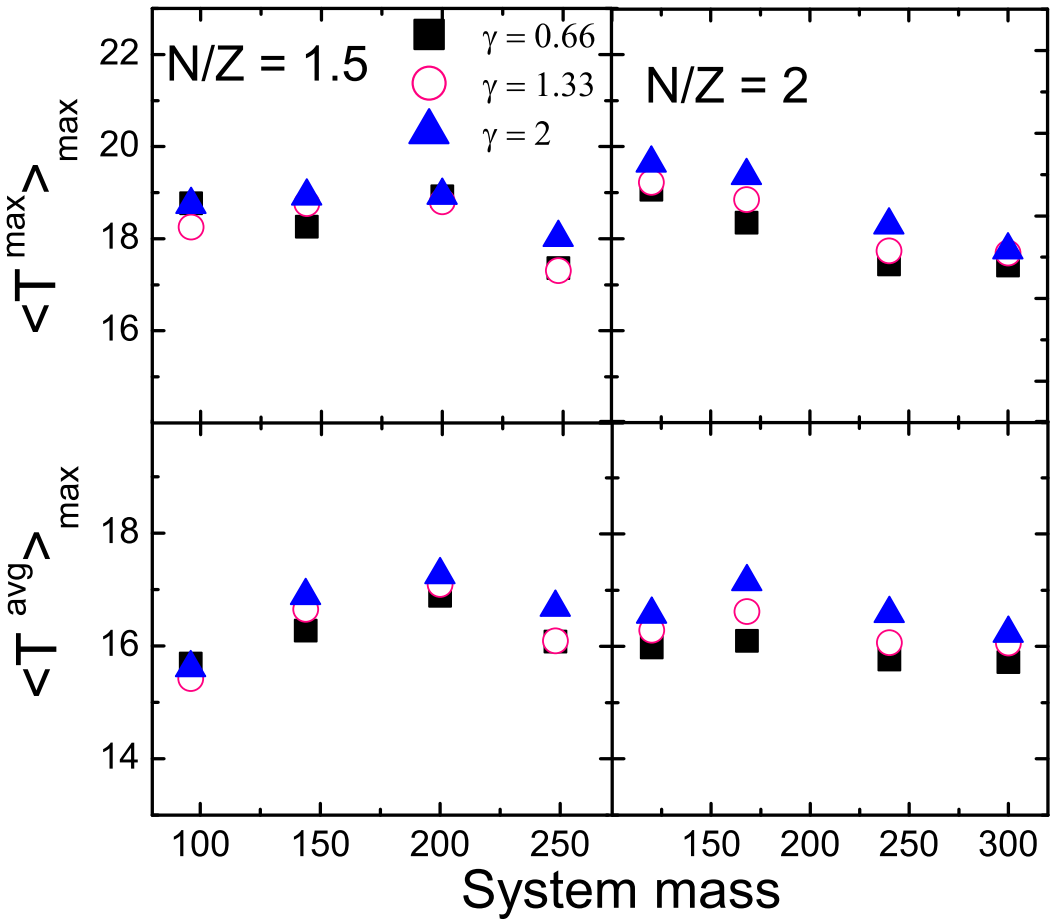

Figure 6.5: The system size dependence of the maximum value of maximum temperature and average temperature, for different N/Z ratios.

In Fig. 6.6, we display the time evolution of the anisotropy ratio $< R_P >$ for the reactions of ${}^{40}_{20}Ca + {}^{40}_{20}Ca$, ${}^{60}_{20}Ca + {}^{60}_{20}Ca$, ${}^{58}_{28}Ni + {}^{58}_{28}Ni$ and ${}^{84}_{28}Ni + {}^{84}_{28}Ni$, for the symmetry energies of 32 MeV and $32.(\rho/\rho_o)^{0.66}$ MeV at the incident energies of 100 MeV/nucleon and 400 MeV/nucleon, to study the effect of symmetry energy on global nuclear stopping. It has been observed that at the incident energy of 100 MeV/nucleon, reaction dynamics is dominated by the mean field potential. On the other hand, the nucleon-nucleon scattering becomes dominant at the incident energy of 400 MeV/nucleon [265, 296].

The phenomenon of nuclear stopping originates from the participant zone, due to which it is affected by the various forms of the symmetry energy (i.e. constant and density dependent). This is due to the variation in the strength of symmetry energy under the extreme conditions produced in heavy-ion collisions along the participant zone. The nuclear stopping tends to decrease for the density dependent symmetry energy ($\gamma =$

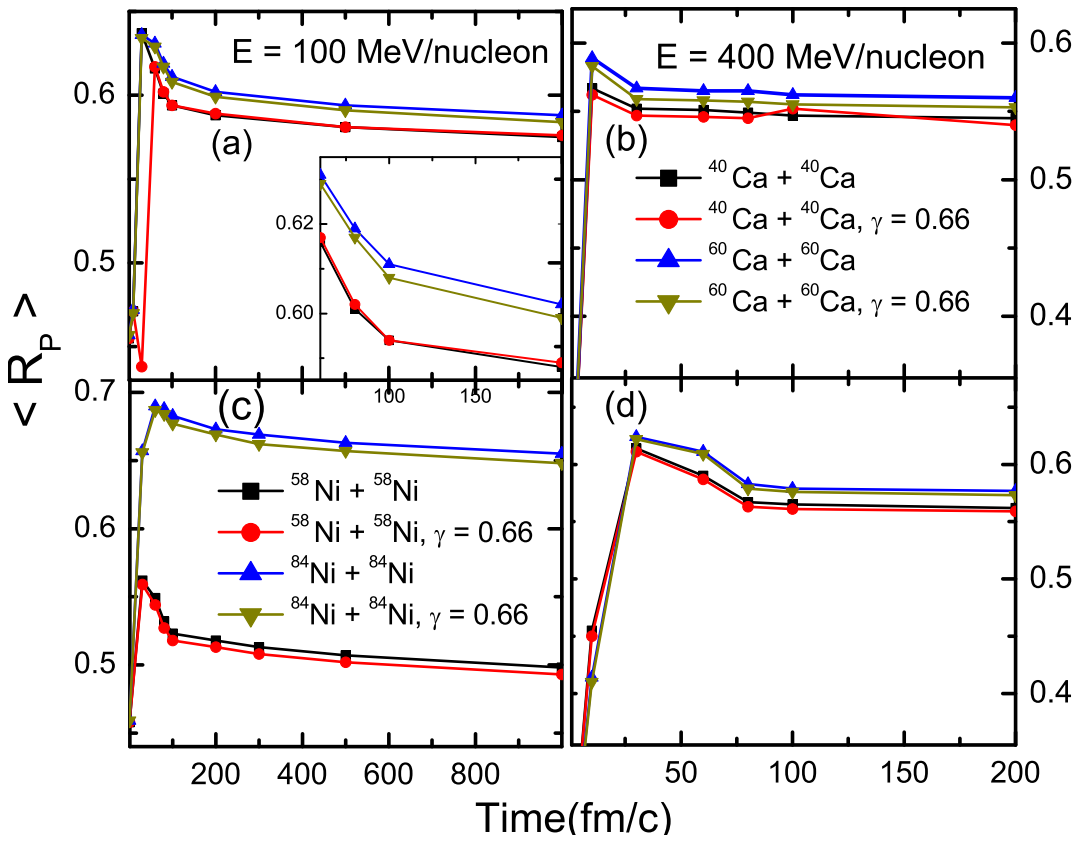

Figure 6.6: Time evolution of the anisotropy ratio, for the isotopes of systems Ca + Ca (a,b) and Ni + Ni (c,d) using symmetry energy (32 MeV) and density dependent symmetry energy, $E(\rho) = E(\rho_o)(\rho/\rho_o)^{\gamma}$, for $\gamma = 0.66$, at the incident energies of 100 MeV/nucleon and 400 MeV/nucleon respectively. The impact parameter of reaction b = 0.3 b_{max}.

0.66), compared to the constant form of the symmetry energy. For $\gamma = 0.66$, the symmetry energy tends to play a significant role across the high density region, i.e. the participant zone. The repulsion produced due to the symmetry energy tends to affect the nuclear stopping.

The density dependent symmetry energy ($\gamma = 0.66$) does not seem to affect the symmetric systems with N ≈ Z. However, a mild effect can be observed in the case of isospin asymmetric system $^{84}_{28}Ni + ^{84}_{28}Ni$ $(N/Z = 2)$. The effect of symmetry energy can be observed for an asymmetric system with $\gamma = 0.66$ as compared to the full symmetry energy strength i.e. 32 MeV. This concludes that the role of symmetry energy tends to increase as one moves away from the isospin symmetric nuclear matter. The nuclear stopping does not seem to be affected by density dependent symmetry energy ($\gamma = 0.66$)

on a large scale in comparison with the constant form of the symmetry energy due to the small variation in the symmetry energy. However, for the stiff density dependence of the symmetry energy (γ = 1.33, 2), it is possible to have a large symmetry energy variation (60 - 70 MeV) depending upon the density achieved in the collision.

Further, to explore the role of isospin, we analyze the nuclear stopping of protons & neutrons, which can act as a tool to extract the strength of symmetry energy in HIC's. We here attempt to investigate the role of isospin in heavy-ion collisions by calculating the individual contribution of neutrons and protons in nuclear stopping for different systems having different isotopic content.

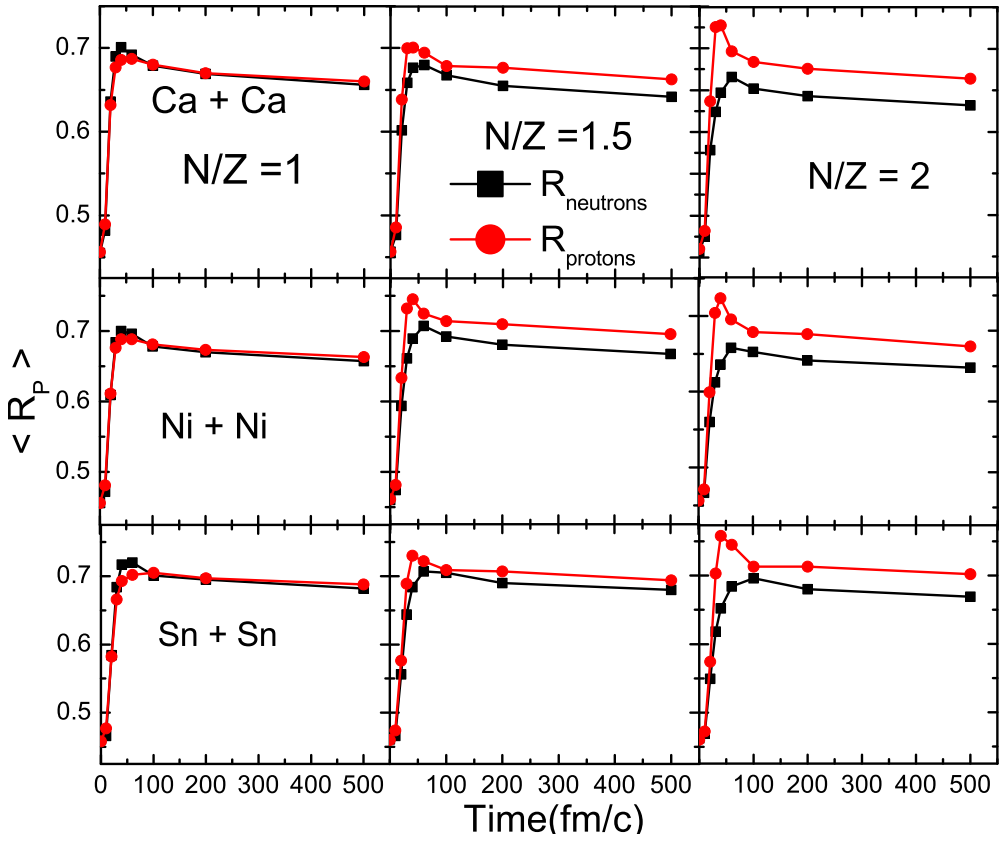

Figure 6.7: Time evolution of the anisotropy ratio(nuclear stopping) for the protons and neutrons, for the reactions of Ca + Ca (upper panel), Ni + Ni (middle panel), Sn + Sn (bottom panel) having different isotopic content at the incident energy of 100 MeV/nucleon. The impact parameter $\hat{b} = 0.3$.

The nuclear stopping in HIC's being an indicator of thermalization depends both on the mean field and in-medium NN cross sections [243, 263, 281, 286]. In a major

contribution, Kumar *et al.* [183] showed the direct relation of the nuclear stopping with symmetry energy. To have an actual picture of the reaction dynamics, the inclusion of the density dependence of the symmetry energy is necessary. We have performed our calculations with density dependence of symmetry energy for $\gamma = 0.66$.

In Fig. 6.7, we display the time evolution of the anisotropy ratio (nuclear stopping) for neutrons and protons for different systems having different N/Z values along with density dependent symmetry energy (for $\gamma = 0.66$). The trends observed through our simulations gives a clear picture of the larger contribution of protons towards nuclear stopping. The contribution considered from the protons and neutrons seems to vary along with the N/Z ratio. The protons have the larger value of anisotropy ratio as compared to the neutrons. This behavior is found to increase along with the isospin asymmetry of the system. The larger nuclear stopping exhibited by the protons is due to the Coulomb repulsion. The charged particles (protons) due to repulsion are stopped by the target protons earlier than the neutral particles (neutrons).

6.3.5 N/Z dependence of nuclear stopping

In order to obtain a more clear picture about the isospin effect on nuclear stopping, we display the N/Z dependence of the anisotropy ratio for the protons and neutrons in Fig. 6.8. The contribution of protons is found to increase as that of neutrons decreases for the larger N/Z ratios. This is due to the fact that the pp and the nn force has automatically isospin T = 1 and the main interactions come preferentially from S =0 and L = 0. This excludes the strong tensor force. The proton-neutron interaction allows also the isospin T = 0 and thus S = 1 and L = 0, which includes the strong tensor force, which is mainly responsible for the increased stopping of the protons with increasing N/Z. The larger difference in value of anisotropy ratio ($< R_{protons} > \; - \; < R_{neutrons} >$), for the larger N/Z values is because of the larger interplay of the symmetry energy as we move away from the symmetric nuclear matter (i.e., $N/Z > 1$). The term ($< R_{protons} > \; - \; < R_{neutrons} >$) signifies the strength of the symmetry energy. This observation clearly indicates about the phenomenon of nuclear stopping as a tool to probe the form and strength of symmetry energy which is found to play a significant role in the isospin-asymmetric nuclear matter.

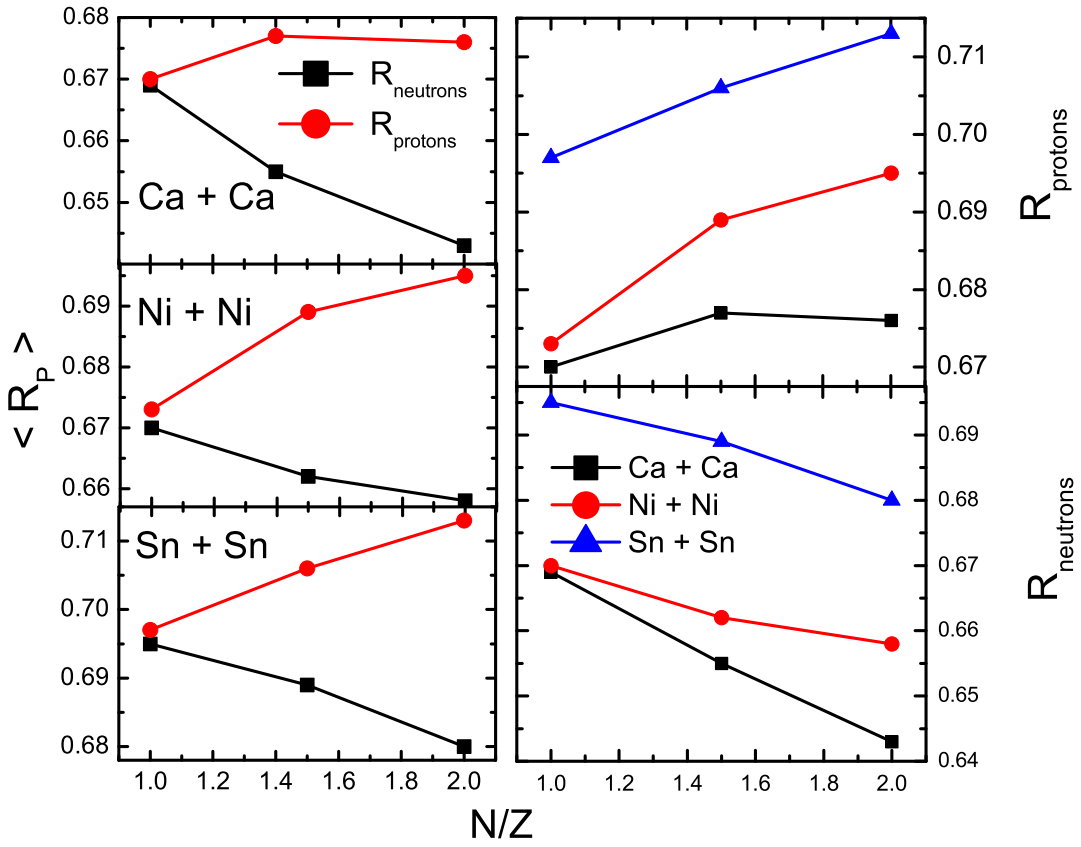

Figure 6.8: The N/Z dependence of anisotropy ratio(nuclear stopping) for protons and neutrons, for the same reactions as shown in Fig. 6.7. The incident energy is 100 MeV/nucleon at $\hat{b} = 0.3$.

Overall, the nuclear stopping for the protons tends to increase with composite mass of the system. This is due to an increase in the participant zone, along with an increase in the system mass. Similar findings are also published in [143, 183], which indicates that the nuclear stopping becomes dominant with an increase in the size of the system.

From Figs. 6.6, 6.7, and 6.8, one can conclude that the role of symmetry energy in nuclear stopping increases with the isospin asymmetry of the nuclear matter, however, more impact of symmetry energy can be observed for stiff forms of the symmetry energy (larger values of γ). Further, to study the effect of various forms of density dependence of symmetry energy on nuclear stopping, we study the rapidity distribution of particles as a function of reduced rapidity in HIC's.

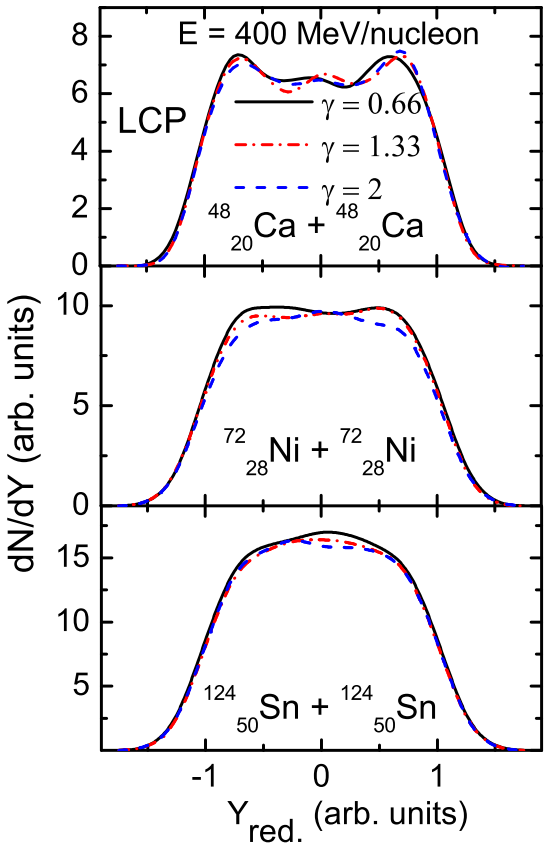

Figure 6.9: The rapidity distribution $\frac{dN}{dY}$ as a function of reduced rapidity for LCP's for the reactions of $^{48}_{20}Ca + ^{48}_{20}Ca$ (upper panel), $^{72}_{28}Ni + ^{72}_{28}Ni$ (middle panel) and $^{124}_{50}Sn + ^{124}_{50}Sn$(bottom panel), for the three different forms of the symmetry energy. The incident energy is 400 MeV/nucleon and impact parameter of reaction b = 0.3 b_{max}.

6.3.6 Rapidity distribution

One can also relate the rapidity with nuclear stopping. For details, please see Refs. [271, 238]. The LCP's (generated from the participant zone) are found to be more sensitive towards symmetry energy due to the pairing nature and also a good indicator for nuclear stopping [186, 288, 297]. Therefore, we display the rapidity distribution $\frac{dN}{dY}$ as a function of the reduced rapidity for LCP's, at the incident energy of 400 MeV/nucleon in Fig. 6.9. For complete stopping, a single Gaussian is observed [271, 238]. One can see that the LCP's emitted in the collisions forms a narrow Gaussian for the lesser value of γ. Thus, the larger values of γ result in the reduction of global nuclear stopping.

6.3.7 Rapidity distribution of particles at different colliding geometries

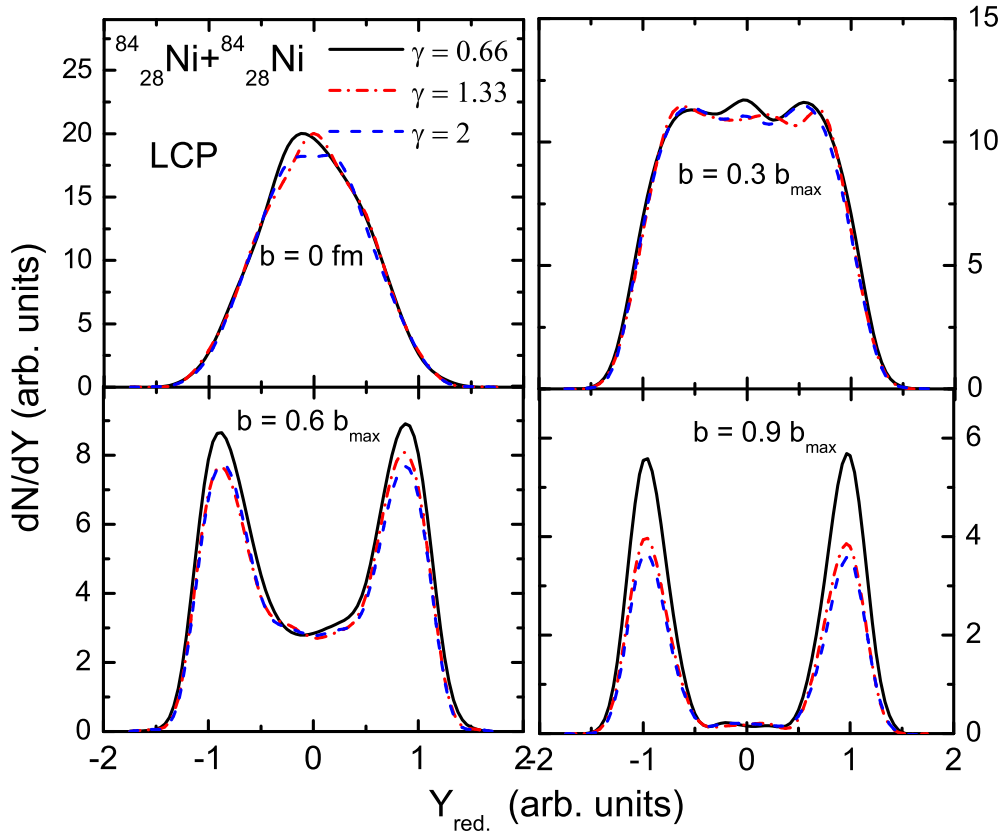

Figure 6.10: The rapidity distribution $\frac{dN}{dY}$ as a function of reduced rapidity for LCP's for the system $^{84}_{28}Ni + ^{84}_{28}Ni$, at the incident energy of 400 MeV/nucleon for different colliding geometries.

In Fig. 6.10, we display the rapidity distribution of LCP's for the different forms of symmetry energy at different colliding geometries. The central collisions do not seem to feel the strength of various forms of density dependent symmetry energy. This is due to the occurence violent phase of collisions at central geomtries. However, at the peripheral collisions, the nuclear stopping decreases due to the lesser overlapping of the target and projectile, i.e., decrease in the participant zone. The effect of density dependent symmetry energy can be clearly observed in the semi-peripheral and peripheral collisions.

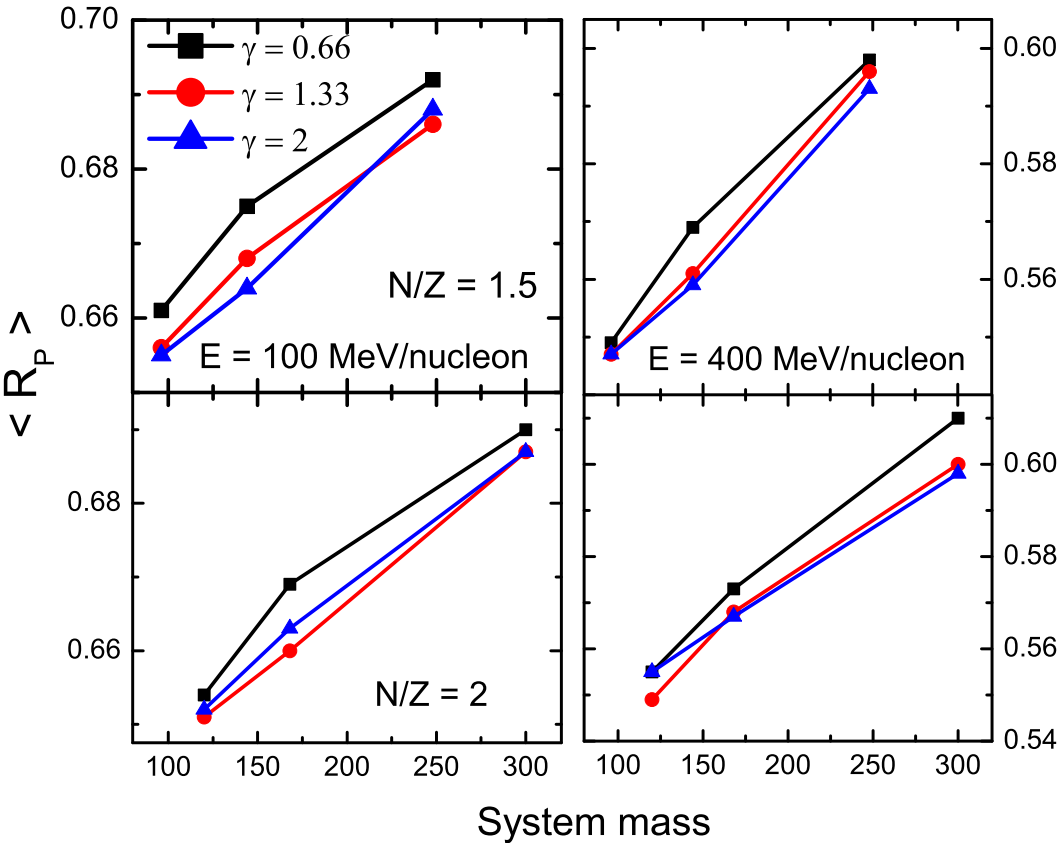

Figure 6.11: The system size dependence of the anisotropy ratio for $\frac{N}{Z} = 1.5$ and $\frac{N}{Z} = 2$, at the incident energies of 100 MeV/nucleon and 400 MeV/nucleon. The impact parameter of reaction b = 0.3 b_{max}.

6.3.8 System size dependence of anisotropy ratio

In Fig. 6.11, we display the anisotropy ratio $< R_P >$, as a function of the composite mass of the system for the different parameterizations of the density dependence of the symmetry energy (γ = 0.66, 1.33 & 2). The analysis has been made for the systems stated above having different isotopic compositions i.e., $\frac{N}{Z}$ = 1.5 and 2, for the incident energies of 100 and 400 MeV/nucleon. We observe a decrease in anisotropy ratio (nuclear stopping) for the larger value of γ. However, the effect is mild, which is due to the small variation in the density at the incident energies at which the present analysis is performed.

The nuclear stopping decreases when the value of γ increases, but the effect is really mild. The larger values of γ corresponds to the larger symmetry energy strength at higher densities and smaller symmetry energy strength at density less than saturation density ($\rho \leq \rho_0$). The density of the system is directly proportional to the incident energy, which

affects the strength of symmetry energy. The dominance of the sub-saturation region of the EOS at the incident energies of 100 and 400 MeV/nucleon reduces the nuclear stopping for larger values of γ. The nuclear stopping is found to increase with the composite mass of the system. This is due to an increase in the participant zone, with an increase in the composite mass of the system. Similar results are also observed in Fig. 6.8 which are in agreement with observations of Refs. [143, 183].

6.3.9 Correlation between temperature and nuclear stopping

The temperature reached in HIC's can also be correlated to the global nuclear stopping. The comparison of the global nuclear stopping with that of the temperature reached in HIC's can help us improve our knowledge for the nuclear matter thermalization and the in-medium properties of the nucleon-nucleon interactions. The observable nuclear stopping can describe the amount of dissipated energy, the amplitude of the large collective motion, and can shed light on the various critical phenomena's related to nuclear physics as well as astro-physics [148].

6.3.9.1 Impact parameter dependence

In Fig. 6.12, we display the maximum temperature, $< R_P >$ and $1/< Q_{zz} >$ as a function of the colliding geometry, subjected to various forms of the density dependence of symmetry energy. The similar behavior for the nuclear stopping $< R_P >$ and temperature is observed along the whole colliding geometry. Therefore, the nuclear stopping can be considered as a probe for the temperature reached in HIC's. Also the $1/< Q_{zz} >$ which seems to decrease monotonically with the decreasing temperature, can yield an estimate for the temperature. These predictions are however potentially important as the nuclear stopping, being statistically correlated to the temperature is itself an indicator of the degree of thermalization and equilibration reached during the collision.

6.3.9.2 Excitation energy dependence

In Fig. 6.13 (left panel), we display the incident energy dependence of the global nuclear stopping $< R_P >$ and comparison with experimental data [148]. The results obtained by theoretical calculations, using different forms of density dependent symmetry

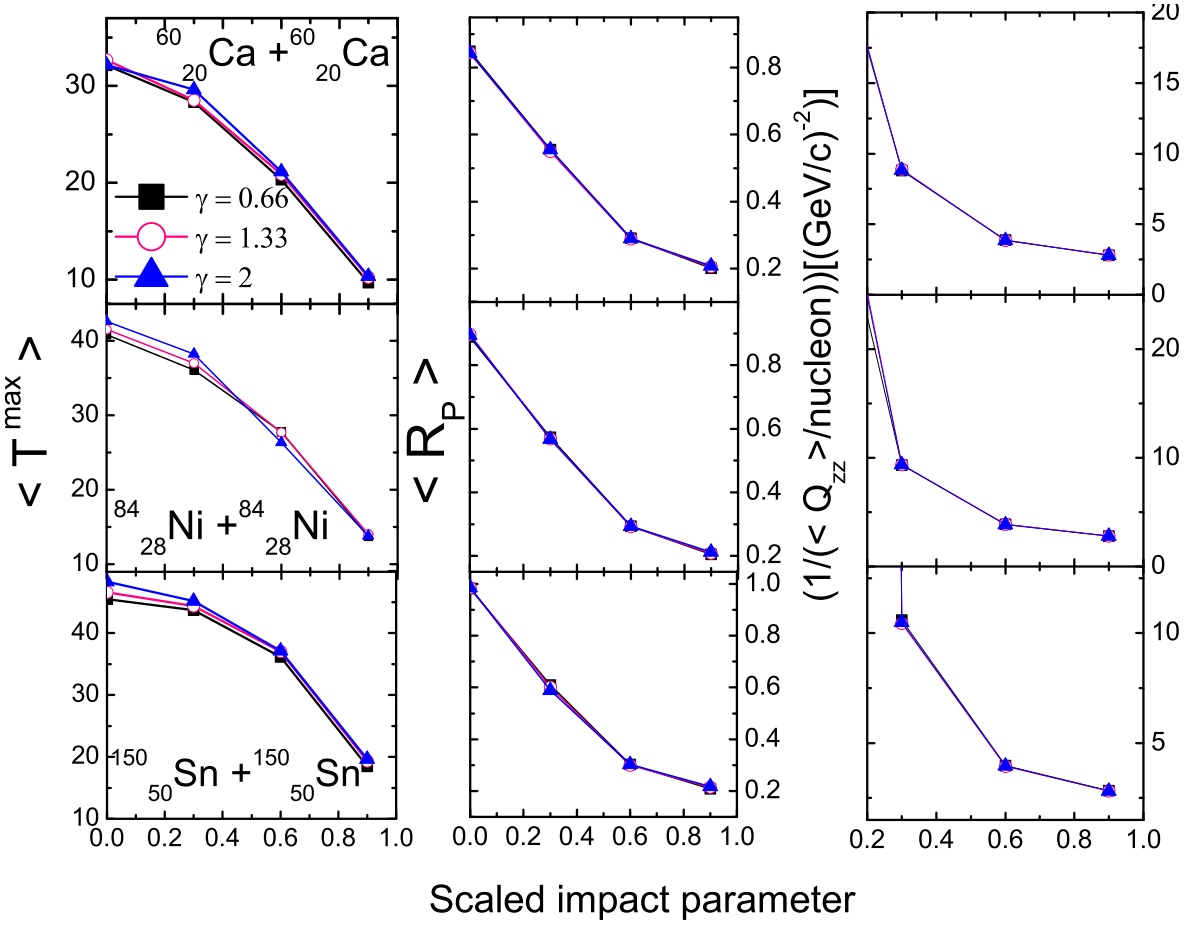

Figure 6.12: The variation of maximum temperature and nuclear stopping($< R_P >$ and $1/(< Q_{zz} >/\text{nucleon})$) with the colliding geometry. The incident energy is 400 MeV/nucleon.

energy, yields a good agreement with the experimental data [148]. However, the theoretical calculations overestimate the value of anisotropy ratio at an incident energy below 80 MeV/nucleon. A small sensitivity of $< R_P >$ to the density dependent symmetry energy can be attributed to the small density achieved during the collision. Our findings are in accordance with the findings of Dutt *et al.* [261], which provides an evidence that at low incident energies, which belong to smaller baryonic densities, the isospin dependence of the mean field potential was shown to yield the same results as obtained with potentials that has no isospin dependence. In a major contribution, Lehaut *et al.* [148] concluded that around incident energies of 40 MeV/nucleon to 100 MeV/nucleon, the isospin content of the system, i.e. the density dependent symmetry energy, does not effect the system as far as the stopping power is concerned.

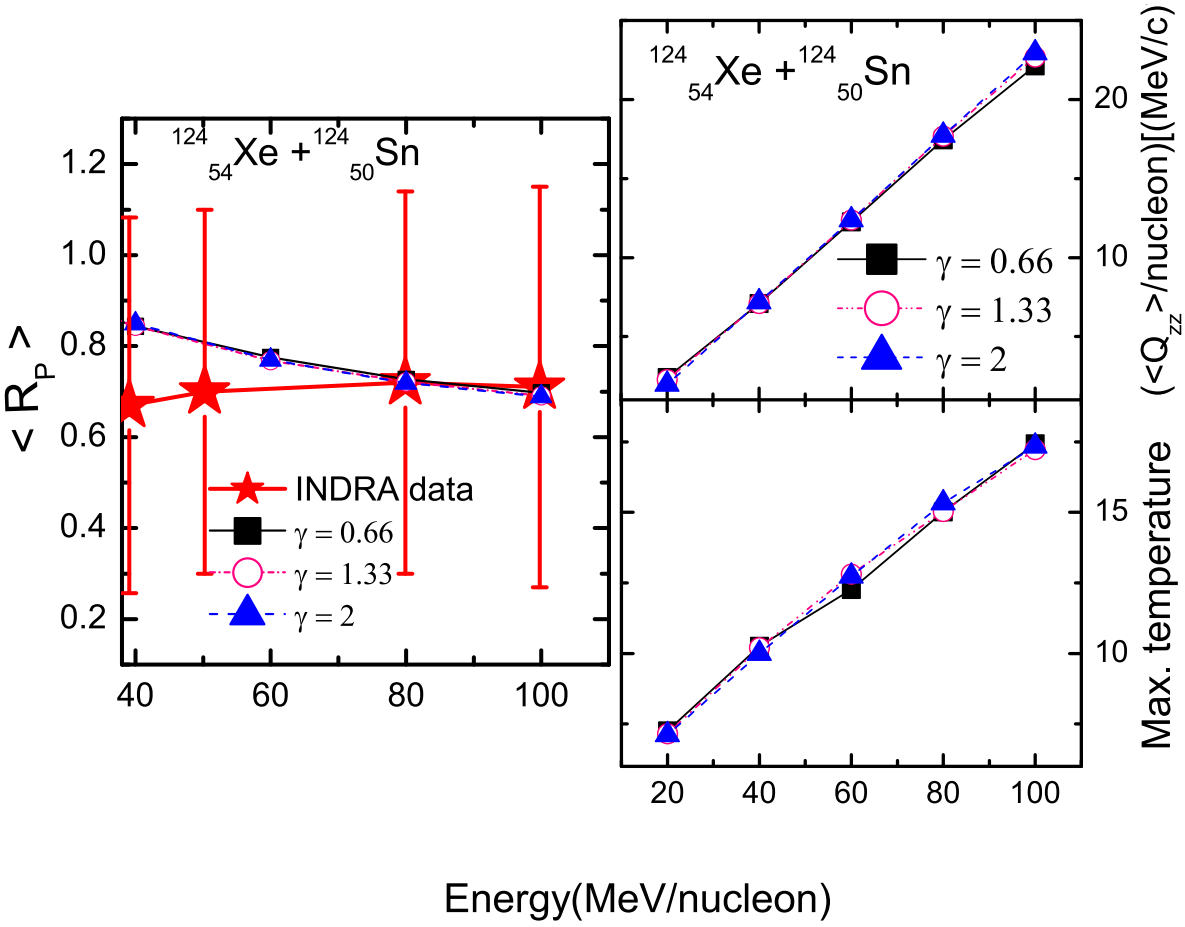

Figure 6.13: The excitation energy dependence of the anisotropy ratio (left panel) and for the $< Q_{zz} >$ and maximum temperature (right panel), for the different parameterizations of the density dependence of the symmetry energy, and comparison with the experimental data [148].

The larger incident energy corresponds to violent collisions, which tends to increase the temperature. However, the nuclear stopping increases at a particular instance of the collision but results in a lesser thermalization of the nuclear matter after the reaction is over. That is why, the nuclear stopping is found to decrease with the incident energy. A comparison has been made for the incident energy dependence of $< Q_{zz} >$ and the temperature in Fig. 6.13 (right panel), for the similar reaction as shown in the left panel of Fig. 6.13. The excitation energy dependence of the nuclear stopping (Q_{zz}) is found to give similar behavior as that of the temperature. Therefore, the temperature reached in HIC's gives an interesting and concrete resemblance with the global nuclear stopping.

One can clearly suspect a linear dependence of the $< Q_{zz} >$ and temperature with

Quantity	$\gamma = 0.66$		$\gamma = 1.33$		$\gamma = 2$	
-	m	c	m	c	m	c
$< Q_{zz} >$	0.24	-2.66	0.257	-3.00	0.262	-3.308
Max. Temp.	0.12	4.918	0.124	4.99	0.128	4.77

Table 6.1: The comparison of the slope for $< Q_{zz} >$ and the temperature for various forms of the density-dependent symmetry energy, i.e. different values of γ.

the incident energy. A linear fit y = mx + c has been performed for the excitation energy dependence of $< Q_{zz} >$ and the maximum temperature for the various forms of the density dependent symmetry energy in Table 6.1. A higher strength of the symmetry energy results in a steady increase in the slope for $< Q_{zz} >$ as well as for the maximum temperature. For a better understanding of the concept of thermalization, we present the global nuclear stopping constrained along the various types and size of rapidity bins and comparison with the experimental findings.

6.3.10 Optimizing the rapidity limit for nuclear stopping

We here perform a systematic study related to nuclear stopping to explore its various aspects through different rapidity distributions. We have divided the rapidity distribution into different ranges in terms of the parameter given below;

$$Y_{red.} = \frac{Y_{c.m.}}{Y_{beam}}. \tag{6.15}$$

where $Y_{c.m.}$ is stated in Eqn. 5.2. To understand the nuclear stopping via. rapidity distribution, we plot the dN/dY as a function of $Y_{red.} = \frac{Y_{c.m.}}{Y_{beam}}$ in Fig. 6.14 (left panel). Also, we plot the dN/dY with respect to Y_{red} for the systems having different isotopic content in the right panel of Fig. 6.14. The rapidity distribution is found to vary drastically throughout the range of rapidity $|Y_{red}| \leq 1.75$. This is a clear indication for the compressed or participant zone around the zero value and the decay into the spectator zone towards both sides of the zero value. Overall, the peak value for the curve increases with an increase in the size of the system due to the larger nuclear stopping.

6.3.10.1 R_P and Q_{zz} as function of system mass

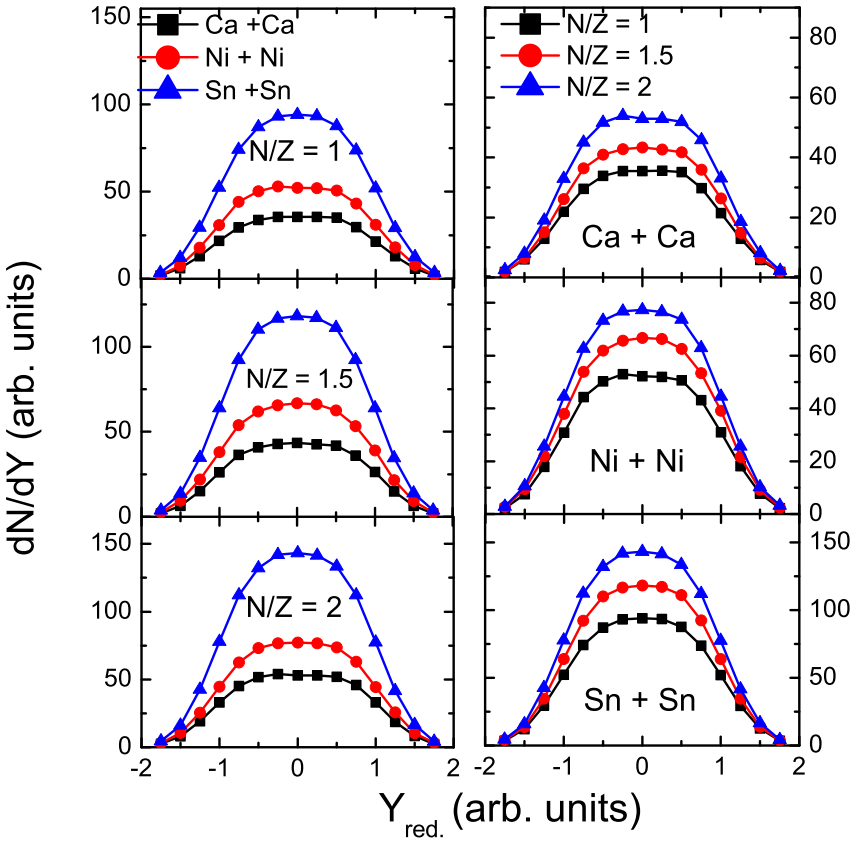

Figure 6.14: dN/dY as a function of $Y_{red.} = \frac{Y_{c.m.}}{Y_{beam}}$ for different systems having different isotopic compositions. The incident energy is 100 MeV/nucleon and $\hat{b} = 0.3$.

In Fig. 6.15, we display the system mass dependence of $< R_P >$ and $< Q_{zz} >$ for the different sizes of rapidity bins taken into account. Our findings clearly indicate the variation in $< R_P >$ and $< Q_{zz} >$ for the whole mass range for the various rapidity bins. The larger size of rapidity bin correspond to the increased contribution of spectator matter results in lesser nuclear stopping along the whole mass range.

6.3.10.2 Impact parameter dependence of R_P and Q_{zz}

The nuclear stopping or thermalization achieved during the collision is directly associated to the impact parameter of the reaction. To study the variation of nuclear stopping with colliding geometry, we display the impact parameter dependence of nuclear stopping for the different rapidity bins is shown in Fig. 6.16. One can clearly observe a linear decrease in the nuclear stopping with an increase in impact parameter of reaction. The larger impact parameter tends to increase the role of spectator matter which results in

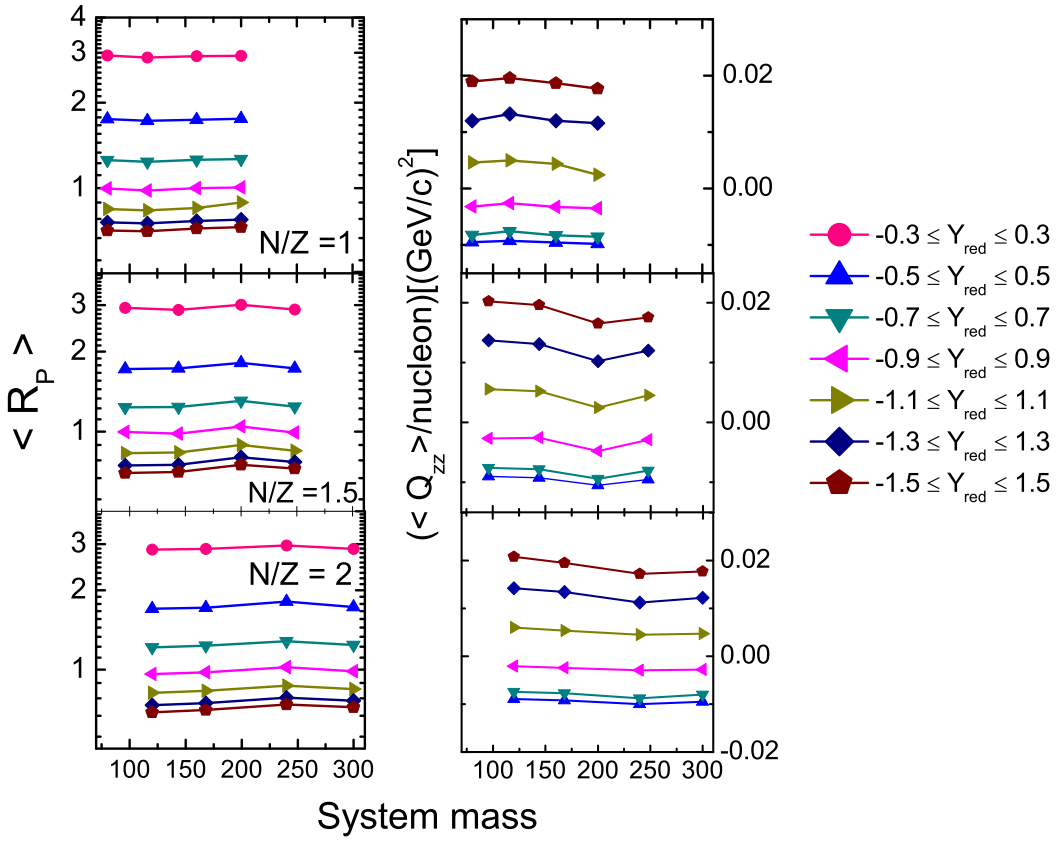

Figure 6.15: $< R_P >$ and $< Q_{zz} >$ as a function of the composite mass of the system for E = 100 MeV/nucleon and $\hat{b} = 0.3$. The different lines correspond to the different sizes of rapidity bins.

lesser value of $< R_P >$ due to the larger dominance of the longitudinal momentum (p_z) of the particles. However, larger participant matter corresponds to the lesser contribution of the p_z component of momenta and the larger contribution of $p_\perp$, which tends to increase the nuclear stopping. Overall, the nuclear stopping decreases with an increase in the size of rapidity bin at all the colliding geometries.

6.3.10.3 Comparison with experimental data

In Fig. 6.17, we display the excitation energy dependence of nuclear stopping with respect to the different rapidity bins and comparison with the experimental data [148]. The expansion of the rapidity bin including mid-rapidity, i.e., larger contribution of the spectator matter results in a clear decrease in nuclear stopping. The larger size of the rapidity bin (including mid-rapidity region) results in close agreement with the experimental data. The increase in size of rapidity bin corresponds to the larger contribution

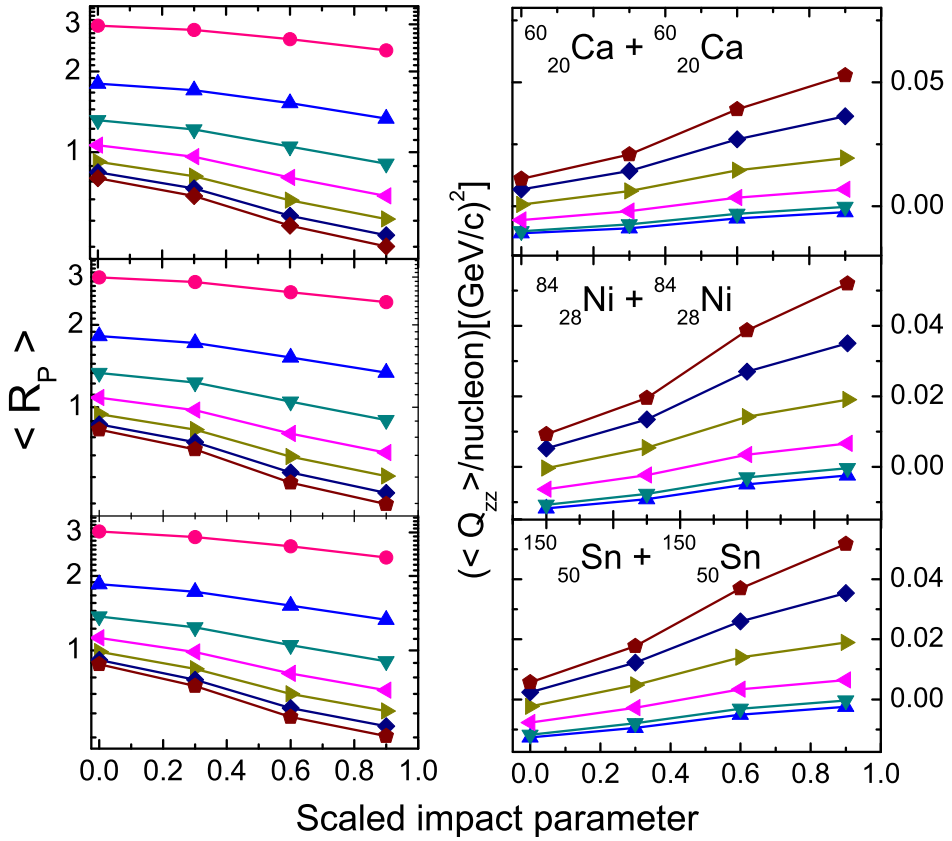

Figure 6.16: Impact parameter dependence of $< R_P >$ and $< Q_{zz} >$. The symbols and lines represent the same meaning as in Fig. 6.15.

of the system towards nuclear stopping which includes the participant matter as well as the spectator matter. However, we consider the term global nuclear stopping which comprises the nuclear stopping caused by the whole system. The global word is due to the fact that it does not depend on the local position. The anisotropy ratio produced by the experimental data is due to the ratio of the transverse momenta to the longitudinal momenta of all particles in the system. Constraining of the nuclear stopping to the mid-rapidity only, the core participant region is considered; that is why, we get the large value of anisotropy ratio (global nuclear stopping). This shows that most of the particles are stopped in the mid-rapidity region. That is why, our findings are not in agreement with the experimental data if we consider the mid-rapidity region only or near to mid-rapidity region. The largest size of rapidity bin yields a good agreement with the experimental findings at the incident energy above 80 MeV/nucleon.

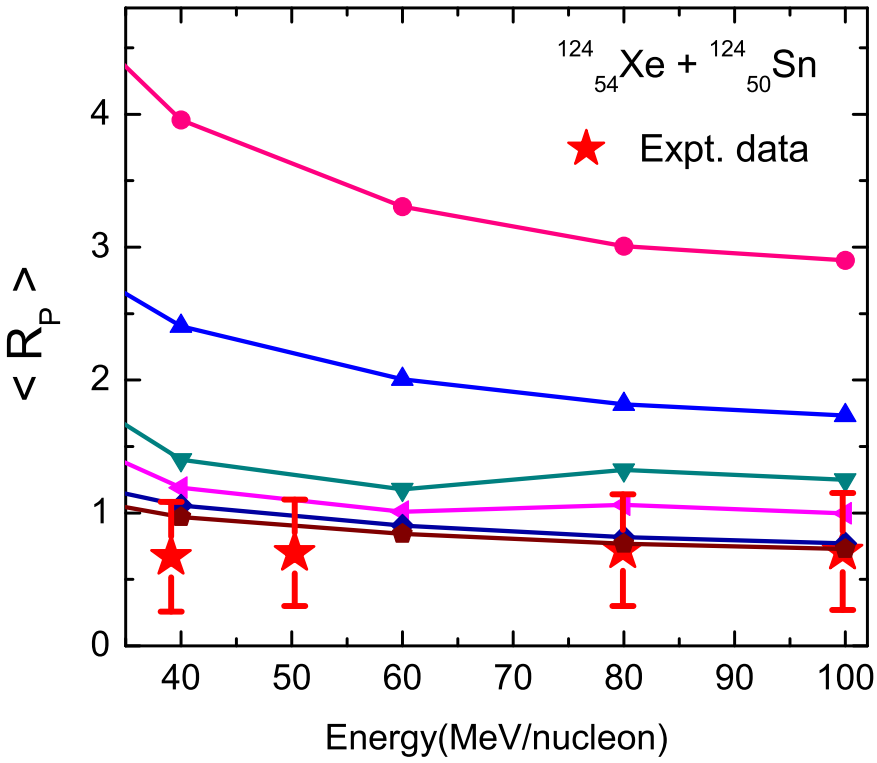

Figure 6.17: The incident energy dependence of nuclear stopping for the different sizes of rapidity bins and comparison with the experimental data [148]. The symbols and lines represent the same meaning as in Fig. 6.15.

6.4 Summary

We have studied the density and temperature reached in HIC's for various systems. Analysis has been carried out for the different forms of density dependent symmetry energy. Our findings with $\gamma = 0.66$, 1.33 & 2, concludes that the density and temperature increases for the larger values of γ. The global nuclear stopping is found to be associated to the temperature of the nuclear matter. This provides us a methodology to associate the global nuclear stopping with the temperature. The nuclear stopping can give us a good estimation of the temperature of the nuclear matter in HIC's.

Also the sensitivity of nuclear stopping to density dependent symmetry energy is analyzed. The nuclear stopping, which is found to increase with the composite mass of the system, shows a minor but considerable sensitivity for the isospin asymmetric systems for the various forms of density dependent symmetry energy. Our findings with $\gamma = 0.66$

- 2, concludes that the effect of density dependent symmetry energy on nuclear stopping cannot be observed at lower incident energies due to the small density achieved during the reaction. However, considerable effect can be observed at peripheral geometries. The nuclear stopping decreases for the stiff density dependence of the symmetry energy.

The investigation of the role of protons and neutrons in nuclear stopping clearly shows the larger contribution of protons towards nuclear stopping, which increases with the isospin asymmetry of the nuclear matter. The size of rapidity bin is found to affect the nuclear stopping drastically for the whole colliding geometry which is due to the larger number of nucleons concentrated to the mid-rapidity region. The participant and spectator region is determined by the impact parameter of the reaction, as the larger impact parameter tends to decrease the participant zone and vice-versa. In the participant region (or mid-rapidity zone) the transverse momentum $p_{\perp}$ achieved is of maximum strength, whereas longitudinal momentum $p_{||}$ vanishes which affects the value of $< R_P >$ and $< Q_{zz} >$. Although larger size of rapidity bin tends to increase the contribution of spectator (target and projectile) matter which strengthens the p_z component of momenta resulting in the lesser anisotropy ratio (nuclear stopping). The larger size of rapidity bin including the mid-rapidity region tends to favor the experimental data.

Chapter 7

Summary and outlook

7.1 Summary

We here presented a schematic analysis of the density dependence of symmetry energy on the various phenomena e.g. multi-fragmentation, elliptical flow and nuclear stopping used to study the heavy-ion collisions at intermediate energies. For the present analysis, we used the Isospin-dependent Quantum Molecular Dynamics *(IQMD)* model to generate the phase space of nucleons. The phase space was then analyzed using the various clusterization algorithms to get useful information regarding various phenomena's listed above.

We present the general introduction of the present work in **Chapter 1**. The importance of intermediate energy HIC's has been discussed in detail. We emphasized on the importance to study the isospin-asymmetric nuclear matter. The isospin asymmetry in the system leads to the evolution of symmetry energy. Also, the details of the density dependent symmetry energy and its role in the reaction dynamics is presented. We review the work done on the density dependence of the symmetry energy and described the different processes (multi-fragmentation, elliptical flow and nuclear stopping) in detail. For the present work, we use the isospin-dependent NN cross-section. **Chapter 2**, includes the brief survey of various theoretical models used in the literature to study the phase space of nucleons. We discussed the *QMD*, *IQMD* model, MST, and MSTM in detail.

In Chapter 3, we explored the various aspects of multi-fragmentation in the intermediate energy HIC's. We carry out an investigation for the evolution of free nucleons

and light mass fragments at, above and below the transition energy (incident energy at which the elliptical flow vanishes). We concluded that there is no particular structure obtained in fragmentation at the transition energy when the squeezed-out flow diminishes completely in the mid-rapidity region (participant zone).

In Chapter 4, we studied the effect of density dependence of symmetry energy on the production of FN's and LCP's for the whole colliding geometry. We see that the variation in fragment production is less than 10 % for the different forms of density dependence of symmetry energy. We see that the symmetry energy affect the fragment production within 2.7 % for FN's, and 4.6 % for LCP's on an average. The collective effect of MDI and symmetry energy affects the fragment production within 7.5 % for FN's, and 10.3 % for LCP's on an average with the variation of stiffness factor γ from 0.66 to 2. The inclusion of MDI & with density dependent symmetry energy ($\gamma = 0.69$) concludes a significant shift in the peak IMF multiplicity and a better agreement with the experimental data. Also, we performed an investigation for the excitation energy and impact parameter dependence of IMF's for the reaction of ${}^{197}_{79}Au + {}^{197}_{79}Au$ and made a comparison with the experimental findings of *ALADIN* Collaboration. Also, we performed an investigation regarding the impact of Coulomb interactions on the evolution of intermediate mass fragments and the results are compared with the *NSCL* data.

In Chapter 5, we study the influence of the density dependence of symmetry energy on the elliptical flow associated with the various fragments. We showed the transverse momentum and excitation energy dependence of the elliptical flow v_2 (second harmonic coefficient of the azimuthal distribution of particles in the reaction plane). We also made a comparison of theoretical predictions with the experimental findings of *INDRA, FOPI* and *PLASTIC BALL* collaborations. The excitation energy dependence of elliptical flow in the mid-rapidity region (core participant zone) yields larger squeeze-out for the protons and Z $\leq$ 2 particles with the inclusion of density dependence of symmetry energy ($\gamma = 0.66$) and a better agreement with the experimental findings. The neutron-proton P_t-differential elliptical flow has high sensitivity towards the momentum dependent equation of state and the isospin dependence of the NN cross section, which can shed light on the

density dependence of the symmetry energy and provide useful information about the complex nuclear matter interactions in the reaction zone.

In Chapter 6, we demonstrated that the maximum/average density and temperature increases with the stiffness of the symmetry energy (larger values of stiffness factor γ). We concluded that the nuclear stopping shows a mild sensitivity towards the different forms of density dependence of symmetry energy, however, considerable effect is observed at peripheral collisions. The nuclear stopping parameters (R and Q_{zz}) shows that the global stopping decreases mildly with the stiffness of symmetry energy. Theoretical predictions yields a good agreement with the experimental data of *INDRA* and *ALADIN* Collaboration. The most important aspects of our finding is that the nuclear stopping has the ability to provide information about the temperature reached during the reaction. Nuclear stopping can give a good generalization of the thermalization and temperature evolved during the reaction.

In summary, we concluded that the symmetry energy as a function of density has small effect on the multifragmentation and nuclear stopping. However, various forms of symmetry energy affect the elliptic flow drastically, which is a critical phenomenon and is generated from the participant zone. The density dependence of the symmetry energy ($\gamma = 0.66$) yields better agreement with the experimental data. The various forms of density dependent symmetry energy have a considerable effect on the maximum/average density and temperature reached during the reaction. Also, the global nuclear stopping can give us a good estimation of the temperature of the nuclear matter.

7.2 Outlook

The different forms of density dependence of symmetry ($\gamma = 0.66 - 2$) affects the fragment production within 10 % on an average. Also, the effect of various forms of density dependence of symmetry energy on nuclear stopping is very small. However, the elliptical flow is a significantly affected by the various forms of the symmetry energy. On the other hand, the exact parametrization for the density dependence of symmetry energy is still an open question for the nuclear physics community. Our findings with

the stiffness parameter $\gamma = 0.66$, yields more squeeze out for the protons and $Z \leq 2$ particles in the mid-rapidity region. The theoretical investigations can be very useful for the investigation of the appropriate parametrization of the density dependence of the symmetry energy. The effect of symmetry energy as well as its density dependence on the participant/spectator matter and other observables associated to the nuclear equation of state (such as photon production) can yield essential facts about the nuclear physics and astro-physics. The photon production is also an another topic of interest for the present day nuclear physics research, which needs an appropriate theoretical treatment for the better interpretation of HIC's.

The momentum dependent equation state is necessary for the proper interpretation of heavy-ion reactions and the better explanation of the experimental findings. The implementation of isospin effect via. momentum dependent interactions and its effects on various observables such as fragmentation, fragment flow and global stopping can be useful to understand the isospin-dependent part of the nuclear equation of state (density dependence of the symmetry energy). The information about the momentum dependence of the symmetry energy is essential to describe the exact parametrization of the density dependence of symmetry energy.

Bibliography

[1] S. S. Malik and Raj. K. Gupta, Phys. Rev. C **39**, 1992 (1989).

[2] P. K. Rath, Phys. Rev. C **79**, 051601(R) (2007).

[3] W. Trautmann *et al.,* Phys. Rev. C **76**, 064606 (2007).

[4] S. Rafi, M. Sharma, D. Pachouri, W. Haider, and Y. K. Gambhir, Phys. Rev. C **87**, 014003 (2013).

[5] A. W. Steiner, M. Prakash, J. M. Lattimer and P. J. Ellis, Phys. Rep. **411**, 325 (2005); M. Kutschera, Phys. Lett. B **340**, 1 (1994).

[6] J. M. Lattimer, M. Prakash, Phys. Rep. **333**, 121 (2000); J. M. Lattimer *et. al.* Astrophys. J. **550**, 426 (2001); A. Carbone *et al.*, Phys. Rev. C **81**, 041301 (2010); M. Prakash *et al.,* Phys. Rep. **280**, 1 (1997).

[7] S. Kubis and M. Kutschetra, Nucl. Phys. A **720**, 189 (2003); S. Kubis, Phys. Rev. C **76**, 025801 (2010).

[8] H. M*ü*ller and B. D. Serot, Phys. Rev. C **72**, 2072 (1995).

[9] B. A. Li and L. W. Chen, Phys. Rev. C **74**, 034610 (2006).

[10] S. Gautam, and R. K. Puri, Phys. Rev. C **85**, 067601 (2012).

[11] J. D. Walecka, Ann. Phys. (NY) **83**, 491 (1974); P. Ring, Prog. Part. Nucl. Phys. **37**, 193 (1996); J. Meng and P. Ring, Phys. Rev. Lett. **77**, 3963 (1996).

[12] G. Mahajan and S. K. Dhiman, Phys. Rev. C **84**, 045804 (2011).

[13] B. K. Agrawal, S. K. Dhiman, and Raj Kumar, Phys. Rev. C **73**, 034319 (2006).

[14] B. A. Li, C. M. Ko, and W. Bauer, Int. J. of Mod. Phys. E **7**, 147 (1998).

[15] P. Danielewicz, R. Lacey, W. G. Lynch, Science **298**, 1592 (2002).

[16] J. M. Lattimer, M. Prakash, Science **304**, 536 (2004).

[17] B. A. Brown, Phys. Rev. Lett. **85**, 5296 (2000).

[18] C. Xu, B. A. Li, L. W. Chen, Phys. Rev. C **82**, 054607 (2010); B. A. Li, L. W. Chen, C. M. Ko, Phys. Rep. **464**, 113 (2008).

[19] A. Bohr and B. R. Mottelson, Nuclear structure 1, (Benjamin, New York) (1969).

[20] C. F. V. Weizsäcker, Z. Physik **96**, 431 (1935); H. A. Bethe and R. F. Bacher, Rev. Ko, S. J. Yennello, Phys. Rev. Lett. **76**, 4492 (1996).

[21] H. Stocker and W. Greiner, Phys. Rep. **137**, 277 (1986).

[22] C. Hartnack *et al.,* Eur. Phys. J. A **1**, 151 (1998); C. Hartnack *et al.,* Phys. Rep. **510**, 119 (2012).

[23] B. A. Li and S. J. Yennello, Phys. Rev. C **52**, R1746 (1995).

[24] B. A. Li *et al.,* Phys. Rev. Lett. **76**, 4492 (1996).

[25] M. B. Tsang, Y. Zhang, P. Danielewicz, M. Famiano, Z. Li, W. G. Lynch, A. W. Steiner, Phys. Rev. Lett. **102**, 122701 (2009).

[26] D. V. Shetty, S. J. Yenello, G. A. Souliotis, Phys. Rev. C **76**, 024606 (2007); D. V. Shetty, S. J. Yennello and G. A. Souliotis, Phys. Rev. C **75**, 034602 (2007); D. V. Shetty *et al.,* Nucl. Instr. and Meth. in Phys. Res. B **261**, 990 (2007).

[27] D. V. Shetty and S. J. Yennello, Pramana J. Phys. **75**, 259 (2010); D. V. Shetty, S. J. Yennello, A. S. Botvina, G. A. Souliotis, M. Jandel, E. Bell, A. Keksis, S. Soisson, B. Stein and J. Iglio, Phys. Rev. C. **70**, 011601 (2004).

[28] M. A. Famiano *et al.*, Phys. Rev. Lett. **97**, 052701 (2006).

[29] E. Galichet, M. Colonna, B. Borderie and M. F. Rivet, Phys. Rev. C **79**, 064615 (2009); E. Galichet *et al.,* Phys. Rev. C **79**, 064614 (2009).

[30] B. A. Li, C. B. Das, S. Das Gupta and C. Gale, Phys Rev. C **69**, 011603(R) (2004).

[31] B. A. Li and L. W. Chen, Phys. Rev. C **72**, 064611 (2005).

[32] M. B. Tsang *et al.*, Phys. Rev. Lett. **92**, 062701 (2004).

[33] Z. G. Xiao, B. A. Li, L. W. Chen, G. C. Yong, M. Zhang, Phys. Rev. Lett. **102**, 062502 (2009).

[34] M. B. Tsang *et al.*, Prog. Part. Nucl. Phys. **66**, 400 (2011).

[35] L. W. Chen, C. M. Ko, and B. A. Li, Phys. Rev. C **68**, 017601 (2003).

[36] B. A. Li, Phys. Rev. C **69**, 034614 (2004).

[37] H. Heiselberg and M. Hjorth-Jensen, Phys. Rep. **328**, 237 (2000).

[38] C. J. Horowitz and J. Piekarewicz, Phys. Rev. C **66**, 055803 (2002).

[39] J. M. Lattimer *et al.,* Astrophys. J. **425**, 802 (1994).

[40] J. R. Stone *et al.,* Phys. Rev. C **68**, 034324 (2003).

[41] R. B. Wiringa, V. Fiks, A. Fabrocini, Phys. Rev. C **38**, 1010 (1988).

[42] B. Liu *et al.,* Phys. Rev. C **65**, 045201 (2002).

[43] N. Kaiser, S. Fritsch, and W. Weise, Nucl. Phys. A **697**, 255 (2002).

[44] C. Fuchs and H. H. Wolter, Eur. Phys. J. A **30**, 5 (2006).

[45] Z. H. Li *et al.*, Phys. Rev. C **74**, 044613 (2006); Y. Zhang, P. Danielewicz, M. Famiano, Z. Li, M. B. Tsang, Phys. Lett. B **664**, 145 (2008).

[46] B. Friedman, V. R. Pandharipande, Nucl. Phys. A **361**, 502 (1981); D. T. Khoa *et al.*, Nucl. Phys. A **602**, 98 (1996).

[47] S. Kumar and Y. G. Ma, Phys. Rev. C **86**, 051601(R) (2012).

[48] E. Khan *et al.*, Phys. Rev. C **82**, 024322 (2010).

[49] P. Russotto *et al.*, Phys. Lett. B **697**, 471 (2011); A. Klimkiewicz, *et al.*, Phys. Rev. C **76**, 051603(R) (2007); M. Centelles, *et al.*, Phys. Rev. Lett. **102**, 122502 (2009).

[50] A. Andronic *et al.*, Phys. Lett. B **612**, 173 (2005).

[51] Q. Li *et al.,* J. Phys. G: Nucl. Part. Phys. **31**, 1359 (2005).

[52] Q. Li *et al.*, J. Phys. G: Nucl. Part. Phys. **32**, 151 (2006); Q. Li *et al.*, J. Phys. G: Nucl. Part. Phys. **32**, 407 (2006).

[53] L. W. Chen, C. M. Ko, and B. A. Li, Phys. Rev. Lett. **94**, 032701 (2005).

[54] B. A. Li, C. B. Das, S. Das Gupta, and C. Gale, Nucl. Phys. A **735**, 563 (2004).

[55] L. W. Chen, V. Greco, C. M. Ko, and B. A. Li, Phys. Rev. Lett. **90**, 062701 (2003).

[56] G. C. Yong, B. A. Li and L. W. Chen, Phys. Rev. C **74**, 064617 (2006).

[57] G. C. Yong, Phys. Rev. C **81**, 054603 (2010).

[58] W. G. Lynch *et al.,* Prog. Part. Nucl. Phys. **62**, 427 (2009).

[59] V. Baran, M. Colonna, V. Greco and M. D. Toro, Phys. Rep. **410**, 335 (2005).

[60] W. Reisdorf *et al.*, Nucl. Phys. A **781**, 459 (2007).

[61] http://groups.nscl.msu.edu/hira/sep.htm.

[62] S. Kumar, Y. G. Ma, G. Q. Zhang, and C. L. Zhou, Phys. Rev. C **85**, 024620 (2012).

[63] B. A. Li *et al.,* Phys. Rev. Lett. **88**, 192701 (2002) and references therein.

[64] B. A. Li, Nucl. Phys. A **708**, 365 (2002).

[65] B. A. Li, G. C. Yong, and W. Zuo, Phys. Rev. C **71**, 044604 (2005).

[66] B. A. Li, L. W. Chen, G. C. Yong, and W. Zuo, Phys. Lett. B **634**, 378 (2006)

[67] Q. Li, Z. Li, S. Soff, M. Bleicher, and H. Stocker, Phys. Rev. C **72**, 034613 (2005); B. A. Li, L. W. Chen, H. R. Ma, J. Xu, and G. C. Yong, Phys. Rev. C **76**, 051601(R) (2007).

[68] B. A. Li, Phys. Rev. C **67**, 017601 (2003); H. H. Wolter, V. Prassa, G. Lalazissis, T. Gaitanos, G. Ferini, M. D. Toro, and V. Greco, Prog. Part. Nucl. Phys. **62**, 402 (2009)

[69] M. Zhang, Z. G. Xiao, B. A. Li, L. W. Chen, G. C. Yong, and S. J. Zhu, Phys. Rev. C **80**, 034616 (2009).

[70] Z. Q. Feng and G. M. Jin, Phys. Lett. B **683**, 140 (2010).

[71] M. Zhang, Z. G. Xiao, and S. J. Zhu, Chin. Phys. C **34**, 1100 (2010).

[72] Y. Gao, L. Zhang, H. F. Zhang, X. M. Chen, and G. C. Yong, Phys. Rev. C **83**, 047602 (2011).

[73] G. C. Yong, B. A. Li, L. W. Chen, W. Zuo, Phys. Rev. C **73**, 034603 (2006).

[74] C. W. Ma *et al.*, Eur. Phys. J. A **48**, 78 (2012).

[75] W. Trautmann *et al.*, PoS BORMIO **2011**, 018 (2011).

[76] P. Marini *et al.,* Phys. Rev. C **87**, 024603 (2013).

[77] J. P. Bondorf, A. S. Botvina, A. S. IIjinov, I. N. Mishustin, and K. Sneppen, Phys. Rep. **257**, 133 (1995)

[78] A. S. Botvina *et al.,* Nucl. Phys. A **584**, 737 (1995).

[79] J. K. Dhawan and R. K. Puri, Phys. Rev. C **75**, 057601 (2007).

[80] B. Jakobsson *et al.,* Nucl. Phys. A **509**, 195 (1990).

[81] J. P. Hubbele *et al.,* Z. Phys. A **340**, 263 (1991).

[82] A. Schüttauf *et al.,* Nucl. Phys. A **607**, 457 (1996).

[83] S. Hudan *et al.,* Phys. Rev. C **67**, 064613 (2003).

[84] A. Bohnet, N. Ohtsuka, J. Aichelin, R. Linden, and A. Faessler, Nucl. Phys. A **494**, 349 (1989).

[85] J. Piekarewicz, Proceedings of the International Conference on Current Problems in Nuclear Physics and Atomic Energy, Kyiv, Ukraine, May 29 - June 3, 2006.

[86] M. B. Tsang, W. A. Friedman, C. K. Gelbke, W. G. Lynch, G. Verde, and H. S. Xu, Phys. Rev. Lett. **86**, 5023 (2001)

[87] G. Peilert, H. Stocker, and W. Greiner, Rep. Prog. Phys. **57**, 533 (1994).

[88] B. Jakobsson *et al.,* Z. Phys. A **307**, 293 (1982).

[89] A. I. Warwick *et al.,* Phys. Rev. C **27**, 1083 (1983).

[90] J. E. Finn *et al.,* Phys. Rev. Lett. **49**, 1321 (1982).

[91] N. T. Porlie, Nucl. Phys. A **681**, 253 (2001); B. K. Srivastva *et al.,* Phys. Rev. C **65**, 054617 (2002); J. B. Elliott *et al.,* Phys. Rev. C **71**, 024607 (2005); L. G. Moretto, C. O. Dorso, J. B. Elliott, and L. Phair, Phys. Rev. C **77**, 037603 (2008).

[92] S. R. Souza *et al.,* Phys. Rev. C **50**, 257 (1994).

[93] L. Phair *et al.,* Phys. Rev. Lett. **75**, 213 (1995); L. Phair *et al.,* Phys. Rev. Lett. **77**, 822 (1996).

[94] T. C. Sangster *et al.,* Phys. Rev. C **46**, 1404 (1992).

[95] D. R. Bowman *et al.,* Nucl. Phys. A **523**, 386 (1991).

[96] P. R. Chomaz *et al.,* Nucl. Phys. A **552**, 508 (1993).

[97] A. Insolia *et al.,* Phys. Rev. C **61**, 044902 (2000).

[98] R. T. de Souza *et al.,* Phys. Lett. B **268**, 6 (1991); T. Li *et al.,* Phys. Rev. Lett. **70**, 1924 (1992); L. Phair *et al.,* Phys. Lett. B **285**, 10 (1992); D. R. Bowman *et al.,* Phys. Rev. C **46**, 1834 (1992); T. Li *et al.,* Phys. Rev. C **49**, 1630 (1994).

[99] C. Williams *et al.,* Phys. Rev. C **55**, R2132 (1997).

[100] M. B. Tsang *et al.,* Phys. Rev. Lett. **71**, 1502 (1993).

[101] S. Piantelli *et al.,* Phys. Rev. C **74**, 034609 (2006); S. Piantelli *et al.,* Phys. Rev. C **78**, 064605 (2008).

[102] R. Planeta *et al.,* Phys. Rev. C **77**, 014610 (2008).

[103] C. A. Ogilvie *et al.,* Phys. Rev. Lett. **67**, 1214 (1991).

[104] J. Hubele *et al.,* Phys. Rev. C **46**, R1577 (1992).

[105] M. Begemann-Blaich *et al.,* Phys. Rev. C **48**, 610 (1993).

[106] G. F. Peaslee *et al.,* Phys. Rev. C **49**, R2271 (1994); N. T. B. Stone *et al.,* Phys. Rev. Lett. **78**, 2084 (1997); A. S. Botvina *et al.,* Phys. Rev. C **74**, 044609 (2006).

[107] B. de Schauenburg,*et al.,* GSI Rep. **98-1**, p. 56 (1997); W. Reisdorf, Nucl. Phys. A **630**, 15c (1998); W. Reisdorf, *et al., ibid.* **2000-1**, p. 45 (1999); W. Reisdorf, Hirschegg, p. **82** (1999); B. Hong *et al.,* Phys. Rev. C **66**, 034901 (2002).

[108] G. Poggi *et al.,* Nucl. Phys. A **586**, 755 (1995); J. Konopka, *et al.,* GSI Rep. **96-1**, p. 65 (1995); J. P. Alard, *et al., ibid.* **97-1**, p. 54 (1996); N. Bastid, *et al., ibid.* **98-1**, p. 54 (1997); A. Andronic, *et al., ibid.* **98-1**, p. 55 (1997).

[109] C. Sfienti *et al.,* Acta Phys. Pol. B **37**, 193 (2006).

[110] see http://www-aladin.gsi.de.

[111] W. Trautmann *et al.,* Int. J. Mod. Phys. E **17**, 1838 (2008); W. Trautmann *et al.,* Nucl. Phys. A **787**, 575 (2007).

[112] C. Sfienti *et al.,* Phys. Rev. Lett. **102**, 152701 (2009).

[113] Y. G. Ma *et al.,* Phys. Rev. C **69**, 031604 (2004).

[114] R. Wada *et al.,* Phys. Rev. C **69**, 044610 (2004); J. Wang *et al.,* Phys. Rev. C **72**, 024603 (2005); R. Wada *et al.,* Phys. Rev. C **71**, 054608 (2005).

[115] D. V. Shetty *et al.,* J. Phys. G: Nucl Part. Phys. **36** , 075103 (2009).

[116] D. V. Shetty, G. A. Souliotis, S. Galanopoulos, and S. J. Yennello, Phys. Rev. C **79**, 034603 (2009).

[117] D. V. Shetty *et al.,* Phys. Rev. C **68**, 054605 (2003).

[118] A. Ono, P. Danielewicz, W. A. Friedman, W. G. Lynch, and M. B. Tsang, Phys. Rev. C **68**, 051601(R) (2003).

[119] A. Ono, P. Danielewicz, W. A. Friedman, W. G. Lynch, and M. B. Tsang, Phys. Rev. C **70**, 041604(R) (2004).

[120] N. Marie *et al.,* Phys. Rev. C **58**, 256 (1998); W. Loveland *et al.,* Phys. Rev. C **59**, 1472 (1999)

[121] J. D. Frankland *et al.,* Phys. Rev. C **71**, 034607 (2005); J. D. Frankland *et al.,* Nucl. Phys. A **689**, 940 (2001).

[122] J. Colin *et al.,* Phys. Rev. C **67**, 064603 (2003).

[123] J. Lukasik *et al.,* Phys. Rev. C **66**, 064606 (2002).

[124] L. Manduci *et al.,* Nucl. Phys. A **811**, 93 (2008).

[125] E. Bohnet *et al.,* Phys. Rev. Lett. **103**, 072701 (2009).

[126] P. Bozek and I. Wyskiel, Phys. Rev C **81**, 054902 (2010).

[127] V. Greco *et al.,* Phys. Lett. B **562**, 215 (2003).

[128] H. Stocker *et al.,* Phys. Rev. C **25**, 1873 (1982); A. R. Raduta and F. Gulminelli, Phys. Rev. C **75**, 024605 (2007).

[129] M. Demoulins *et al.,* Phys. Lett. B **241**, 476 (1990).

[130] H. H. Gutbroad *et al.,* Phys. Lett. B **216**, 267 (1989).

[131] H. H. Gutbroad *et al.,* Phys. Rev. C **42**, 640 (1990).

[132] R. Popescu *et al.,* Phys. Lett. B **331**, 285 (1994).

[133] M. B. Tsang *et al.,* Phys. Rev. C **53**, 1959 (1996).

[134] P. Danielewicz *et al.,* Phys. Rev. Lett. **81**, 2438 (1998).

[135] C. Pinkenburg *et al.,* Phys. Rev. Lett. **83**, 1295 (1999).

[136] K. H. Ackermann *et al.,* Phys. Rev. Lett. **86**, 402 (2001); C. Adler *et al.,* Phys. Rev. Lett. **87**, 182301 (2001); C. Adler *et al.,* Phys. Rev. C **66**, 034904 (2002); J. Adams *et al.,* Phys. Rev. C **72**, 014904 (2005).

[137] Y. Zhang, Z. Li, and P. Danielewicz, Phys. Rev. C **75**, 034615 (2007).

[138] P. Crochet *et al.,* Nucl. Phys. A **624**, 755 (1997).

[139] J. Lukasik, G. Auger, and M. L. Begemann-Blaich *et al.*, Phys. Lett. B **608**, 223 (2005).

[140] A. Andronic *et al.*, Nucl. Phys. A **679**, 765 (2001).

[141] J. Lukasik, *et.al.,* INDRA Collaborations, Int. Workshop on Multifragmentation and related topics (IWM 2003) Caen, France (2003).

[142] W. Reisdorf *et al.,* Phys. Rev. Lett. **92**, 232301 (2004).

[143] W. Reisdorf *et al.,* Phys. Lett. B **595**, 118 (2004).

[144] A. Andronic, J. Lukasik, W. Reisdorf, and W. Trautmann, Eur. Phys. J. A **30**, 31 (2006).

[145] N. Bastid *et al.,* Phys. Rev. C **72**, 011901 (2005).

[146] J. Lukasik *et al.,* Proc. of INPC **2**, 513 (2007).

[147] J. Y. Ollitrault, A. M. Poskanzer, and S. A. Voloshin, Phys. Rev. C **80**, 014904 (2009).

[148] G. Lehaut *et al.*, Phys. Rev. Lett. **104**, 232701 (2010).

[149] P. Danielewicz, Acta Phys. Polon. B **33**, 45 (2002); B. Hong *et al.,* Phys. Rev. C **71**, 034902 (2005); T. Gaitanos, C. Fuchs and H. H. Wolter, Phys. Lett. B **609**, 241 (2005).

[150] S. Pal, S. K. Samaddar, and J. N. De, Nucl. Phys. A **608**, 49 (1996), D. K. Srivastava *et al.,* Nucl-th/0506075 (2005); L. Satpathy, M. Mishra, A. Das, M. Satpathy, Phys. Lett. B **237**, 181 (1990); C. B. Das, A. Das, L. Satpathy, M. Satpathy, Phys. Rev. C **53**, 1833 (1996).

[151] J. P. Bondorf, R.Donangelo, I.N. Mishustin, C.J. Pethick, H. Schulz, and K. Sneppen, Nucl. Phys. A **443**, 321 (1985).

[152] J. P. Bondorf *et al.,* Nucl. Phys. A **444**, 460 (1985); *ibid* **448**, 753 (1986). G. A. Souliotis *et al.,* Phys. Rev. C **75**, 011601 (2007); S. Pal, S. K. Samaddar, J. N. de, and B. Djerroud, Phys. Rev. C **57**, 3246 (1998); A. Das, M. Mishra, M. Satpathy, and L. Satpathy, J. Phys. G: Nucl. and Part. **19**, 319 (1993).

[153] D. H. E. Gross, Rep. Prog. Phys. **53**, 605 (1990).

[154] S. R. Souza, W. P. Tan, R. Donangelo, C. K. Gelbke, W. G. Lynch, and M. B. Tsang, Phys. Rev. C **62**, 064607 (2000).

[155] W. Bauer, D. R. Dean, U. Mosel, and U. Post, Phys. Lett. B **150**, 53 (1985); W. Bauer, U. Post, D. R. Dean, and U. Mosel, Nucl. Phys. A **452**, 699 (1986).

[156] J. Pan, S. D. Gupta, Phys. Lett. B **344**, 29 (1995); J. Pan, S. D. Gupta, Phys. Rev. C **51**, 1384 (1995); S. D. Gupta and J. Pan, Phys. Rev. C **53**, 1319 (1996).

[157] W. A. Friedman, Phys. Rev. C **42**, 667 (1990).

[158] A. K. Kerman and S. E. Koonin, Ann. of Phys. **100**, 332 (1976); P. Bonche, S. Koonin and J. W. Negele, Phys. Rev. C **13**, 1226 (1976); K. T. R. Davies and S. E. Koonin, Phys. Rev. C **23**, 2042 (1981); M. D. Toro, G. Russo, and F. Duggan, Phys. Rev. C **21**, 2054 (1980).

[159] G. F. Bertsch, H. Kruse and S. D. Gupta, Phys. Rev. C **29**, R673 (1984).

[160] J. J. Molitoris, H. Stocker, and B. L. Winer, Phys. Rev. C **36**, 220 (1987); C. Gale *et al.,* Phys. Rev. C **41**, 1545 (1990); W. Cassing, W. Metag, U. Mosel, and K. Nitta, Phys. Rep. **188**, 363 (1990).

[161] H. Kruse, B. V. Jacak, and H. Stocker, Phys. Rev. Lett. **54**, 289 (1985); J. J. Molitoris, A. Bonasera, B. L. Winer, and H. Stocker, Phys. Rev. C **37**, 1020 (1988).

[162] E. Suraud, C. Gregoire, and B. Tamain, Prog. Part. Nucl. Phys. **23**, 357 (1989).

[163] A. Bonasera, G. F. Burgio, and M. D. Toro, Phys. Lett. B **221**, 233 (1989); A. Bonasera, G. Russo, and H. H. Wolter, Phys. Lett. B **246**, 337 (1990).

[164] L. Wilets, Y. Yariv, and R. Chestnut, Nucl. Phys. A **301**, 359 (1978); A. R. Bodmer, C. N. Panos, and A. D. MacKellar, Phys. Rev. C **22**, 1025 (1980); A. Vicentini, G. Jacucci and V. R. Pandharipande, Phys. Rev. C **31**, 1783 (1985).

[165] H. Feldmeier and J. Schnack, Rev. Mod. Phys. **72**, 655 (2000).

[166] J. Aichelin, Phys. Rep. **202**, 233 (1991).

[167] J. Aichelin and H. Stocker, Phys. Lett. B **176**, 14 (1986).

[168] J. Aichelin, A. Rosenhaur, G. Peilert, H. Stocker, and W. Greiner, Phys. Rev. Lett. **58**, 1926 (1987).

[169] G. Peilert, H. Stocker, W. Griener, A. Rosenhauer, A. Bohnet, and J. Aichelin, Phys. Rev. C **39**, 1402 (1989); G. Peilert *et al.,* Mod. Phys. Lett. A **3**, 459 (1988).

[170] J. Aichelin, G. Peilert, A. Bohnet, A. Rosenhauer, H. Sö*c*ker and W. Greiner, Phys. Rev. C **37**, 2451 (1998).

[171] E. Lehmann, R. K. Puri, A. Faessler, G. Batko and S. W. Huang, Phys. Rev. C **51**, 2113 (1995).

[172] A. Bohnet *et al.*, Phys. Rev. C **44**, 2111 (1991).

[173] P. B. Gossiaux, D. Keane, S. Wang, and J. Aichelin, Phys. Rev. C **51**, 3357 (1995); G. Q. Li *et al.,* Nucl. Phys. A **537**, 631 (1992); C. Fuchs, A. Faessler, E. Zabrodin, and Y. M. Zheng, Phys. Rev. Lett. **86**, 1974 (2001).

[174] Z. X. Li , C. Hartnack, H. St*ö*cker and W. Greiner, Phys. Rev. C **44**, 824 (1991).

[175] J. Jaenicke, J. Aichelin, N. Ohtsuka, R. Linden and A. Faessler, Nucl. Phys. A **536**, 201 (1992).

[176] M. Colonna *et al.,* Phys. Rev. C **57**, 1410 (1998).

[177] S. A. Bass, C. Hartnack, H. Stöcker, and W. Greiner, Phys. Rev. C **51**, 3343 (1995).

[178] B. J. VerWest and R. A. Arndt, Phys. Rev. C **25**, 1979 (1982).

[179] J. Y. Liu *et al.,* Phys. Rev. Lett. **86**, 975 (2001).

[180] J. Singh, S. Kumar, and R. K. Puri, Phys. Rev. C **62**, 044617 (2000); *ibid.* **65**, 024602 (2002).

[181] R. K. Puri and S. Kumar, Phys. Rev. C **57**, 2744 (1998).

[182] S. Kumar, S. Kumar, and R. K. Puri, Phys. Rev. C **78**, 064602 (2008).

[183] S. Kumar, S. Kumar, and R. K. Puri, Phys. Rev. C **81**, 014601 (2010).

[184] S. Kumar, Ph.D Thesis 1999, Punjab University, Chandigarh (India).

[185] S. Kumar and R. K. Puri, Phys. Rev. C **58**, 320 (1998).

[186] S. Kumar, S. Kumar, and R. K. Puri, Phys. Rev. C **81**, 014611 (2010).

[187] K. S. Vinayak and S. Kumar, Phys. Rev. C **83**, 034614 (2011).

[188] K. S. Vinayak and S. Kumar, Phys. Part. Nucl. Lett. **9**, 583 (2012); K. S. Vinayak, M. Singh, and S. Kumar, 5th Chandigarh Science Congress (CHASCON), PUNJAB UNIVERSITY, (CHANDIGARH), **PS-16**, Page-56 (2011): K. S. Vinayak and S. Kumar, Journal of Physics Conference Series **381**, 012032 (2012); K. S. Vinayak and S. Kumar, DAE Symposium for Nuclear Physics, BITS (PILANI), Vol. **55**, 496 (2010); K. S. Vinayak and S. Kumar, Pramana Journal of Physics (Accepted).

[189] K. S. Vinayak and S. Kumar, Eur. Phys. J. A **47**, 144 (2011); S. Kumar and K. S. Vinayak, DAE symposium for Nuclear Physics, Andhra University, (Vishakhapatnam), Vol. **56**, 814 (2011); K. S. Vinayak and S. Kumar, AIP Proceedings **1524**, 228 (2013); S. Kumar and K. S. Vinayak, DAE symposium for Nuclear Physics, University of Delhi, (New Delhi), Vol. **57**, 704 (2012).

[190] K. S. Vinayak and S. Kumar, J. Phys. G: Nucl. Part. Phys. **39**, 095105 (2012); K. S. Vinayak and S. Kumar, Eur. Phys. J. A **48**, 96 (2012); K. S. Vinayak and S. Kumar, Phys. of Atomic Nucl. **76**, 286 (2013); K. S. Vinayak and S. Kumar, DAE Symposium on Nuclear Physics, Andhra University, (Vishakhapatnam), Vol. **56**, 770 (2011).

[191] J. W. Negele, Rev. Mod. Phys. **54**, 913 (1982); H. Stocker and W. Greiner, Phys. Rep. **137**, 277 (1986); F. Sakata *et al.,* Phys. Rev. C **50**, 138 (1994); D. Lacroix.

and P. Chomaz, Phys. Rev. C **58**, 1604 (1998); A. S. Umar and D. Oberacker, Phys. Rev. C **74**, 024606 (2006); S. S. Chandel, S. K. Dhiman, R. Shyam, Phys. Rev. C **68**, 054320 (2003).

[192] J. Cugnon and C. Volant, Z. Phys. A **334**, 435 (1989); J. Cugnon, D. Kinet, and J. Vandermeulen, Nucl. Phys. A **379**, 553 (1982); J. Cugnon, Phys. Rev. C **22**, 1885 (1980).

[193] H. Sorge, H. Stöcker and W. Greiner, Ann. Phys. **192**, 266 (1989).

[194] H. Sorge, Phys. Rev. C **52**, 3291 (1995).

[195] M. Belkacem *et al.,* Phys. Rev. C **58**, 1727 (1998); A. Dumitru *et al.,* Phys. Rev. C **57**, 3271 (1998); S. A. Bass *et al.,* Prog. Part. Nucl. Phys. **41**, 255 (1998).

[196] K. A. Waged, Phys. Rev. C **67**, 064610 (2003); *ibid.* C **70**, 014605 (2004); *ibid.* C **71**, 044607 (2005).

[197] J. Aichelin and G. Bertsch. Phys. Rev. C **31**, 1730 (1985).

[198] J. Molitoris, J. B. Hoffer, H. Kruse, and H. Stocker, Phys. Rev. Lett. **53**, 899 (1984); S. M. Kiselew and Y. E. Polrowskil, Sov. Journ, Nucl. Phys. **38**, 46 (1983).

[199] G. Batko, J. Randrup and T. Vetter, Nucl. Phys. A **536**, 786 (1992); *ibid.* A **546**, 761 (1992).

[200] J. Cugnon, T. Mizutani, and J. Vandermeulen, Nucl. Phys. A **352**, 505 (1981).

[201] T. Maruyama, A. Ono and H. Horiuchi, Phys. Rev. C **42**, 386 (1990).

[202] S. W. Huang, *Ph.D. thesis*, Tubingen (Germany) (1994).

[203] G. Peilert, J. Randrup, H. Stöcker and W. Greiner, Phys. Lett. B **260**, 271 (1991); G. Peilert *et al.*, Phys. Rev. C **46**, 1457 (1992).

[204] J. Konopka, H. Stöcker and W. Greiner, Nucl. Phys. A **583**, 357c (1995).

[205] M. Trefz, A. Faessler and W. H. Dickhoff, Nucl. Phys. A **443**, 499 (1985); N. Ohtsuka, R. Linden, A. Faessler and F. B. Malik, Nucl. Phys. A **465**, 550 (1987).

[206] V. Ramillien *et al.,* Nucl. Phys. A **587**, 802 (1995).

[207] R. K. Puri *et al.,* Nucl. Phys. A **575**, 733 (1994); R. K. Puri, J. Singh, J. Aichelin and A. Faessler, in Horizon of Physics, edited by R. K. Gupta (Narosa, New Delhi, India).

[208] Q. Li, Z. Li and H. Stöcker, Phys. Rev. C **73**, 051601 (2006).

[209] R. K. Puri, E. Lehmann, A. Faessler and S. W. Huang, Z. Phys. A **351**, 59 (1995).

[210] H. Feldmeier, Nucl. Phys. A **515**, 147 (1990); H. Feldmeier and J. Schnack, Prog. Part. Nucl. Phys. **39**, 393 (1997).

[211] A. Ono, H. Horiuchi, T. Maruyama, and A. Ohnishi, Phys. Rev. Lett. **68**, 2898 (1992); A. Ono and H. Horiuchi, Phys. Rev. C **51**, 299 (1995).

[212] N. Itagaki *et al.,* Phys. Rev. C **70**, 054307 (2004).

[213] M. Papa, T. Maruyama and A. Bonasera, Phys. Rev. C **64**, 024612 (2001); M. Papa, G. Giuliani and A. Bonasera, J. Comp. Phys. **208**, 403 (2005).

[214] M. Hoffmann *et al.,* Phys. Lett. B **478**, 161 (2000); Y. Akimura *et al.,* Eur. Phys. J. A **25**, 405 (2005).

[215] D. Lacorix, A. V. Lauwe, and D. Durand, Phys. Rev. C **69**, 054604 (2004).

[216] Total cross-sections for reactions of high energy particles, edited by A. Baldini, V. Flaminio, W. G. Moorhead, and R. R. O. Morrison (Springer-Verlag, Berlin, 1988).

[217] S. K. Charagi and S. K. Gupta, Phys. Rev. C **41**, 1610 (1990); G. Alkahzov *et al.,* Nucl. Phys. A **280**, 365 (1977).

[218] G. Q. Li and R. Machleidt, Phys. Rev. C **48**, 1702 (1993).

[219] B. Remaud, C. Grëgoire, F. Sebille, and P. Schuck, Nucl. Phys. A **488**, 423c (1988); M. Farine, T. Sami, B. Remaud, and F. Sebille, Z Phys. A **339**, 363 (1991); L. G. Sobotka, Phys. Rev. C **50**, R1272 (1994).

[220] P. E. Hodgson, *Nuclear Reactions and Nuclear Structure* (Clarendon, Oxford, 1971), Chap. 9.3.

[221] B. A. Li, C. B. Das, S. D. Gupta, and C. Gale, Nucl. Phys. A **735**, 563 (2004).

[222] P. E. Hodgson, The Nucleon Optical Model, World Scientific, Singapore, 1994.

[223] C. B. Dass, S. D. Gupta, C. Gale, B. A. Li, Phys. Rev. C **67**, 034611 (2003).

[224] H. Kruse, B. V. Jacak, and H. Stocker. Phys. Rev. Lett. **54**, 289 (1985).

[225] J. J Molitoris and H. Stocker, Phys. Rev C **32**, R346 (1985).

[226] M. Kutschera, Phys. Lett. B **340**, 1 (1994).

[227] S. Kubis and M. Kutschera, Acta. Phys. Pol. B **30**, 2747 (1999); *ibid.* Nucl. Phys. A **720**, 189 (2003).

[228] L. J. Ye, G. W. Jun, X. Y. Zhong, L. X. Guo, Chin. Phys. Lett. **22**, 65 (2005).

[229] L. G. Arnold *et al.,* Phys. Rev. C **25**, 936 (1982); G. Passatore. Nucl. Phys. A **95**, 694 (1967).

[230] G. F. Bertsch and S. Das Gupta, Phys. Rep. **160**, 189 (1988).

[231] P. Danielewicz and G. F. Bertsch, Nucl. Phys. A **533**, 712 (1991).

[232] S. Huber and J. Aichelin, Nucl. Phys. A **573**, 587 (1994).

[233] V. Kaur *et al.,* Phys. Lett. B **697**, 512 (2011).

[234] H. Sorge, Phys. Rev. Lett. **78**, 2309 (1997).

[235] J. Y. Ollitrault, Phys. Rev. D **46**, 229 (1992).

[236] S. Kumar, V. Kaur and S. Kumar, Cent. Eur. J. Phys. **9(4)**, 986 (2011).

[237] D. J. Magestro, W. Bauer, G. D. Westfall, Phys. Rev. C **62**, 041603(R) (2000); D. J. Magestro, Ph. D thesis, NSCL, MSU, USA (2000).

[238] J. K. Dhawan and R. K. Puri, Phys. Rev. C **75**, 057901 (2007); J. K. Dhawan and R. K. Puri, Phys. Rev. C **74**, 054610 (2006).

[239] S. Kumar *et al.,* Chin. Phys. Lett. **27**, 062504 (2010).

[240] B. Jakobsson *et al.*, Nucl. Phys. A **509**, 195 (1990); H. W. Barz *et al.*, Nucl. Phys. A **548**, 427 (1992); J. Colinet *et al.*, Phys. Rev. C **67**, 064603 (2003); R. P. Scharenberg *et al.*, Phys. Rev. C **64**, 054602 (2001); J. P. Bondorf, A. S. Botvina, and I. N. Mishustin, Phys. Rev. C **58**, R27 (1998); J. Pochodzalla *et al.*, Nucl. Phys. A **583**, 553 (1995); D. Sisan *et al.*, Phys. Rev. C **63**, 027602 (2001); N. Marie *et al.*, Phys. Lett. B **391**, 15 (1997); D. Dore *et al.*, Phys. Rev. C **63**, 034612 (2001).

[241] A. D. Sood and R. K. Puri, Phys. Rev. C **69**, 054612 (2004).

[242] C. Gale, G. F. Bertsch, and S. D. Gupta, Phys. Rev. C **35**, 1666 (1987); C. Gale, G. M. Welke, M. Prakash, S. J. Lee, and S. D. Gupta, Phys. Rev. C **41**, 545 (1990).

[243] S. W. Huang, A. Faessler, G. Q. Li, R. K. Puri, E. Lehmann, D. T. Khoa, and M. A. Matin, Phys. Lett. B **298**, 41 (1993).

[244] J. Y. Chen, W. Zuo, L. Ma, and B. A. Li, Chin. Phys. Lett. **24(1)**, 76 (2007).

[245] S. Kumar and R. K. Puri, Phys. Rev. C **60**, 054607 (1999).

[246] Q. Pan and P. Danielewicz, Phys. Rev. Lett. **70**, 2062 (1993); J. Zhang, S. D. Gupta, and C. Gale, Phys. Rev. C **50**, 1617 (1994).

[247] H. S. Xu *et al.*, Phys. Rev. Lett. **85**, 716 (2000).

[248] K. Hagel *et al.,* Phys. Rev. Lett. **68**, 2141 (1992).

[249] B. A. Li and D. H. E. Gross, Nucl. Phys. A **554**, 257 (1993).

[250] A. Andronic *et al.*, Phys. Rev. C **67**, 034907 (2003).

[251] P. Danielewicz, Nucl. Phys. A **685**, 368c (2001).

[252] M. Colonna, J. Rizzo, P. Comaz, and M. D. Toro, Nucl. Phys. A **805**, 454C (2008).

[253] V. Baran, M. Colonna, M. D. Toro, and V. Greco, Phys. Rev. Lett. **86**, 4492 (2001).

[254] B. Blättel, V. Koch, W. Cassing and U. Mosel, Phys. Rev. C **38**, 1767 (1988); C. M. Ko, Q. Li and R. Wang, Phys. Rev. Lett. **59**, 1084 (1987).

[255] B. Blättel, V. Koch, K. Weber, W. Cassing and U. Mosel, Nucl. Phys. A **495**, 381c (1989); W. Cassing and U. Mosel, Prog. Part. Nucl. Phys. **25**, 235 (1990); C. M. Ko and Q. Li, Phys. Rev. C **37**, 2270 (1988).

[256] G. D. Westfall *et al.,* Nucl. Instrum. Methods Phys. Res., Sect. A **238**, 347 (1985).

[257] T. Li *et al.,* Phys. Rev. Lett. **70**, 1924 (1993).

[258] E. Plagnol *et al.,* (INDRA Collaboration) Phys. Rev. C **61**, 014601 (1999).

[259] S. Hudan, Doctorate de 1' Universite' de Caen, GANIL T **01**, 07 (2001).

[260] J. D. Frankland *et al.,* Contribution to International Workshop on multifragmentation and related topics (IWM 2001), LNS Catania, Italy, Nov. 28 - Dec 1, (2001).

[261] I. Dutt and R. K. Puri, Phys. Rev. C **81**, 047601 (2010); I. Dutt and R. K. Puri, Phys. Rev. C **81**, 044615 (2010).

[262] Z. Q. Feng, Phys. Rev. C **84**, 024610 (2011).

[263] Y. Vermani, S. Goyal, and R. K. Puri, Phys. Rev. C **79**, 064613 (2009).

[264] W. J. Llope *et al.,* Phys. Rev. C **51**, 1325 (1995).

[265] G. D. Westfall *et al.,* Phys. Rev. Lett. **71**, 1986 (1993).

[266] W. Bauer *et al.,* Phys. Rev. C **62**, 041603(R) (2000).

[267] Y. M. Zheng, C. M. Ko, B. A. Li, B. Zhang, Phys. Rev. Lett. **83**, 2534 (1999).

[268] B. A. Li, A. T. Sustich, B. Zhang, Phys. Rev. C **64**, 054604 (2001).

[269] C. Alt *et al.,* Phys. Rev. C **68**, 034903 (2003).

[270] S. Voloshin and Y. Zhang, Z. Phys. C **70**, 665 (1996).

[271] P. B. Gossiaux and J. Aichelin, Phys. Rev. C **56**, 2109 (1997).

[272] R. Snellings, New J. Phys. **13**, 055008 (2011).

[273] T. Z. Yan *et al.,* Chin. Phys. lett. **26**, 112501 (2009).

[274] C. Fuchs, Prog. Part. Nucl. Phys. **56**, 1 (2006).

[275] S. Gautam, A. D. Sood, R. K. Puri and J. Aichelin, Phys. Rev. C **83**, 034606 (2011).

[276] Y. Zhang, Z. Li, Phys. Rev. C **74**, 014602 (2006).

[277] S. Kumar, Rajni, S. Kumar, Phys. Rev. C **82**, 024610 (2010).

[278] D. T. Khoa *et al.,* Nucl. Phys. A **542**, 671 (1992).

[279] A. D. Sood, R. K. Puri and J. Aichelin , Phys. Lett. B **594**, 260 (2004).

[280] J. L. Nagle, I. G. Bearden, W. A. Zajc, New J. Phys. **13**, 075004 (2011).

[281] D. T. Khoa *et al.*, Nucl. Phys. A **548**, 102 (1992).

[282] R. K. Puri, E. Lehmann, A. Faessler, S.W. Huang, J. Phys. G: Nucl. Part. Phys. **20**, 1817 (1994).

[283] M. D. Toro *et al.,* Prog. Part. Nucl. Phys. **42** 125 (1999).

[284] W. Zhan *et al.,* Int. J. Mod. Phys. E **15**, 1941 (2006).

[285] Y. Yano, Nucl. Inst. Meth. B **261**, 1009 (2007).

[286] W. Bauer, Phys. Rev. Lett. **61**, 2534 (1988); G. F. Bertsch *et al.,* Nucl. Phys. A **490**, 745 (1988).

[287] L. Q. Feng *et al.*, Chin. Phys. Lett. **19**, 321 (2002).

[288] B. A. Li *et al.,* Phys. Rev. C **71** 054603 (2005).

[289] J. Y. Liu, Phys. Rev. C **70**, 034610 (2004).

[290] T. Li *et al.,* Phys. Rev. C **81** 034309 (2010).

[291] J. Piekarewicz *et al.,* Phys. Rev. C **79** 054311 (2009).

[292] L. Trippa *et al.,* Phys. Rev. C **77** 061304 (2008).

[293] F. Sebille *et al.,* Nucl. Phys. A **822** 51 (2009).

[294] A. D. Sood *et al.,* Phys. Rev. C **79**, 064618 (2009).

[295] M. Barronco, J. Treiner, Nucl. Phys. A **351**, 269 (1987).

[296] R. Pak *et al.,* Phys. Rev. C **53**, R1469 (1996).

[297] G. Q. Zhang *et al.,* Phys. Rev. C **84**, 034612 (2011).